Comparison of different Line Source Model approaches for analysis of Thermal Response Test in a U-pipe Borehole Heat Exchanger

PATRICIA M. MONZÓ

Master of Science Thesis
Stockholm, Sweden 2011

KTH Industrial Engineering
and Management

Comparison of different Line Source Model approaches for analysis of Thermal Response Test in a U-pipe Borehole Heat Exchanger.

Patricia M. Monzó

Master of Science Thesis Energy Technology 2011
KTH School of Industrial Engineering and Management
Division of Applied Thermodynamic and Refrigeration
SE-100 44 STOCKHOLM

KTH Industrial Engineering and Management

Master of Science Thesis EGI 2011-017 MSC

Comparison of different Line Source Model approaches for analysis of Thermal Response Test in a U-pipe Borehole Heat Exchanger.

Patricia M. Monzó

Approved	Examiner Björn Palm	Supervisor José Acuña
	Commissioner	Contact person

Abstract

Ground Source Heat Pumps (GHSPs) is a relevant application and around 3 millions installations are setting up at the beginning of 2010 (IEA ECES Annex 21). The improvements in GSHPs are currently focused on the optimization of the system and the reduction of costs installations. The thermal conductivity of the ground and thermal resistance of the Borehole Heat Exchanger (BHE) are important design parameters for Borehole Thermal Energy Storage (BTES) systems. The Thermal Response Test (TRT), which has been used up to now in the GHE design, only allows estimating mean values for thermal conductivity of the surrounding ground and borehole resistance. However, the ground thermal conductivity and borehole thermal resistance may present local variation along the borehole depth. For improving conventional TRT, the optical fiber technology is applied to collect information about the temperature profiles in the borehole. Thermal Response Test (TRT) logs the inlet and outlet fluid temperatures; meanwhile, the Distributed Thermal Response Test (DTRT) carries out a profile of the temperature along the borehole depth, in this case with fiber optic cables.

This Master of Science Thesis focuses on the comparison and analysis of DTRT measurements in a U-pipe borehole in order to estimate the thermal conductivity and the borehole thermal resistance along the borehole. The comparison and the analysis are carried out by:

- Comparing the differences of TRT results depending on the heat power rate considered – constant and by steps-.

- Comparing the results from two different resolution Distributed Test Sensing (DTS) equipments: Halo and Sentinel DTS.

- Comparing the differences of TRT results as depending on the analytical procedure based on the line source theory: line source model and line source approximation.

Acknowledgements

Firstly, I would like to sincerely thank to my advisor José Acuña for sharing his knowledge, support, good will and orientation. I would also like to thank Björn Palm for his help to coordinate this project.

I would like to dedicate this report to my mother, Mª Teresa, for her support, infinite patience and comprehension, to my brother, Juan Antonio for making me laugh and his support. I would also like to dedicate this report to my father, Antonio.

I would like also to thank all my colleagues from UPV: Isaac, Ana, Andrea, Sandra, Teo and Javi for making a nice environment during the Master.

Thank to all my friends: Bego, María, Padi, Tere, Yésica and Coke for encouraging me every day from Spain, and Carlos, Álvaro, Victor, Alexandra, Itziar, Sergio and Manu for making me laugh in Sweden.

Abbreviations

GSHP… Ground Source Heat Pump

BHE… Borehole Heat Exchanger

GHE… Ground Heat Exchanger

TRT… Thermal Response Test

DTRT… Distributed Thermal Response Test

DTS… Distributed Test Sensing

Nomenclature

a… Ground Thermal diffusivity [m^2/s]

c_p... The volumetric heat capacity [J/m^3K]

c… Volumetric heat capacity [J/m^3]

c_{cyl}… Cylinder heat capacity per m borehole [J/m K]

E_1… The exponential integral

G… Cylindrical source function

H… Effective borehole depth [m]

h… $2\pi\lambda_{ground}R_b$

J_0, J_1, Y_0, Y_1… Bessel functions

K_{geo}… Temperature gradient in the semi-infinite region.

k… slope

m... the ordinate at the origin

p… r/r_0

Q… Injected heat power rate [W]

q… heat flux [W/m]

r… radius [m]

r_b… borehole radius [m]

r_0… references radius [m]

R_b… Borehole thermal resistance [K m/W]

R_r… Rock thermal resistance [K m/W]

R_T… Total ground thermal resistance [K m/W]

t… Time [sec]

T… Temperature [^oC]

T_b… Borehole wall temperature

T_f... Fluid mean temperature in the collector

T_0… Undisturbed ground temperature [^oC]

U… Heat conductance [K/(W/m)]

x… $\frac{r_b^2}{4 \cdot a_{ground} \cdot t}$

z… Fourier's number

α_1… $\frac{2\pi \cdot r_b^2 \cdot c_{ground}}{c_{cy1}}$

λ… Borehole thermal conductivity [W/m K]

γ… Euler's constant

ρ… Density [kg/m³]

τ… $\tau_N(t) = \sum_{n=1}^{N} \frac{q_n - q_{n-1}}{q_{ref}} \cdot \ln(t - t_n)$

ζ… $\frac{a_{ground} \cdot t}{r_b^2}$

Subscripts

b… Borehole

bhf… Borehole filling

bhw… Borehole wall

fill… filling

f… fluid

m... mean

p_i… pipe (inner)

p_o… pipe (outer)

ug… undisturbed ground

Table of Contents

Index of Figures.

1. Introduction.

Ground source heat pumps (GSHPs) systems are now well established to provide heating or cooling in commercial and residential buildings. GSHPs are the most relevant geothermal application and around 3 millions installations are setting up at the beginning of 2010 (IEA 2010).A GSHP system includes a conventional heat pump unit and a group of borehole heat exchangers (BHEs), which are connected with the pump. The improvements in GSHPs are currently focused on the optimization of the system and the reduction of costs installations.

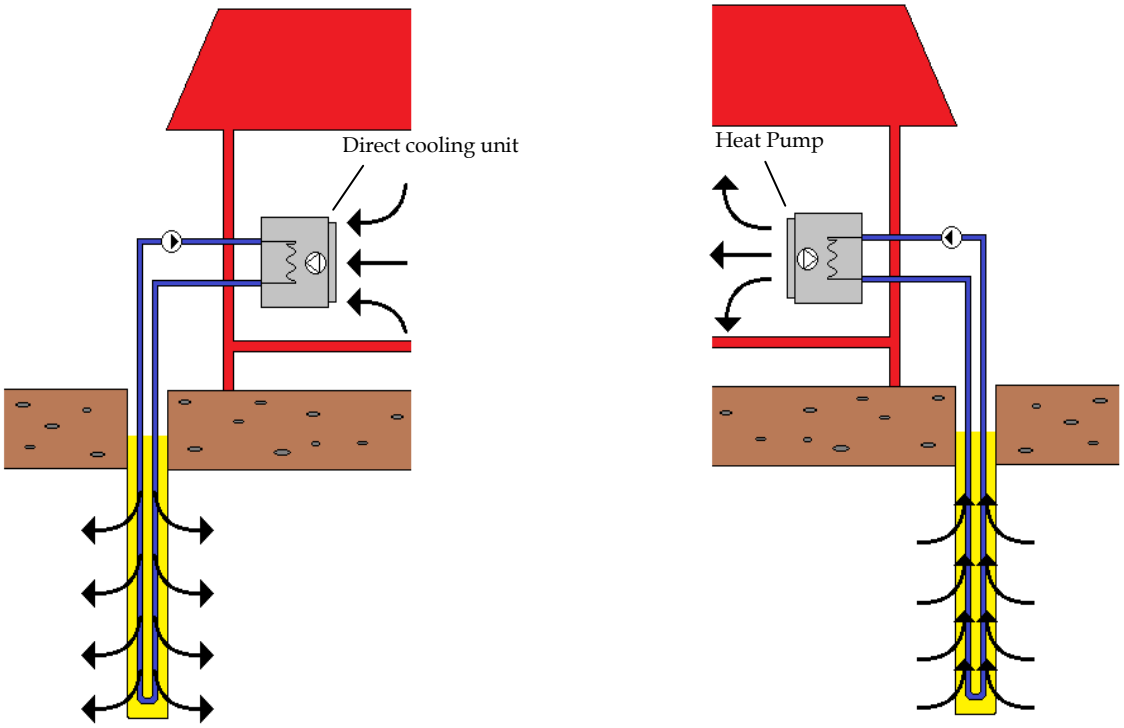

Figure 1. *Borehole heat exchanger cooling (left) and heating (right) applications.*

The length of the ground heat exchanger (GHE) is crucial for an optimal design and low cost. Moreover, for the design of larger BHE systems is necessary to know some points such as the effective heat transfer capacity of the borehole, sizes and configuration as well as backfill materials of BHEs. Thus, thermal conductivity of the ground and thermal resistance of borehole heat exchanger require being determined for the design of BHE system.

1.1. Thermal Resistance and Ground Thermal Conductivity.

As above pointed out, the most important factors for an optimal thermal performance of the borehole are its thermal resistance and the ground thermal conductivity.

The total ground thermal resistance (R_T) contains the ground thermal resistance and the borehole thermal resistance, so that it can be defined as a sum of both resistances. The ground thermal resistance (R_r) comprises the resistance of the rock surrounding the borehole wall. The thermal resistance of borehole (R_b) is the thermal resistance between the heat carrier fluid in the borehole flow channels and the borehole wall.

$$R_T = R_b + R_r \qquad (1)$$

The thermal resistance of the borehole includes the thermal resistance of the fluid circulating inside the pipe, the wall pipe thermal resistance as well as thermal resistance of filling material. The borehole thermal resistance can be defined as an addition of these three components:

$$R_b = R_f + R_{bhf} + R_{bhw} \qquad (2)$$

The thermal resistance fundamental is enclosed in *Figure 2*.

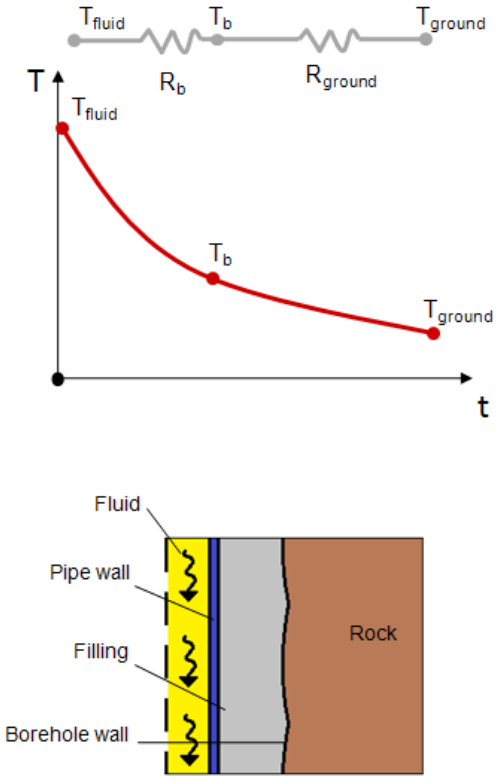

Figure 2. *Thermal resistance fundamental in borehole heat exchanger.*

The difference of the temperature between the fluid in the collector *(T_f)* and the borehole wall *(T_b)* is connected with the fluid-to-borehole wall thermal resistance *(R_b)* as well as the specific the heat transfer rate q (W/m):

$$T_f - T_b = R_b \cdot q \quad (3)$$

It can be interpreted from equation (3) that the heat transfer rate is proportional to the temperature difference between the heat carrier fluid and the borehole wall. Thus the borehole thermal resistance is dependent on the disposition of the flow channels and thermal properties of materials implicated. A small thermal borehole resistance value is suitable for the design.

The thermal conductivity of the ground is the capacity of the rock to transfer the heat from the borehole walls to its surrounding ground and vice versa. The volumetric heat capacity (c_p) is the ground capability for the thermal energy storage. These parameters are related to the diffusivity (α), which can be defined as a relation between the ground capacity to conduct the heat and its capacity to store the energy.

$$\lambda = \rho \cdot c_p \cdot \alpha \quad (4)$$

According to borehole grouting, there are different materials using to fill the space between the pipes and the borehole wall, such as bentonite, concrete. These materials usually have a good thermal conductivity. However, the groundwater, which has a low thermal conductivity, is usually used as a grouted material in Sweden. In spite of its low thermal conductivity, the heat transfer between the heat exchanger and the surrounding ground is enhanced by a natural convection occurred in the groundwater. Depending on the geological materials (sand, gravel) or fractures in bedrocks, the groundwater flow can be relevant in the borehole design.

There are some ways to evaluate the ground properties, for instance in Europe ground thermal conductivity and thermal resistance between heat carrier fluid and borehole wall are taken into account. However, the ground thermal conductivity and grout thermal conductivity are analyzed in American methods. (Gehlin 2002)

1.2. Thermal Response Test

Thermal Response of the borehole is the change occurring in its temperature when a heat carrier fluid circulates through the borehole heat exchanger for a certain period of time.

The study of the fluid temperature versus time enables the estimation of thermal properties in an around the borehole. For instance, a rapid temperature response manifests a low thermal conductivity. As well as, the thermal resistance of the borehole

heat exchanger is indicated by the temperature difference between the heat carrier fluid and the surrounding ground. Analytical solutions of heat equation can provide an assessment of the temperature change in the heat carrier fluid.

There are different methods to estimate the ground thermal property at the location of the BTES system by means of standard values for the type of rock or laboratory methods (Sundberg 1998). However, these methods do not offer complete information of the ground characteristics.

Nowadays, thermal response test (TRT) is widely utilized to determine the ground thermal properties as well as the heat-transfer performance between the ground and the BHE. The *Figure 3* shows an outline of the principle of thermal response test. Mogensen (1983) was the first who applied this method to determine the in situ ground thermal conductivity and thermal resistance of the borehole. It is based on constant heat (or cool) flux extraction by means of a heat carrier fluid which circulates through a BHE system. The temperature data of the inlet and outlet fluid from the BHE are measured and logged. The heat transfer process is described by a mathematical model and this is compared with the experimental field data of temperature over time. In mathematical model, the values of the ground thermal conductivity and borehole thermal resistance have to be primarily assumed. Although conventional TRT is not an accurate system, it has widely been applied to determine the optimum design BHE.

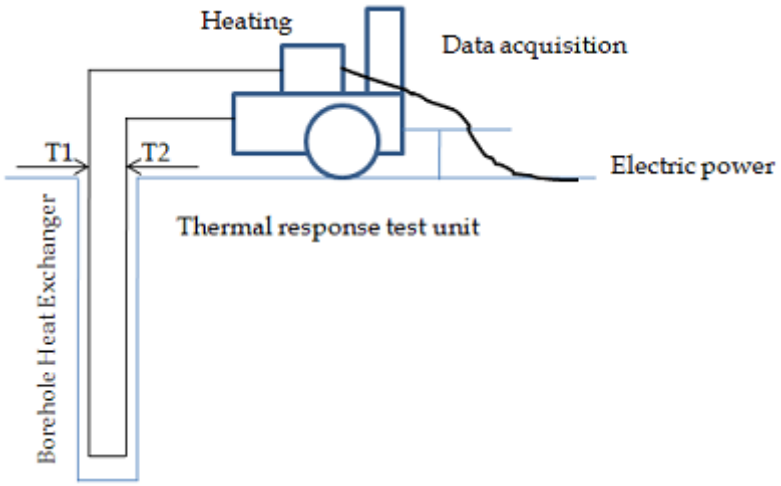

Figure 3. *Thermal response test. (Gehlin et al. 2001)*

The first TRT mobile measurement device was introduced in Sweden in 1995. Since then, this method has been extended into Europe and North America. At the same time, a variety of analytical and numerical data analyses have been developed to improve this method. In Europe, the common model for evaluation of the response test data is line source due to its ease of operation and speedy response. However, the cylinder source combines with numerical models is the usual in the USA.

In 1995-1996, "TED", the Swedish response test apparatus was developed at the Luleå University of Technology (Eklöf and Gehlin 1996; Gehlin and Nordell 1997) to determine ground thermal conductivity and the influence of the effect such as groundwater flow and natural convection in the boreholes. More details about the response test apparatus can be found in Gehlin (1998).This methodology is further studied by Gehlin et al. (2002).

1.3. Analysis of TRT-Theory.

Analytical and numerical models are developed to assess the temperature data of TRT, which will be described in details subsequently. (Gehlin et al. 2002)

For the purpose of the thermal response test evaluation, the following assumptions are taken into account in analytical and numerical models:

- Convective heat transfer in the ground is neglected. Conduction heat is only considered by models.
- Thermal process is symmetry in the radial direction from the borehole axis.
- In the direction along the borehole axis, heat conduction is negligible.

1.3.1. Analytical models.

The main analytical direct models used to evaluate thermal response data are line source and cylinder source approaches. The heat transfer problem between the borehole and the nearby infinite region is assumed as an analytical solution of line and cylinder source model. According to the geometry of the borehole and the heat exchanger pipe configuration, these models require the simplifications of several assumptions.

1.3.1.1. Line source model.

Mogensen (1983) was the first who applied the line source model to estimate the ground thermal conductivity by means of an experimental field test. This model is commonly used because of its simplicity and rapid results. The temperature field on the ground can be written as a function depending on time (t) and radius (r) around a line source with a constant heat injection rate (q) from a line along the vertical axis of the borehole in an infinite solid (Carlslaw and Jaeger 1959):

$$T(r,t) = \frac{q}{4\pi\lambda}\int_{\frac{r^2}{4at}}^{\infty}\frac{e^{-u}}{u}du = \frac{q}{4\pi\lambda}E_1\left(\frac{r^2}{4at}\right) \quad (5)$$

It should be noted that the line-source temperature is evaluated at the borehole radius ($r = r_b$), so that it is necessary to take into account the effect of the thermal resistance between the fluid inside the pipe and the borehole wall (R_b).

$$T_f^q(t) = T_b^q(t) + q \cdot R_b \quad (6)$$

It should be emphasized that the heat extraction rate q [W/m] along the vertical axis of the borehole is constant, the ground temperature is undisturbed and its BHE surrounding is homogeneous and isotropic. As well as the above assumptions mentioned, the equation (6) can be written as:

$$T_f^q(t) = \frac{q}{4\pi\lambda}\int_{\frac{r^2}{4at}}^{\infty}\frac{e^{-u}}{u}du + q \cdot R_b + T_0 \quad (7)$$

With an error less than 2%, the equation can be used for cylindrical heat injection ducts (Ingersoll and Plass 1948) if:

$$t > \frac{20r_b^2}{a} \quad (8)$$

The usual time in a borehole is around the interval ranged from 10 to 20 hours.

The essential method developed by Mogensen (1983) is followed by the researchers. Thus, the approach described is implementing in different ways to obtain a simple method for the evaluation of ground thermal properties. Subsequently, the most relevant line source approximations are compiled.

In the equation (5), the exponential integral E_1 can be simplified for large values of the parameter ($\alpha t/r^2$).

$$E_1\left(\frac{r^2}{4at}\right) = ln\left(\frac{4at}{r^2}\right) - \gamma \qquad \frac{at}{r^2} \geq 5 \quad (9)$$

where γ (Euler's constant)=0.5772

It is reported that the maximum error is 2.5% for values of (at/r^2)≥20 and 10% for ($\alpha t/r^2$)≥ 5.

Taking into consideration equation (7) and the aforementioned exponential integral approximation equation (9), the fluid temperature can be expressed as:

$$T_f(t) = \frac{q}{4\pi\lambda} \cdot \left(ln\left(\frac{4at}{r^2}\right) - \gamma\right) + q \cdot R_b + T_o \quad (10)$$

Eklöf and Gehlin (1996), Gehlinand Nordell (1998), Sanner et al. (2000) and Cruickshanks et al. (2000), who assumed the line source solution (5), approximate equation (10) to a linear equation.

$$T_f(t) = k \cdot lnt + m \quad (11)$$

Being *k* the slope of the curve, which is related to the thermal conductivity as expressed in equation (12):

$$k = \frac{q}{4\pi\lambda} \quad (12)$$

And *m* comprises the magnitude of the value when the time is zero, it is known as the ordinate at the origin. If thermal resistance is considered as a constant value over time, m can be connected with this parameter by means of the following equation:

$$m = q \cdot \left[R_b + \frac{1}{4\pi Lk}\left(ln\frac{4a}{R^2} - \gamma\right)\right] + T_{ground} \quad (13)$$

It should be noted that this equation is valid when the thermal process within the borehole is near steady-state condition. Therefore the initial hours of thermal response test require to be neglected.

On the contrary, if the variation of the thermal resistance over time is required, this parameter will be determined by means of the equation (10), as follows:

$$R_b = \frac{T_f(t) - T_o}{q} - \frac{1}{4\pi\lambda}\left(\ln\left(\frac{4\alpha t}{r^2}\right) - \gamma\right) \quad (14)$$

The power supply is not constant during the test and it is difficult to maintain a constant heat flux injection during the thermal response test (Gehlin and Eklöf (1996)). Therefore, the mean temperature in the borehole may be considered as an addition of heat input contribution for time intervals considered. Eskilson (1987) and Hellström (1991) describe this step-analysis.

$$\Delta T(q_1, q_2, \dots, q_n) \equiv \Delta T(q_1) + \Delta T(q_2) + \cdots + \Delta T(q_n) \quad (15)$$

The heat input may be accounted as stepwise of constant heat pulses that are then super imposed in time. For a heat pulse analysis, the following method is used:

$$q(t) = \begin{cases} q_1, & t_1 < t < t_2 \\ q_2, & t_2 < t < t_3 \\ & \dots \\ q_n, & t_{n-1} < t < t_n \end{cases} \quad (16)$$

being t_1 the initial time of TRT (t_1=0).

Considering the principle of super positioning, the temperature in the bedrock can be expressed as a sum of the input of each heat step:

$$T_f = \sum_{n=1}^{N} \frac{q_n - q_{n-1}}{4\pi\lambda} \cdot \ln(t - t_N) + \left[q_N \cdot \left(\frac{1}{4\pi\lambda} \left(ln\left(\frac{4\alpha}{r_0^2}\right) - \gamma \right) + R_b \right) + T_0 \right] \quad (17)$$

This equation can be defined as a function of dimensionless parameter (τ_N), as given in equation (18), being t the time in the interval $t_N + \frac{r_0^2}{5\alpha} < t < t_{n+1}$:

$$\tau_N(t) = \sum_{n=1}^{N} \frac{q_n - q_{n-1}}{q_{ref}} \cdot \ln(t - t_n) \quad (18)$$

Notice that q_0 is equal to zero and q_{ref} can be given any value except zero.

Thus the equation (17) can be also defined as:

$$T_f = \frac{q_{ref}}{4\pi\lambda} \cdot \tau_N(t) + \left[q_N \cdot \left(\frac{1}{4\pi\lambda} \left(ln\left(\frac{4\alpha}{r_0^2}\right) - \gamma \right) + R_b \right) + T_0 \right] \quad (19)$$

According to equation (19), there is a linear relation between the temperature and τ_N parameter. The slope of its line, k, is related to thermal conductivity by means of the following equation:

$$\lambda = \frac{q_{ref}}{4\pi k} \quad (20)$$

For effective conductivity estimation is necessary to consider the stepwise change in the heat injection; however, the ground heat capacity buffers the effect so that the stepwise of shorter than 2-3 hours may not be considered.

Taking into account equation (19), R_b can be estimated as follows:

$$R_b = \frac{T_f(t) - \frac{q_{ref}}{4\pi\lambda} \cdot \tau_N(t) - T_0}{q_N} - \left(\frac{1}{4\pi\lambda} \left(ln\left(\frac{4\alpha}{r_0^2}\right) - \gamma \right) \right) \quad (21)$$

According to the exponential integral simplification, Gehlin (2002) contemplates the results about the continuous line source described in equation (5), in which the exponential integral E_1 is assumed as an approximation of a serial function (Abramowitz and Stegun (1964)):

$$E_1(x) \approx -\gamma - lnx + A \cdot x - B \cdot x^2 + D \cdot x^3 - E \cdot x^4 + F \cdot x^5 \quad (22)$$

where

A=0.99999193; B=0.24991055; D= 0.05519968; E=0.00976004; F=0.00107857;

Notice that this serial development is valid for a small value of x, and x is ($r^2/(4\alpha t)$).

1.3.1.2. Cylinder source model.

The cylinder source model approaches the borehole heat exchanger as an infinite cylinder with a constant heat flux through U-pipe exchangers. Besides the ground loop heat exchanger is considered as a single coaxial pipe with an equivalent diameter of the two pipes of U-pipe exchanger. The line source model is considered as a simplification of the cylinder source model. The following equation describes the cylindrical source solution:

$$T^q(r,t) = \frac{q}{\lambda} \cdot G(z,p) = \frac{q}{\lambda} \cdot G\left(\frac{at}{r^2}, \frac{r}{r_0}\right) \quad (23)$$

Being G(z,p) is the cylindrical source function as described by Ingersoll (1954):

$$G(z,p) = \frac{1}{\pi^2}\int_0^\infty f(\beta)d\beta \quad (24)$$

$$f(\beta) = \left(e^{-\beta^2 z} - 1\right) \cdot \frac{[J_0(p\beta)Y_1(\beta) - Y_0(p\beta)J_1(\beta)]}{\beta^2[J_1^2(\beta) + Y_1^2(\beta)]} \quad (25)$$

In above equation, J_0,J_1,Y_0,Y_1 are Bessel functions of the first and second kind.

The general equation can be written as presented in equation (26):

$$T_f(t) = \frac{q}{\lambda} G(z,p) + q \cdot R_b + T_o \quad (26)$$

Carslaw and Jaeger (1959) develop a model based on cylinder source theory, in which solutions are obtained varying boundary conditions for regions bounded by cylinder geometry. The borehole heat exchanger is represented as a cylinder filled with a backfill material and the fluid temperature for larges value of the time or a small radius can be determined with the following approach cylinder theory:

$$T(t) = T_{ug} + \frac{Q}{4\pi\lambda_{ground}H}\left(2h + ln\frac{4\zeta}{C} - \frac{4h - \alpha_1}{2\alpha_1\zeta} + \frac{\alpha_1 - 2}{2\alpha_1\zeta} \cdot ln\frac{4\zeta}{C} + \cdots\right) \quad (27)$$

where

$$h = 2\pi \cdot \lambda_{ground} \cdot R_b \qquad \alpha_1 = \frac{2\pi \cdot r_b^2 \cdot c_{ground}}{c_{cy1}} \qquad \zeta = \frac{a_{ground} \cdot t}{r_b^2} \quad (28)$$

$$a_{ground} = \frac{\lambda_{ground}}{c_{ground}} \qquad C = e^{\gamma} \qquad \gamma = 0.5772 \ldots \quad (29)$$

Deerman and Kavanaugh (1991) and Kavanaugh and Rafferty (1997) develop a methodology based on the cylinder source theory that uses an iterative procedure. In this procedure, the effective thermal conductivity is calculated by means of the reverse process used to obtain the length of the ground heat exchanger. The thermal conductivity and diffusivity are introduced in a dimensionless cylinder-source function to obtain the thermal resistance, which is compared with its measured value of a short-term in-situ test.

1.3.2. Numerical models.

As outlined above, other way to assess the thermal response data are the numerical models. Since line source and cylinder source models represent the ground loop heat exchanger as a simple geometrical design, the numerical models allow designing in details the borehole geometry and thermal properties of the fluid, pipe, borehole filling as well as modifying heat transfers rates. However, these models can be too much difficult and time-consuming if the requirements of input data are too many extensive.

Berberich (1994) develops a parameter-estimation-based method, which used a two-dimensional finite difference model in order to solve the method. In this model, the temperature is measured along the borehole by sensors located on its wall. The ground thermal conductivity and the volumetric heat capacity are considered variables, whereas the temperature is an input data. Implementing the aforementioned method, the heat flow is calculated in both the vertical and the radial directions.

In the same way, Shonder et al. (1999) describe a procedure for the TRT evaluation, which is based on parameter-estimation and a one-dimensional finite difference model. As cylinder-source representation, the inlet and outlet pipes of the U-pipe borehole are represented as a single cylinder. In addition, a thin film, which adds a resistance without heat capacity and a layer ground with different ground thermal properties from the surrounding region are taken into account. Notice that if thin film is zero and the thermal characteristics of the grout are similar to the soil, this is equivalent to solve a cylindrical heat source problem in an infinite medium (23).

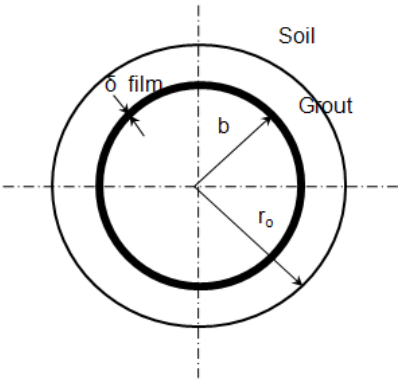

Figure 4. *One-dimensional numerical model geometry for Oak Ridge National Laboratory Method.*

(Shonder, et al. 1999)

As a whole, there are nine parameters involved in this solution – the undisturbed temperature, the effective pipe radius; the thickness of the thermal film; the thermal conductivity of the soil, grout and thermal film; the volumetric heat capacity of the soil, grout and thermal film. On the other hand, heat flux and the temperature are known due to these are measured at the film surface. It is not possible to determine all of these with a single experiment, because some of these parameters may depend on the others. For a trial value of the parameters and the measured heat flux, a predict value of the ground temperature as a function of time is given by the numerical model. The predicted and the measured temperature values are compared by means the sum of the squared errors. According to the Gauss method, the most minimum value of sum of the squared error gives the best fit for the parameters estimated.

A transient two-dimensional numerical finite model is developed for ground parameter estimation by Austin (1998) and Austin et al. (2000) even when the power input is variable. This model utilizes the 2nd order differential equation for conduction heat transfer in cylindrical coordinates; the boundary condition is that the outer radius is adiabatic considering a large enough domain and the initial condition is that all temperatures are at the far-field temperature. Owing to symmetry, this model approximates U-pipes by "pie-sectors", in which a constant flux is accepted. The grid resolution is determined by an algorithm which takes into account the borehole and U-pipe geometry. The grid dimension of conventional borehole is around 100 finite volume cells in the angular direction and 150 to 200 cells in the radial direction. Considering the boundary and initial conditions, the energy balance equation is established in each finite volume cell for the heat flux through a particular control volume in the solution domain. The numerical model assumed a 5 minutes time step, fitting in with the experimental measurements. For establishing identical conditions in this two-dimensional model, it attempts to simulate the heat transfer conditions. Thus, a heat generation in "fluid" cells is required to represent the power in the model. In these "fluid" cells, a high thermal conductivity and a low volumetric specific heat are assumed in order to consider the effect of dissipating the energy without any fluid thermal resistance. Moreover, the pipe is evaluated in a one volume control inside each

pie-shaped sector´s control volumes. The thermal conductivity is calculated in each of those particular control volumes by means of a resistance circuit. This resistance circuit represents the pipe thermal resistance as a sum of two resistances that represents convection heat and thermal conductivity of the material pipe. Hence the convection resistance inside the U-pipe is not neglected for the estimation of the pipe material conductivity.

Therefore, design parameters such as the fluid properties, borehole depths and far-field temperature are given as an input data in Austin et al. (2000). The model also requires the power and the temperature in time intervals studied as well as the mean temperature and the input power, which are both determined experimentally. Introducing a boundary-fitted grid, this methodology is improved by Spiltler et al. (2000).

Regarding numerical model, Gehlin et al (2002) describe a model based on a numerical one dimensional finite difference (FDM) method. In this model, the U-pipe is approximated by a coaxial pipe which is surrounded by the borehole filling material. The thermal process in the borehole is represented by two components - a thermal resistance between the fluid and the borehole filling material and a thermal resistance between the borehole filling material and the borehole wall-.

$$R_b = R_{bhf} + \frac{R_{pipe}}{2} \quad (30)$$

where

$$R_{pipe} = \frac{ln\left(\frac{r_{p\_o}}{r_{p\_i}}\right)}{2\pi\lambda_{pipe}} \quad (31)$$

Similarly, the thermal resistance of the borehole filling material can be divided into a thermal resistance between the outer surface pipes and the borehole filling material and a thermal resistance between the filling material and the borehole wall.

$$R_{bhf\_bhw} = 0.33 \cdot R_{bhf} \qquad R_{fl\_bhf} = (1 - 0.33) \cdot R_{bhf} \quad (32)$$

The heat conductance between the fluid and borehole filling, the one for the borehole filling and the borehole wall, and the ground conductance are defined as follows:

$$U_{fl\_bhf} = \frac{1}{\frac{R_{pipe}}{2} + R_{fl_{bhf}}} \qquad U_{bhf\_bhw} = \frac{1}{\frac{ln\frac{r_m}{r}}{2\pi\lambda} + R_{bhf\_bhw}} \qquad U_{ground} = \frac{2\pi\lambda}{ln\frac{r_m}{r_m - \Delta r}} \quad (33)$$

The evaluation of the difference of the temperature and the heat conductance between two points separated a radial distance from the borehole centre results in the specific heat flow. The change in the temperature depends on the time while the change in the specific heat flow does it over time and the specific heat capacity. In this numerical method, the ground thermal conductivity and the borehole thermal resistance are varied methodically. The minimum difference in the sum of the squares of the errors between the calculated and the measured values gives the best approach of these, which is known as Nelder-Mead Downhill technique.

Mostly models, as line source or cylinder source as well as numerical models are based on cylinder approximation. Although variables are implicated in the methods, most models require a parameter estimation to calculate the ground thermal conductivity.

The main difference between the models is the characterization and analysis of the borehole. For instance, the borehole heat capacity is not taken into account by line source model whereas cylinder source approaches may do it. The advantage of cylinder models is the possibilities to consider the borehole in details, as borehole geometry, heat capacity of filling material, heat carrier fluid properties.

Since most models require the ground thermal properties estimation, a parameter estimation procedure is required to get the solution. This procedure consists of obtaining the minimum difference between an experiment and analytical or numerical response by adjusting model input. Thus borehole thermal resistance and ground thermal conductivity are considered variable values and these are systematically varied. Consequently, the minimum difference between experimental and modelled values gives the best estimation of these parameters.

1.4. Thermal response test - state of the art -

A proper design of a ground source energy system requires a good estimation of the ground thermal properties. Although thermal response test is a recognized method for determining of the heat transfer properties in BHE, TRT results depend on the conditions of the test as well as the analytical or numerical models predicting the thermal conductivity of the ground. Therefore, research efforts are currently focused on carrying out further development of this technique, which allows the optimal design BHE. Eklöf and Gehlin (1996) and Austin (1998) were the first who started with the actual TRT development. Since then, several research activities have been carried out so that some enhanced results have been compiled in this thesis.

Several sources may explain the deviation between the estimated and the real values of ground thermal properties, such as random, experimental error, the duration of test, the estimations considered in analytical or numerical model and the far field temperature.

Austin (1998) discusses the uncertainties due to different analysis procedures with different test equipment. The results show that the error in the measurement of heat transference is on the order of ±10%, which is a similar percentage error in the estimation ground parameters. A minimum experimental error can be got if care is taken in the measurement of heat transfer rate.

The assumption of constant heat rate may be the reason in uncertainties due to analysis procedure. In line source model, significant variations in the heat transfer rate to borehole mean highly variable thermal conductivity estimation (Austin 1998). So that models, which do not assume a constant heat transfer rate, can provide better thermal parameter estimation. However, Witte et al. (2002) demonstrate that the assumption of constant heat transfer rate in both line source model and parameter estimation methods may result in similar BHE parameter.

Regards as the model uncertainties, it should be noted the comparison of four two-variable parameter estimation models develops by Gehlin (2002). Both differences and analogies between these four models are discussed and drawn. The first model is a line source-based solution and its solution results from equation (22), the second one is also based on the line-source theory, which solution is given by equation (10), the third model is a cylinder source-based solution from equation (27) and the fourth is a numerical one-dimensional finite difference model above mentioned based on the evaluation of temperature and heat conductance (33). The following outcomes are established:

- Two line-source models compared present similar results. However, cylinder source and numerical model manifest higher values of ground thermal parameters. This may be related to thermal mass of the material inside the borehole in cylinder source method.

- The line-source models describe closest results in keeping with the measured temperature for evaluated data sets.

- In the numerical model, there is a trend to overestimate the borehole temperature for the initial test hours and more time is required to evaluate the data.

- The line source model is the fastest and simplest model, whilst numerical model responds better for variable heat injection conditions.

Since the numerical model only can provide a suitable solution for the aforementioned assumption, Signorelli et al. (2007) start to deal with the traditional assumption considered in the TRT evaluation. Thus the best time required in TRT is evaluated as well as the influence of other effects such as borehole length, subsurface heterogeneity

or groundwater is taken into account by 3D finite element numerical model from theoretical data.

More recently, Marcotte and Pasquier (2008) develop line source functions considering Fast Fourier Transform and analytical interpolations to obtain a greater accuracy in the estimation of borehole parameters in less time. In the same way, Bandos et al. (2009) apply a semi-infinite line source model to achieve a better fit of GHE parameters.

According to convection heat in ground, Raymond et al. (2010) develop a numerical groundwater flow and heat transfer model in BHE for non-ideal conditions. For this purpose, the HydroGeoSphere simulator is used. The numerical model developed is successfully compared to the line source model, in which the numerical analysis is performed in standard conditions. Moreover, this numerical model is used to analyze a test performed in a geological setting where the line-source assumptions cannot be justified. The numerical model provides a more reliable estimation of the thermal conductivity particularly in complex geological settings where some assumptions cannot be met by lineal model.

The optimum design of the ground heat exchanger installations is difficult to estimate by means of a conventional TRT method. Although this method has been used up to now in the GHE design, TRT only allows estimating medium values for thermal conductivity of the surrounding ground and borehole resistance. The change in the temperature along the borehole depth and for the period of thermal response test have been robustly illustrated by some authors as Signorelli et al. (2007), Marcotte and Pasquier (2008) and Bandos et al. (2009). Thus TRT do not always provide the suitable thermophysical property data of the ground.

Optical fiber thermometer appears in the late 1980s as a facility to collect information about the temperature profiles in the borehole. Thus optical fiber thermometer allows measuring the temperature along a length in time intervals. Fujii et al. (2006) develop a pioneer system to determine the thermal conductivity variations along the borehole depth by means optical fiber sensors. However, this system needs to be improved because the distance between the sensor and the U-pipe walls has a strongly influence on the temperature measurements.

More recently, Fujii et al. (2009) go further on this field. They measure inlet and outlet temperature in the borehole as well as the temperature inside the borehole using retrievable an optical fiber sensor, which is set inside the down-flow U-pipe and has an accuracy of 1ºC.Therefore, the temperature is logged along the depth of the borehole. These temperature measured data and the change in the outlet and inlet temperature are processed in a program based on cylindrical source function G (Ingersoll et al., 1954) to estimate the distribution of thermal conductivity along the borehole by means of non regression lineal method. Considering the geological and groundwater

conditions of the borehole, the results from this method are nearly approached with the ground characteristics. Moreover the groundwater flow is reflected on the recovery temperature, which is quicker in intervals with groundwater flow than intervals without this flow.

Improvements for the TRT equipment is described by Wang et al. (2009), who develop an innovative constant heating temperature method (CHTM) for TRT. While, conventional TRT equipment try to provide a constant heating flux during the test, the improved TRT equipment ensures a constant inlet fluid temperature (CHFM). Furthermore, the improved TRT can operate effectively as the heat-injection mode as the heat-extraction one. A mathematical model based on cylindrical-source model is used to evaluate this data. For this purpose, a program based on Visual Basic 6.0 is used to obtain analytical solutions of G-functions. In comparison with CHFM-based, the CHTM-based TRT presents several advantages in operating modes, as well as in operation of control, stability and accuracy. The most relevant advantage is that the time for reaching a steady heat-transfer state between the BHE and its surrounding is reduced. However, there are some barriers such as high control requirement, a complex model to evaluate the data as well as a high cost that should be overcome.

Another point is 3D simulation of thermal response test, to which Schiavi (2009) implements the governing partial differential equations of heat transfer. The effective heat rates exchanged in TRT are evaluated by means of the software so-called COMSOL Multyphysics® environment. Thus the borehole temperature distribution during the TRT is determined by this tri-dimensional model as well as the ground parameters are estimated through the line-source model. The results shows that TRT evaluated by 3D simulator, which is based on line source model, gives an adequately estimation for ground parameters in U-pipe configurations. However, it is necessary a more developed 3D simulation study for a more complex geometric configuration.

In addition to thermal response along the borehole, Acuña (2010) has developed a method to measure the fluid temperature inside the U-pipe by fiber optic cables, which is known as Distributed Thermal Response Test (DTRT). The difference between the researches carried out by Fujii (2009) is the measurement procedure. While Fujii measures the temperature inside the pipe in the down flow tube, Acuña (2010) makes it in both tube of U-pipe heat exchanger. Thus fiber optical cables go down and up through the down and upwards channels of the BHE. These measurements are carried out by means of Distributed Temperature Sensing (DTS) technology, which gives as a result a clear picture of the temperature along the borehole length at anywhere depth and at any time intervals. Furthermore, the distributed temperature sensing with optical fiber cables technology is complemented by other widely known techniques such as thermocouples, resistance thermometers, loggers, groundwater level meter. The results show the influence of pumping power on the assessment of undisturbed ground temperature during TRTs and there is a difference between the thermal resistance estimated by conventional TRT and innovative DTRT.

The increasing interest of TRT and the research activities all over the world make International Energy Agency establishes a working work (IEA ECES Annex 21), which is concerned to compile TRT experiences and achieve further development and the promotion of this technology since June 2006. The annex 21 program is divided into different fields: TRT state of the art, new TRT development, TRT evaluation methods and developments, standard TRT procedures, diffusion activities. The attention is focuses on TRT state of the art, evaluation methods as well as developments areas, which are considered to be of significant importance for this thesis (IEA ECES Annex 21. Subtask 3 "Evaluation methods and developments" 2010). According to analytical methods, it is said that there are studies for a better fit of line source approximation and cylinder source, which will be reported at IEA ECES next meetings. According to the groundwater flow, annex 21 is noted that the convergence of the result in infinite linear source approximation will not occur if the influence of ground water is high. Moreover, annex 21 compiles some important items and common mistakes should be taken into account, such as not matches and not calibrated temperature sensors, the assessment of undisturbed ground temperature and the active length and deviation of the borehole.

1.5. Objective

The aim of this Master Science Thesis is the analysis and the comparison of distributed thermal response test measurements in a U-pipe borehole in order to estimate the most accurate profile of the thermal conductivity and thermal resistance along the borehole. The comparison and the analysis are carried out by:

- Comparing the differences of TRT results as depending on the heat power rate considered – constant and by steps-.

- Comparing the results from two different resolution Distributed Test Sensing (DTS) equipments: Halo and Sentinel DTS.

- Comparing the differences of TRT results as depending on the analytical procedure based on the line source theory: line source model and line source approximation.

These comparisons may suggest the suitable test equipment to carry out TRT measurements and the uncertainties due to the heat power variations and the analytical procedure. These results may provide the most accurate estimations of the ground thermal conductivity and borehole thermal resistance along the depth of BHE.

2. Methodology.

The installation studied in this thesis is established in the south of Stockholm, Sweden. This installation comprises 6 boreholes, which are separated from each other at least 4 meters. The borehole is 140 mm in diameter and has a depth of 260 meters water filled. Taking into account the ground water level, its active borehole length is around 254.5 m. The carrier fluid is an aqueous solution of 20% ethanol volume concentration and its flow rate is held constant during the test. More details about the installation are described in Acuña (2010).

To analyze the ground properties along the whole borehole, 12 sections of 20 meters in depth were considered in the borehole as shown in *Figure 5*. It should be noted that the first ten meters and the last ten meters depth are neglected. Thus, the influence of the ambient air and the hemispherical heat transfer around the borehole bottom are eliminated, respectively.

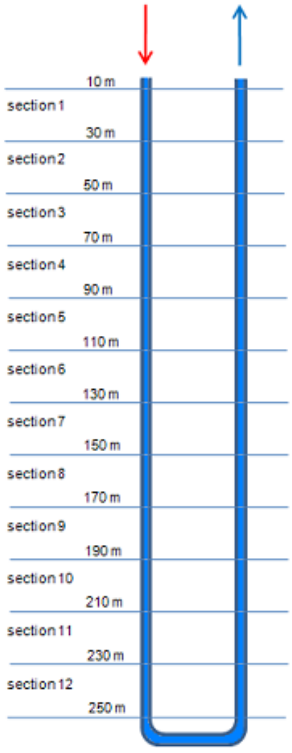

Figure 5. *Studied Section in the borehole.*

Firstly, it should be noticed some considerations according to the borehole operation in the previous periods to the period in which the measurements analyzed in this thesis were carried out. This borehole installation was operative during December 2007 and

December 2008. Consequently, the ground temperature varied from its undisturbed ground temperature. To recover the undisturbed conditions, the installation was not operative for one year, until December 2009. When the borehole recovered its undisturbed conditions, the ground temperature was measured along the borehole length. As shown in *Figure 6*, the undisturbed ground temperature is not constant along the depth of borehole. Since the test equipments use the ground temperature as reference, the undisturbed ground temperature profile is approximated to a line and then a correction factor, which is estimated from the approximation carried out in the ground temperature profile, is applied to determine the value of temperatures during the heating phase of DTRT.

Previously DTRTs, the borehole was characterized in detail. Thus the groundwater flow and its deviation from the vertical were determined. Since boreholes are often deviated from the vertical direction, BHE pipes do not extend to the desire depth. For this installation, the results from the deviation measurements can be found in section 2.1 Acuña (2010). Regarding groundwater, it is noticed that no significant flow does exist (0.4 l/min after decreasing ground water level). More details about how it was determined and its results can be found in Acuña (2010).

DTRT carried out in this thesis, consists of four test phases and it lasts around 160 hours. In the first phase, the undisturbed ground temperature was measured circulating no fluid during three days. Followed by second phase, in which a pre-circulation fluid without heating was carried out for 24 hours. Subsequently, in the third phase, a constant heat power (9kW) was injected for 48 hours. The data logged in this phase allows determining the value of the thermal resistance and the rock thermal conductivity along the BHE. Finally, in the fourth phase, the borehole recovery was observed measuring the temperature with no heating or fluid circulation during 24 hours. For estimating ground properties, data from the first and the third phases are accounting in this thesis.

As mentioned above, distributed temperature is measured along the borehole depth by optical fiber cables, which are installed on the groundwater as well as inside U-pipe. The internal fiber optic cable, placed inside the U-pipe, measures the secondary fluid temperature along the total length of the exchanger. On the other hand, the external fiber optic cable, which is instrumented between the BHE and the rock, measures the groundwater temperature along BHE depth. Since optical fiber cables measure the temperature as a function of the voltage difference, these optical fiber cables are connected with DTS equipment to read and interpret them as magnitude of temperature. In this thesis, the measurements are carried out by means of two different DTS equipments: Halo and Sentinel-DTS. Both are from Sensornet and the main difference between these both equipments is its spatial resolution along the cable. While Halo has a two meters spatial resolution, Sentinel-DTS has a one-meter resolution. The temperature measurements were carried out with an integrating time of 5 minutes and a measurement length interval of 10 m. However, in this thesis the

data has been analyzed with an integrating time of 25 minutes and with the same length interval.

Regarding DTS technology, it is important to bear in mind that the more acquisition data per unit time and per unit length in the borehole are read, the more accuracy is obtained in the results. However, the relation between the photon density and the boreholes length is inversely proportional. Meaning that for a large sectioned studied, the amount of information scan may be smaller. Hence, on account of the desired measurement quality in a fiber optic cable, the expected precisions for temperature, time and space must be compromised previously. For more details about this technology and its accuracy, it should be checked section 1.7 in Acuña (2010).

According to the undisturbed ground temperature, it was determined in each section before the borehole was taken into service during the first phase of DTRT, as mentioned beforehand. The results show that the increase in temperature is around 2.5 degrees in the first 10 meters. Moreover, the temperature gradient is negative between 10 and 110 meters in depth. Since then, the temperature gradient turns into positive until the end of the borehole. Thus, the temperature has a minimum at 110 meters in depth. More information about the procedure to determine the undisturbed temperature can be found in Acuña (2010). Next figure shows the undisturbed ground temperature measured along borehole depth.

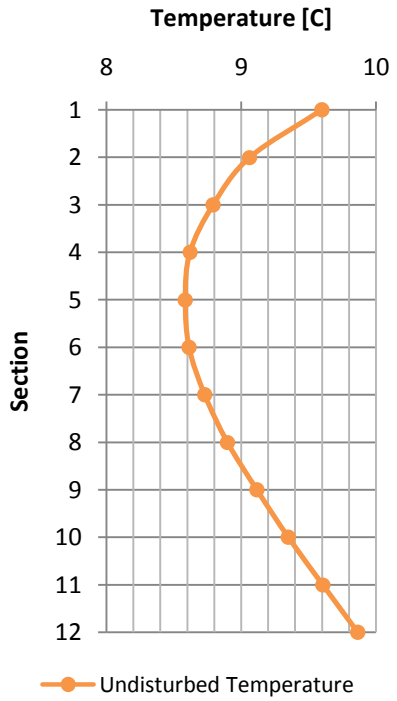

Figure 6. *Undisturbed Temperature profile.*

For determining thermal conductivity and thermal resistance along the borehole, the undisturbed temperature profile and the temperature data logged during the third phase in each section along the borehole are assessed using a linear approach based on the line-source theory; as explained in section 1.3.1.1. Since the heat power injected is required for calculations, this parameter is calculated as the fluid temperature difference (ΔT_s) between temperature at the inlet and at the outlet in each borehole section for every 25 minutes, as follows in equation (34):

$$q(t) = \rho \cdot V \cdot c_p \cdot \Delta T_s(t) \quad (34)$$

On account of the difficulty to maintain constant the power supply in the third phase, as illustrated in section 2.3. Acuña (2010), the data have been analyzed in three different cases of heat power supply:

- Case A, a constant heat power is assumed during the third phase of DTRT.
- Case B, it is considered a stepwisely constant heat power every 7.5 hours.
- Case C, the heat power injection is assumed as a stepwisely constant every 25 minutes during DTRT third phase.

It is important to bear in mind some considerations as regard as the heat power injected in the borehole during DTRT. Hence it should be noted that it is not taking into account the heat power injected during the first 15 hours of the DTRT heating phases for all the calculations carried out in this thesis. Moreover, the deviation in temperature due to the pre-circulation phase is neglected because of no heating fluid. Thus, the heat power in the carrier fluid due to the circulation pump is assumed negligible for all calculations of this thesis.

Subsequently, the methodology, which carried out in three different cases of heating power, is explained widely.

2.1. Case A: Constant heat power

The first case studied – case A- assumes a constant heat power during the third phase of DTRT test. Thus the injected heat power is calculated as average of the heat flow injected during the thermal response test.

Firstly, the measured temperature is plotted against natural logarithm of time. As aforementioned, the slope of the curve is related to thermal conductivity according to equation (12); therefore, considering the inclination of the line and taking q as average of the injected heat flow in DTRT, the thermal conductivity is calculated in each section.

The next step is R_b calculation. This parameter is calculated using equation (14), being $T_f(t)$ the temperature measured every 25 minutes along the third phase test and q is the mean value of the heat flow injected during this phase. As a result, R_b is estimated for every pair of $T_f(t)$ and t using the value of λ, which is determined previously . To analyze the results, it is also obtain the average of the thermal resistance value in each section. Subsequently, the flow chart is shown in *Figure 6*.

To evaluate how the estimated parameters describe the real situation in BHE, the temperature in each borehole section is calculated by the estimated thermal parameters and its calculated temperature profile is compared with the profile of temperature measurements. Since the heat injected power q is known for every 25 minutes during 3rd DTRT phase, the calculated temperature is estimated using equation (19), in which the thermal conductivity and the thermal resistance take the value determined as explained in this section. Notice that τ_N is calculated for every 25 minutes in equation (19).

Subsequently, the comparison between the measured and calculated temperature profiles is established by calculating the difference between the calculated temperature and the measured temperature in each interval of time (25 minutes), as expressed in equation (35):

$$Difference\ T_{fcalc.} - T_{fmeas.}(C) = T_{fcalculated}(t) - T_{fmeasured}(t) \quad (35)$$

To assess the uncertainties due to assuming a constant heat power during the heating phase, the mean value of these differences and its standard deviation is determined. The mean value of ($T_{fcalculated}$ – $T_{fmeasured}$) and its deviation from its mean value, which is expressed as its mean value ± its standard deviation, is plotted in a graph with together the results of the other cases of heat power supply –case B and C- .

Next figure illustrates the flow chart of calculations carried out in case A.

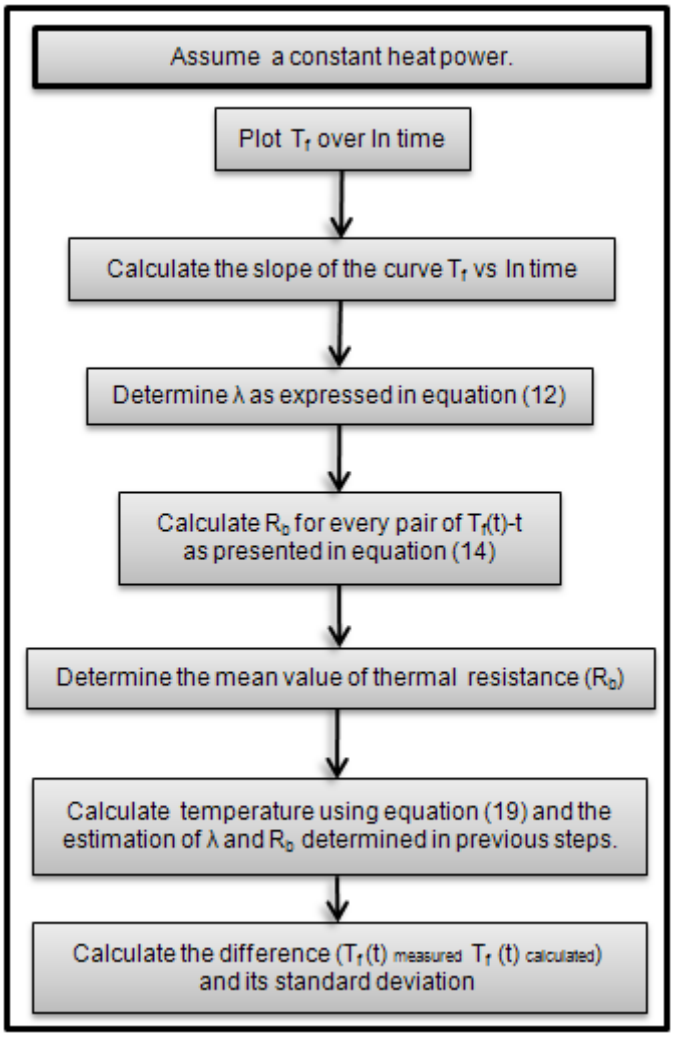

Figure 7. *Flow chart for a constant heat injection during DTRT.*

2.2. Case B: 7.5 hours stepwisely constant heat power.

In case B, it is assumed every 7.5 hours stepwisely constant heat power. In this case, six heat pulse of 7.5 hours and one more step pulse of 75 minutes, which belongs to the last period of the test, are considered for calculations.

Firstly, assuming the above mentioned about heat power steps, the dimensionless parameter $\tau_N(t)$ is calculated using equation (18). Then, the temperature measured is plotted against the value of $\tau_N(t)$, which has been calculated previously. As mentioned earlier, the slope of this curve is connected with thermal conductivity, as expressed in equation (20); therefore, the thermal conductivity is estimated.

Subsequently, R_b is determined as expressed equation (21). For this calculation, q_N is the average of heat injected in each 7.5 hours stepwisely constant heat power that has

been assumed in this case. Since R_b is determined for every pair of T_f and $\tau_N(t)$, the mean value is then calculated for the borehole section.

In the same way as case A, the temperature is calculated for the heat power injected every 25 minutes, as expressed in equation (19). In equation (19), λ and R_b take the values estimating in this case B and τ_N is defined for every 25 minutes stepwise change in heat power. Lastly the calculated temperature is compared with the measured temperature by calculating the difference between both temperatures in every interval of time - 25 minutes -, as expressed in equation (35). And its standard deviation from the average difference in temperature is also determined. *Figure 7* shows a flow chart for the calculations carried out in this case.

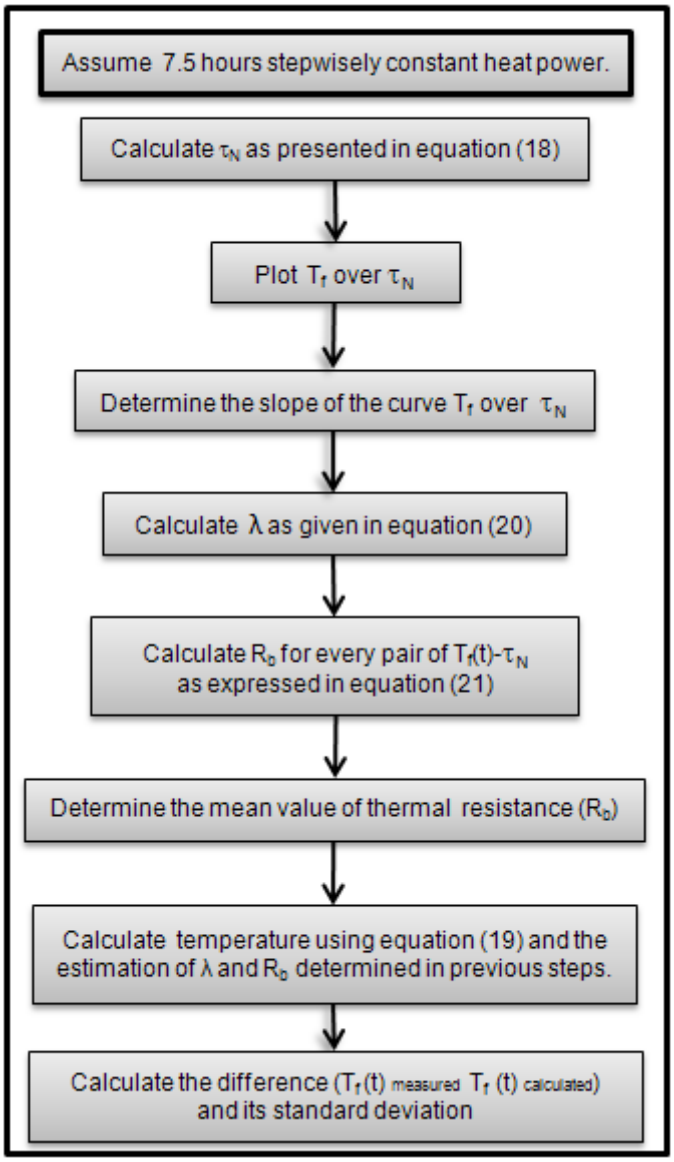

Figure 8. *Flow chart for a heat pulse injection of 7.5 hours during TRT.*

2.3. Case C: 25 minutes stepwisely constant heat power.

In case C, a 25 minutes stepwisely constant heat power is assumed during the third phase of DTRT test. Firstly, $\tau_N(t)$ is calculated according to the heat step assumed in this case – 25 minutes -. Subsequently, the temperature measurements are plotted against $\tau_N(t)$ and its slope allows calculating λ, as expressed in equation (21). Then, for every pair of T_f and $\tau_N(t)$ a value of thermal resistance is determined by means of equation (21). Moreover, the mean value of R_b is calculated in each section. In equation (21), q_N is the heat injected in each 25-minute interval during DTRT.

Similarly above cases, the temperature is evaluated for the heat power injected every 25 minutes as expressed in equation (19). Besides, it is done using the values of λ *and* R_b determined in this case. For evaluating the values of the estimated parameter, the calculated temperature is compared with the measured temperature by calculating the difference between both, as expressed in equation (35). *Figure 9* illustrates the flow chart of calculation in case C.

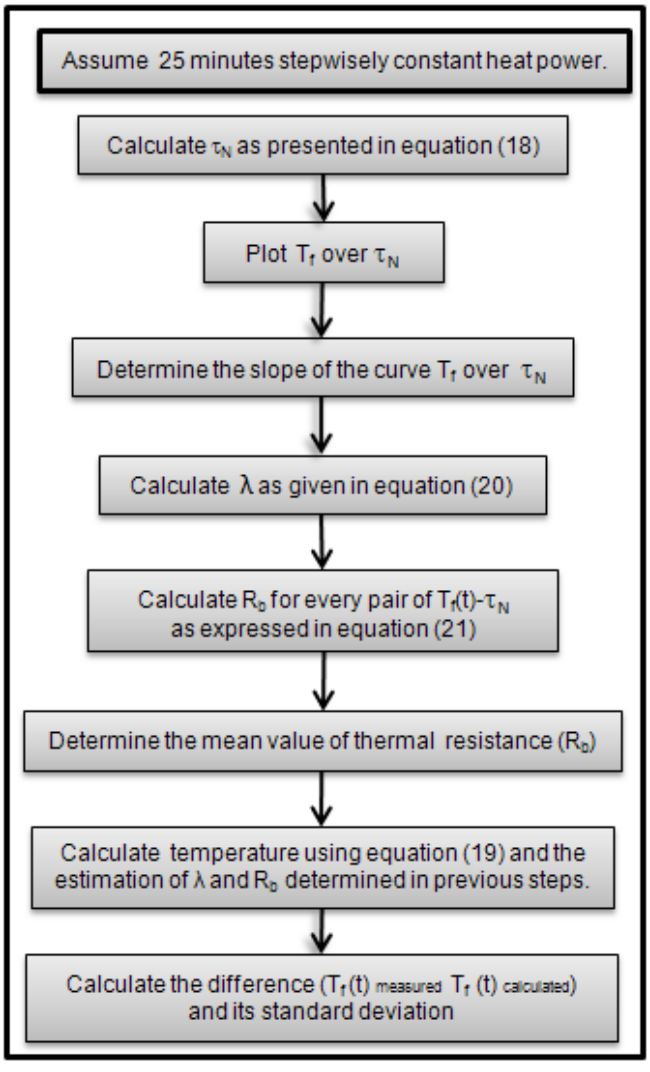

Figure 9. *Flow chart for a heat pulse injection of 25 minutes during DTRT.*

The data from HALO equipment are evaluated by this methodology in each case of heat supply. As well as, these calculations have been applied to each 20 m section along the borehole.

The data from SENTINEL DTS-equipment is only evaluated by the methodology described in case A, in which is assumed a constant heat power supply during the whole heating phase. It is applied in each 20 meters section for the data from SENTINEL equipment. Sentinel data have not been analyzed by heat power steps because the heat power injected between two measurements consecutive differs highly and the results present anomalous values of the estimates. In *Figure 10* is shown the heat power input measured by Halo and Sentinel DTS equipment together with the difference between both in section 5. These kind of heat power variations happen in all section measured by Sentinel DTS-equipment.

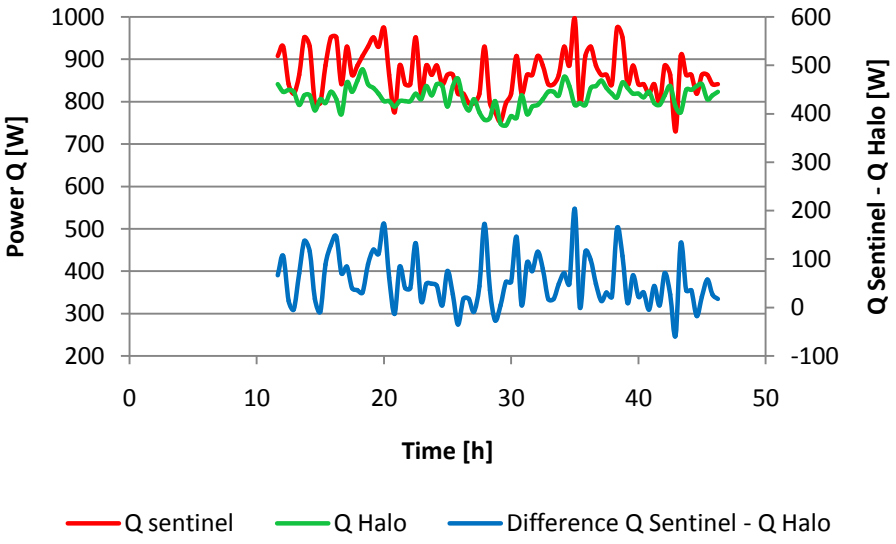

Figure 10. *Heat power input measured by Halo and Sentinel DTS-equipment in section 5.*

Notice that Sentinel data are only analyzed during the last thirty hours of the heating phase. The effects from the first 11.5 hours are neglected.

Thus the thermal conductivity and thermal resistance are determined in three different cases of heat power injection along the borehole sections from HALO measurements. By SENTINEL data, the thermal conductivity and thermal resistance are estimated in each borehole section assuming a constant heat power supply.

Moreover, the results of this thesis from Halo data, which are analyzed by assuming a constant heat power, are compared with the results obtained from Sentinel data and the estimates of Integral method from Acuña (2010) in each 20 meter borehole section. Besides, the results of Halo data in each case of heat supply – constant and by steps- are compared with the results of Integral Method from Acuña (2010), which were

evaluated as the line source model presented by Ingersoll - equation (7)-. For further information, these calculations are described in detail in Acuña (2010).*Figure 11* illustrates the outline of the analysis carried out in this thesis.

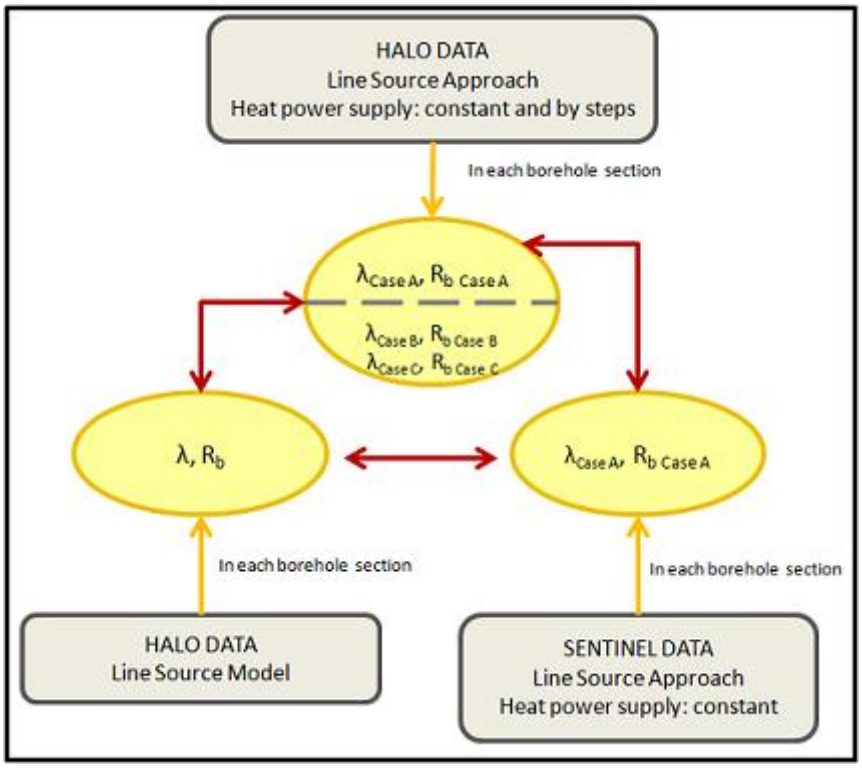

Figure 11. *Flow chart of the analysis carried out in this thesis.*

3. Results and Discussion.

In this chapter, the results from measurements of Halo and Sentinel DTS-equipment are compiled.

Firstly, the results from data of Halo equipment, which is the device with lower resolution, are shown in each 20 meter section of the borehole. The first figure present the profiles of thermal resistance together with the heat power supply assumed in each case. It is done against time. Next figure presents, the mean value of the thermal resistance and its variation according to its standard deviation (mean value ± standard deviation). Furthermore, the profiles of the measured and calculated temperature, which are calculated in each heat power supply, are presented together in other figure. The last figure shows the average value of the differences between $T_{fcalculated}$ and $T_{fmeasured}$ in each case of heat power supply. Notice that the whiskers in this figure show how much dispersion there is from the mean value of ($T_{fcalculated}$–$T_{fmeasured}$), which is calculated as its mean value ± its standard deviation. These four graphics results are presented in each borehole section. After evaluating each borehole section, the vertical distribution along the borehole depth of the thermal conductivity and the thermal resistance – calculating according to its mean value in each borehole section- are compiled in *Figure 62* in each case of heat power supply.

Next point in chapter, section 3.2., shows the results from data of Sentinel equipment in each borehole section. The first figure presents the thermal resistance profile together with the heat power supply and the heat power assumed in calculations. The second figure presents the mean value of thermal resistance and its variation, expressed as its mean value ± its standard deviation together with the results of Halo for a constant heat power. Then, the measured and calculated temperatures of Halo and Sentinel data are compared in other figure against 3rd phase DTRT time. The last figure presents the average difference between these both temperature profiles and its variation for Halo and Sentinel cases -constant heat power-, respectively. All these four graphics results are presented in each borehole section. Finally, the profiles of thermal conductivity and thermal resistance, which is determined by its mean value, are presented in *Figure 113*.

Subsequently, the results from Halo are compared with results of the Integral Method from Acuña (2010). In the same way, the results from Sentinel are compared with results from Acuña (2010). Finally, in section 3.3.3, the results from Halo and the result from Sentinel assuming a constant heat power supply are compared with the results obtained in Acuña (2010). Notice that the results from Acuña (2010) have been termed "Integral Method".

3.1. Results from Halo equipment.

- *SECTION 1*

In Section 1, the thermal conductivity estimated is 3.42 [W/Km] in case A, 2.76 [W/Km] in case B and 2.86 [W/Km] in case C. *Figure 12* shows the profile thermal resistance in each case of heat power studied during the 3rd DTRT phase. It can be observed the influence of the heat power supply in the estimation of the thermal resistance. It can be observed that case B presents the lowest profile thermal resistance.

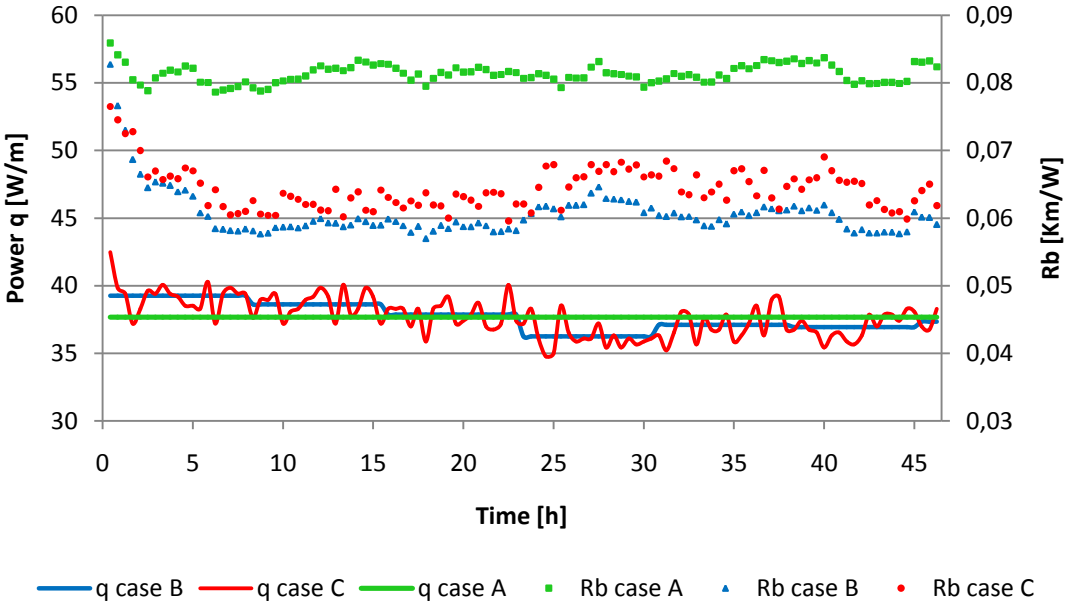

Figure 12. *Section 1: Thermal resistance profiles according to three different cases of power supplied.*

Thus, the profile of thermal resistance in case C presents the highest variations. *Figure 13* shows the mean value of thermal resistance in each case and its variation, which has been calculated as above explained.

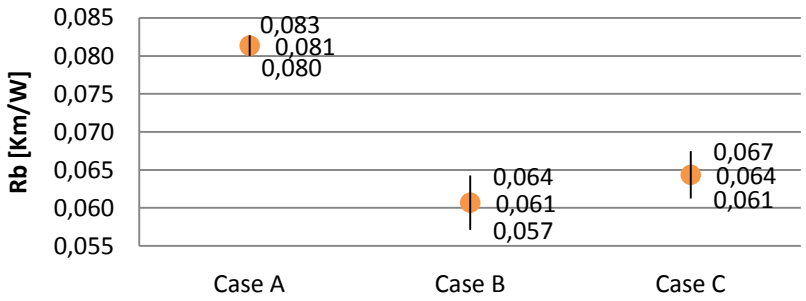

Figure 13. *Section 1: Average thermal resistance and its variation in each case of power supplied.*

Figure 14 presents the profile of the temperature measured during the DTRT 3rd phase and the profile of the temperatures calculated in each case of heat power assumed. It can be observe that the profile from case B and C present better fit than case A profile during the whole phase. Besides, the temperature describing by case B is very close to the profile described in case C.

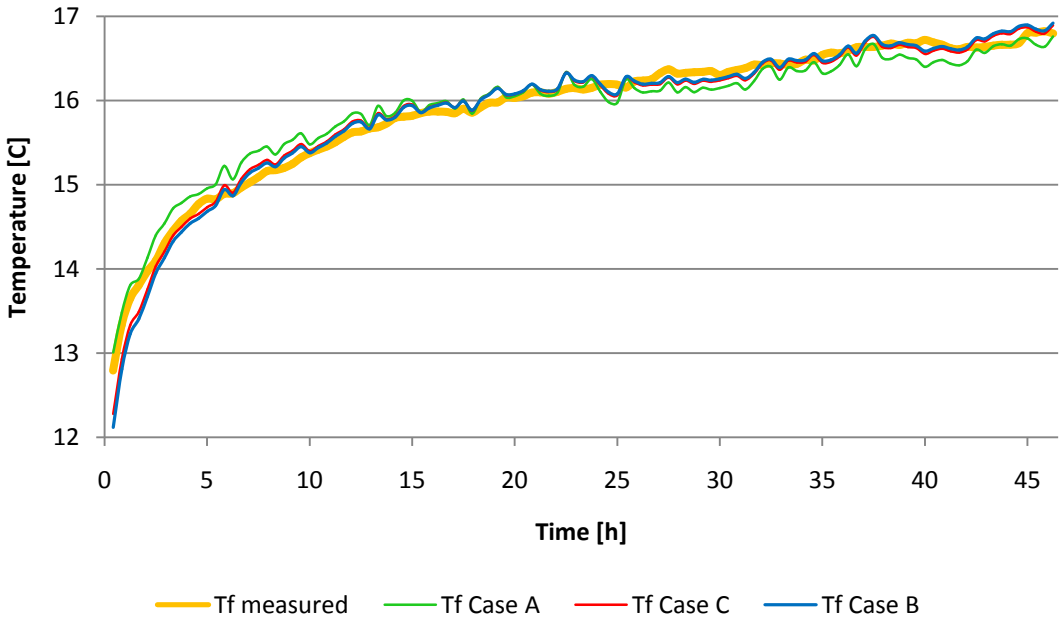

Figure 14. *Section 1: Temperatures measured and temperatures calculated in each power supplied case.*

Next figure reflects the differences showed in *Figure 15*. In section 1, case A presents the highest value of the average of ($T_{fcalculated}$–$T_{fmeasured}$) while case B and C present similar values, which are close to zero. According to its dispersion, case A also presents the highest value.

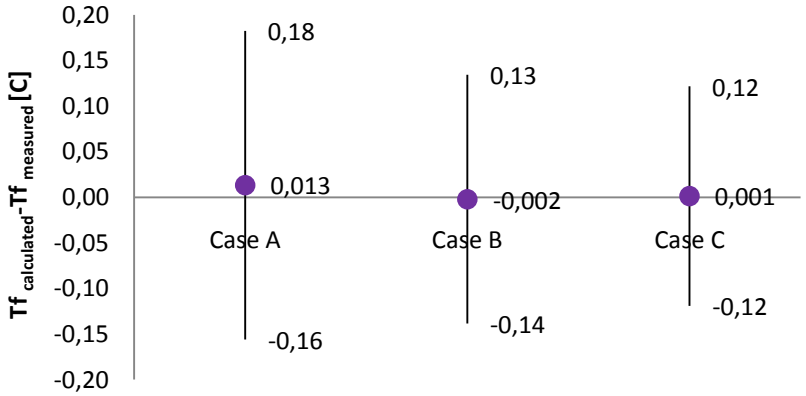

Figure 15. *Section 1: Average of ($Tf_{calculated}$- $Tf_{measured}$) and its variation in each power supplied case.*

Moreover, in this section it is included the results obtained if the temperature is calculated by means of the thermal parameters assuming a constant heat power and the mean value of the heat power injected during the interval of time considered. It can be observed that the profile of measured temperature fits greater than the profile calculated assuming 25 minutes stepwisely heat power.

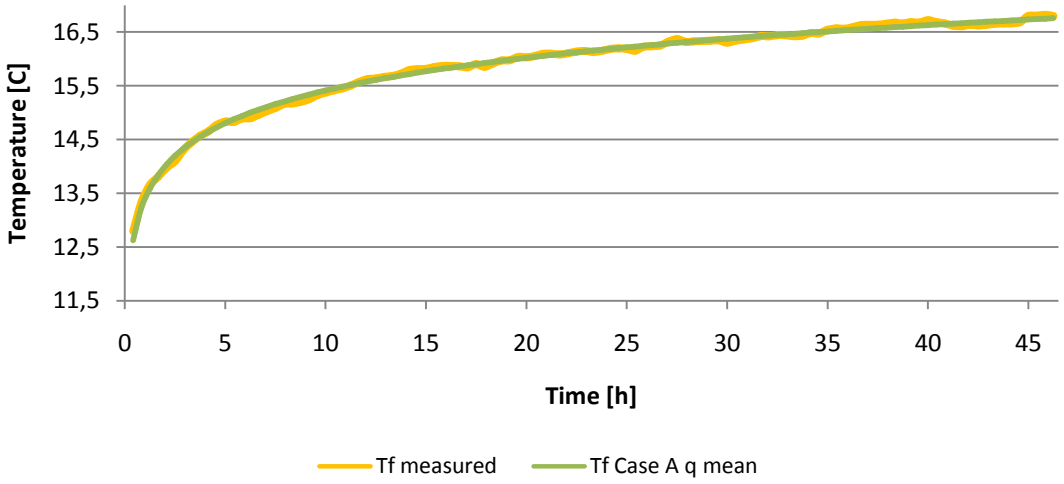

Figure 16. *Section 1: $Tf_{measured}$ and $Tf_{calculated,,}$ which is calculated using taking the thermal parameters from case A and assuming a constant heat power for the whole analysis.*

In next figure, it is shown the temperature calculated using the estimates from case B and considering the power injected as 7.5 stepwisely heat power during the test. The measured temperature fit better than the profile of calculated temperature assuming 25 minutes stepwisely heat power. However, this fit is better when the heat power is assumed constant during the whole test.

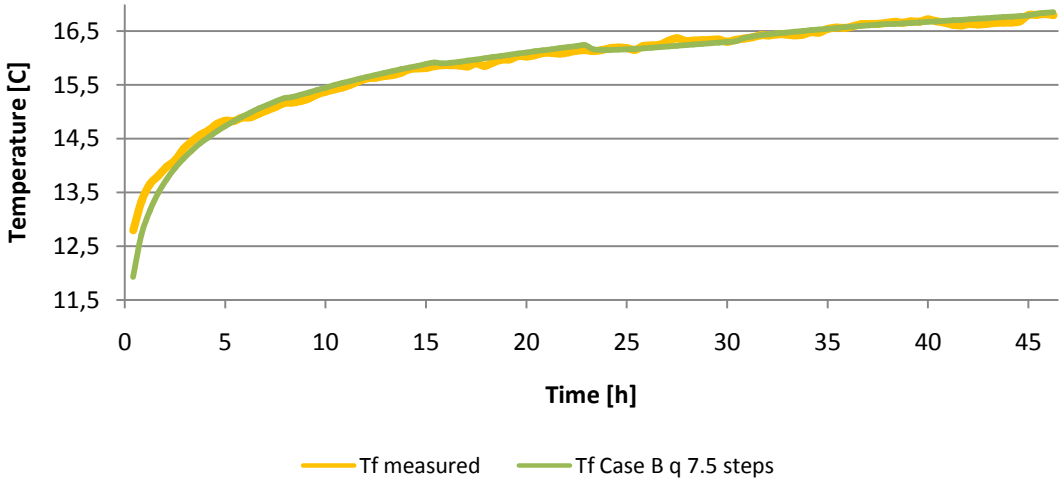

Figure 17. *Section 1: $Tf_{measured}$ and $Tf_{calculated,,}$ which is calculated using taking the thermal parameters from case B and assuming 7.5 hours stepwisely heat power during the analysis.*

- ***SECTION 2***

In Section 2, the thermal conductivity estimated is 3.47 [W/Km] in case A, 3.08 [W/Km] in case B and 3.33 [W/Km] in case C. *Figure 18* reflects the effect of heat power supply on the estimation of the thermal resistance. Thus, the less constant heat power is assumed, the more variation is attributed to thermal resistance. During the whole test, case B presents the lowest values of thermal resistance profile.

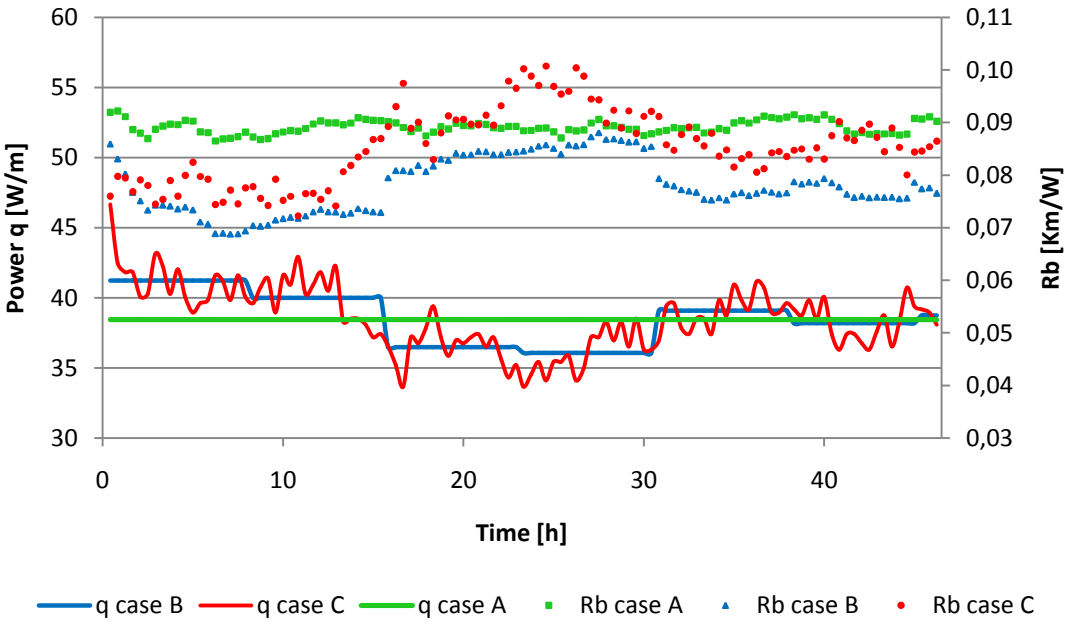

Figure 18. *Section 2: Thermal resistance profiles according to three different cases of power supplied.*

In section 2, case B presents the lowest value of the average thermal resistance, showing accordance with *Figure 19*. And Case C presents the highest variation in thermal resistance.

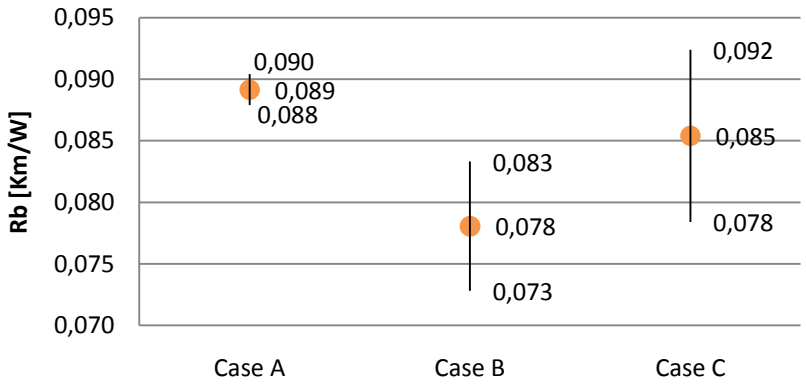

Figure 19. *Section 2: Average thermal resistance and its variation in each case of power supplied.*

Figure 20 shows the profile of the temperatures measured and calculated in each case. At the beginning, case B and case C fit better to the temperature measurements; however, three cases have similar behavioral profile since fifteen DTRT hours. The most significant differences show up in the interval 5 hours and 25 hours is probably attributed to input power variations, as it shown in *Figure 18*.

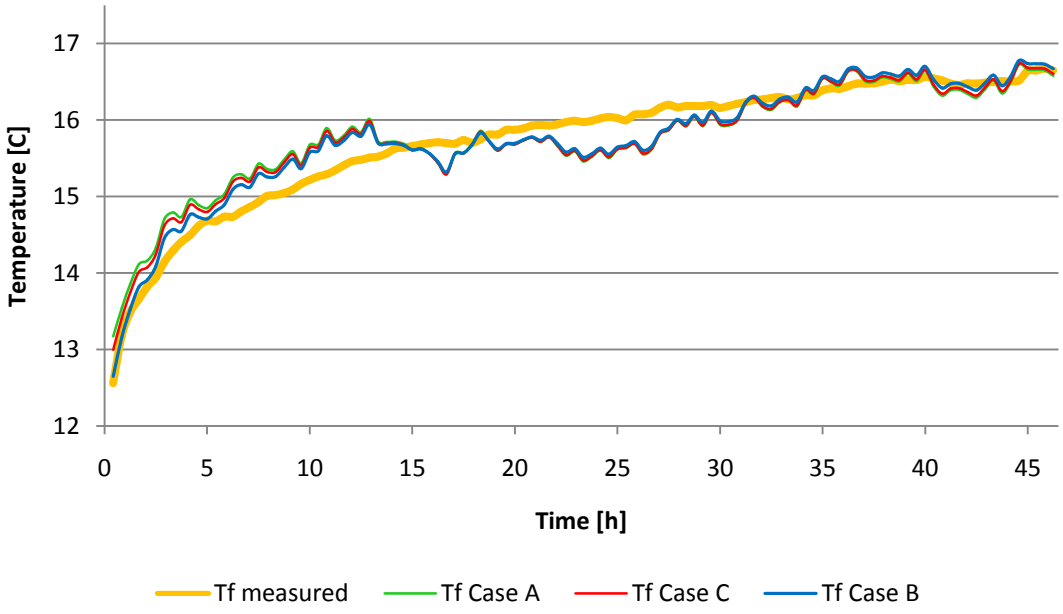

Figure 20. *Section 2: Temperatures measured and temperatures calculated in each power supplied case.*

Calculating the difference between $T_{fcalculated}$ and $T_{fmeasured}$, case B presents the smallest average difference and dispersion, which is only about 0.01 and 0.13, respectively. In contrary, case A shows the highest value of both deviation factors.

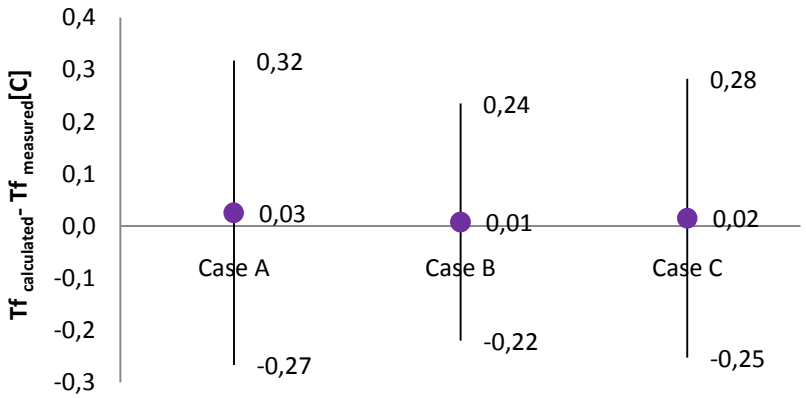

Figure 21. *Section 2: Average of ($Tf_{calculated}$- $Tf_{measured}$) and its variation in each power supplied case.*

- ***SECTION 3***

In Section 3, the thermal conductivity estimated is 3.79 [W/Km] in case A, 2.95[W/Km] in case B and 3.18 [W/Km] in case C. It can be observed the influence of the input power variations on the estimated thermal resistance, being higher in case C. This fact shows a good accordance with the input heat variations.

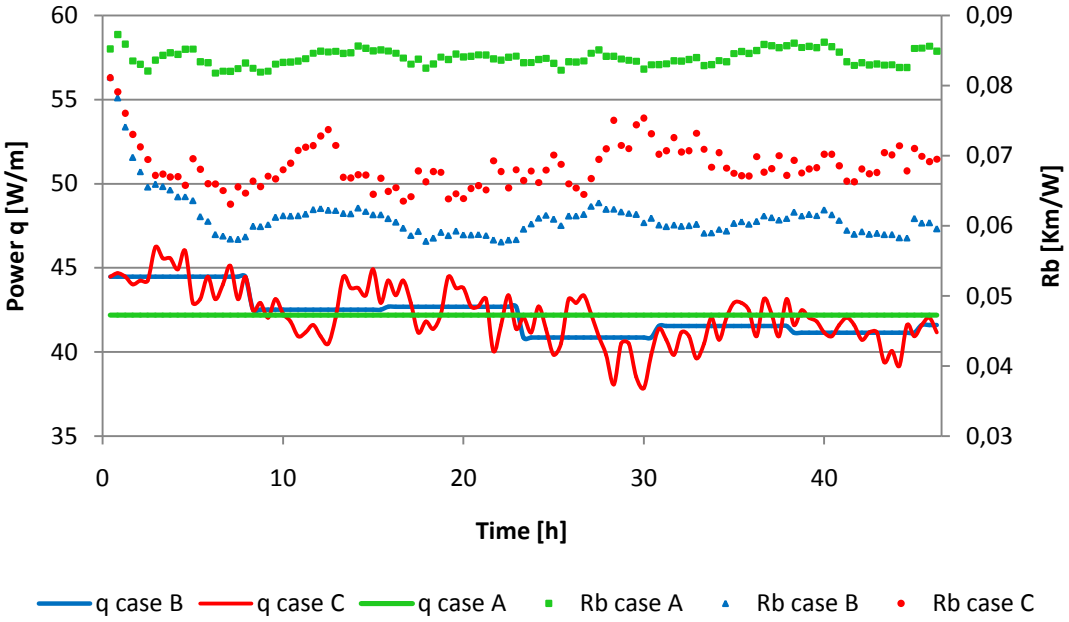

Figure 22. *Section 3: Thermal resistance profiles according to three different cases of power supplied.*

Averaging thermal resistance for the cases studied, case B presents the lowest value of the average thermal resistance, as it can be seen in *Figure 23*. According to thermal resistance deviation, case A barely varies from its mean value. Furthermore, the thermal resistance variation respect to its mean value in case B and C is only about 0,004 [Km/W].

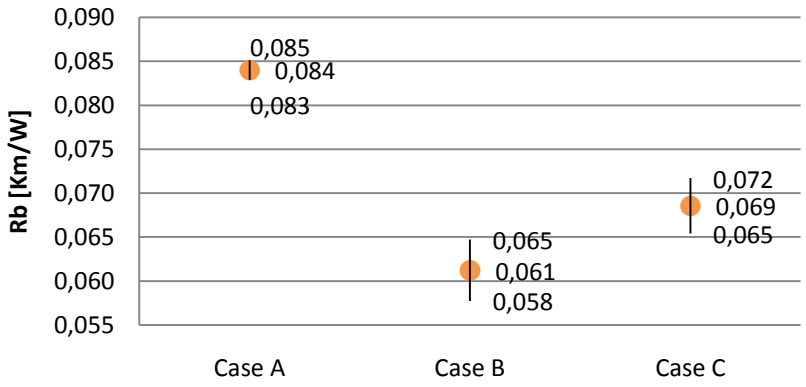

Figure 23. *Section 3: Average thermal resistance and its variation in each case of power supplied.*

In section 3, the profile of the temperatures describing by case B and C fitted better to temperature measurements for the whole test. However, Case A presents a good fit during the period between 15 and 25 DTRT hours, which the heat power shows less variations in its supply, as can be observed in *Figure 22*.

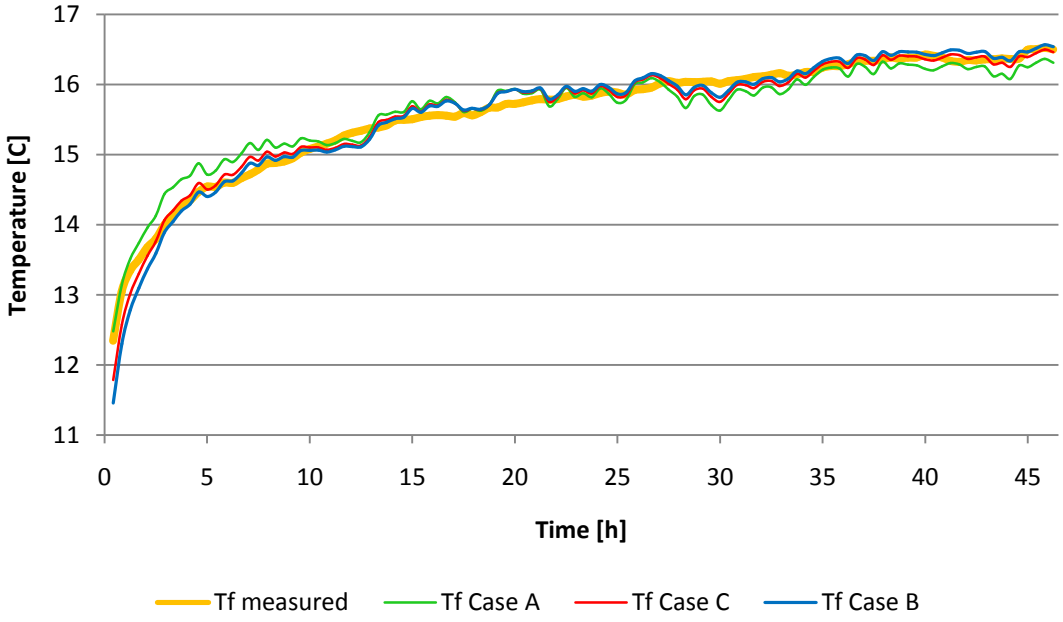

Figure 24. *Section 3: Temperatures measured and temperatures calculated in each power supplied case.*

In accordance with *Figure 24*, case A presents the highest difference between measured and calculated temperature, it is about 0,018 on average. Furthermore, this case also shows the most significant deviations. In contrast, case B presents the lowest value of average ($T_{fcalculated}$-$T_{fmeasured}$) and, its variation is very close to case C.

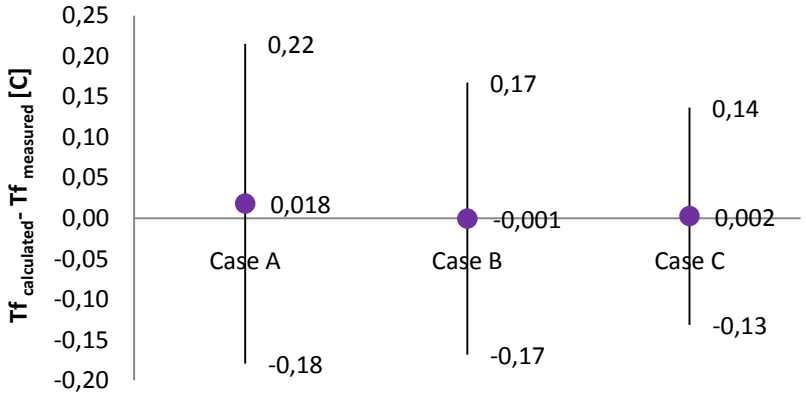

Figure 25. *Section 3: Average of ($Tf_{calculated}$- $Tf_{measured}$) and its variation in each power supplied case.*

- ***SECTION 4***

In Section 4, the thermal conductivity estimated is 3.65 [W/Km] in case A, 3.08 [W/Km] in case B and 3.09 [W/Km] in case C. In *Figure 26*, it can be observed that case B and C present a similar profile of thermal resistance. They are lower than profile for case A. Moreover, it can be observed the relation of heat power to thermal resistance, being inversely proportional.

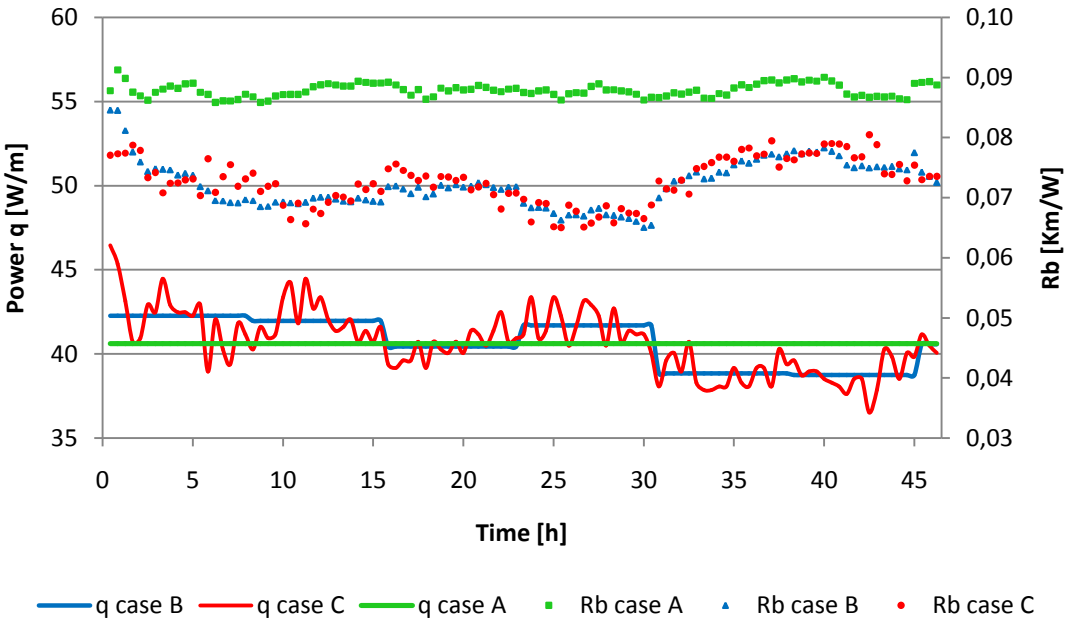

Figure 26. *Section4: Thermal resistance profiles according to three different cases of power supplied.*

Figure 27 shows that the thermal resistance presents a very close value in case B and C, and their variations are very similar too. Comparing with case A, it is distinguished a difference about 0,015 [Km/W]. Besides, the thermal resistance deviation is lower in case A, in accordance to heat power variation.

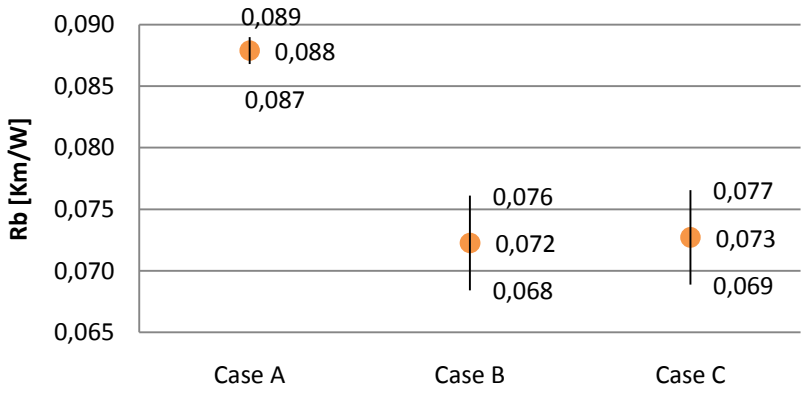

Figure 27. *Section 4: Average thermal resistance and its variation in each case of power supplied.*

Figure 28 shows the profile of temperatures measured and calculated in section 4. It can be observed that case B and C presents a better fit than case A for most time. Case A shows a good fit during the period of 15 and 30 hours.

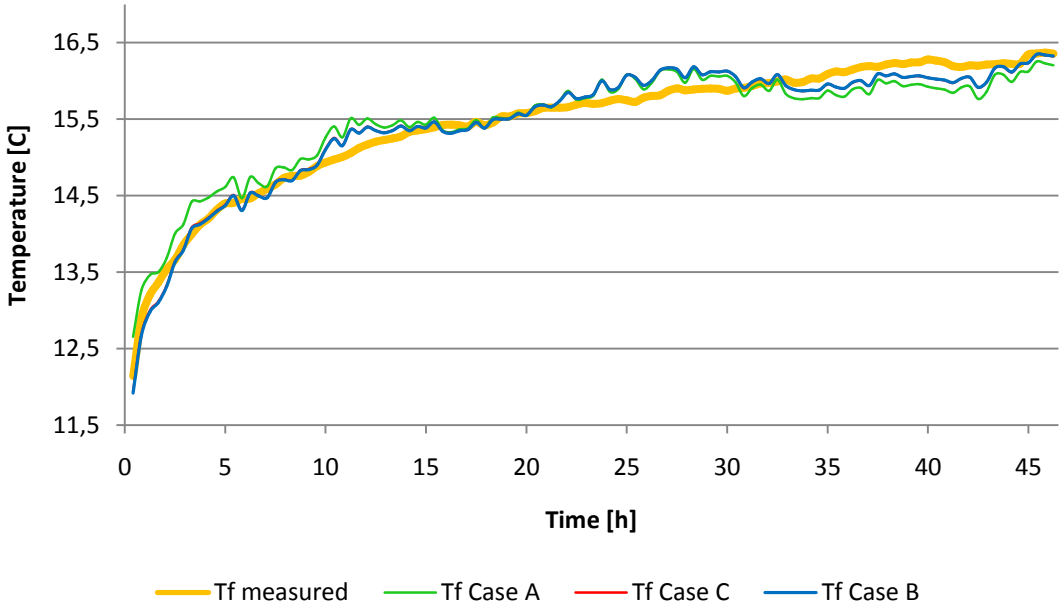

Figure 28. *Section 4: Temperatures measured and temperatures calculated in each power supplied case.*

As mentioned above, case A presents the highest difference between $T_{fmeasured}$ and $T_{fcalculated}$, on average. Its dispersion is also bigger than rest of cases, which is about 0.22 [C]. On the other hand, case B and C presents lower difference respect to the measured temperature. Besides, the dispersion of ($T_{fmeasured}$-$T_{fcalculated}$) is similar in both cases and it is around 0,15 [C].

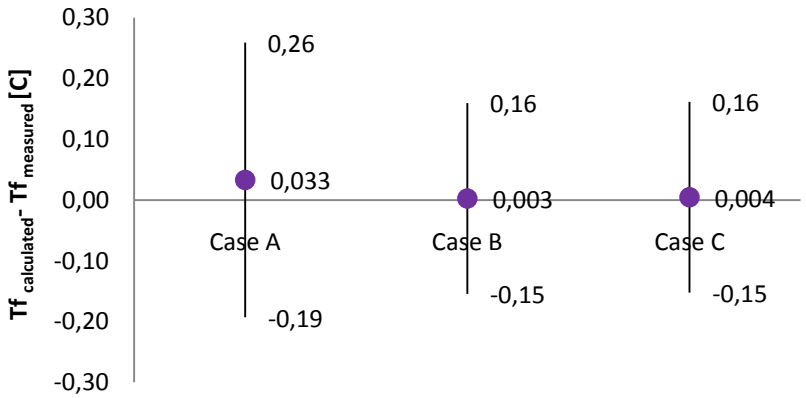

Figure 29. *Section 4: Average of ($Tf_{calculated}$- $Tf_{measured}$) and its variation in each power supplied case.*

- ***SECTION 5***

In Section 5, the thermal conductivity estimated is 3.66 [W/Km] in case A, 3,25 [W/Km] in case B and 3,34 [W/Km] in case C. Case C presents the most irregular profile of thermal resistance, which is attributed to input power variations. Furthermore, it can be observed that the values of case B profile are the lowest, whereas case A presents the highest ones.

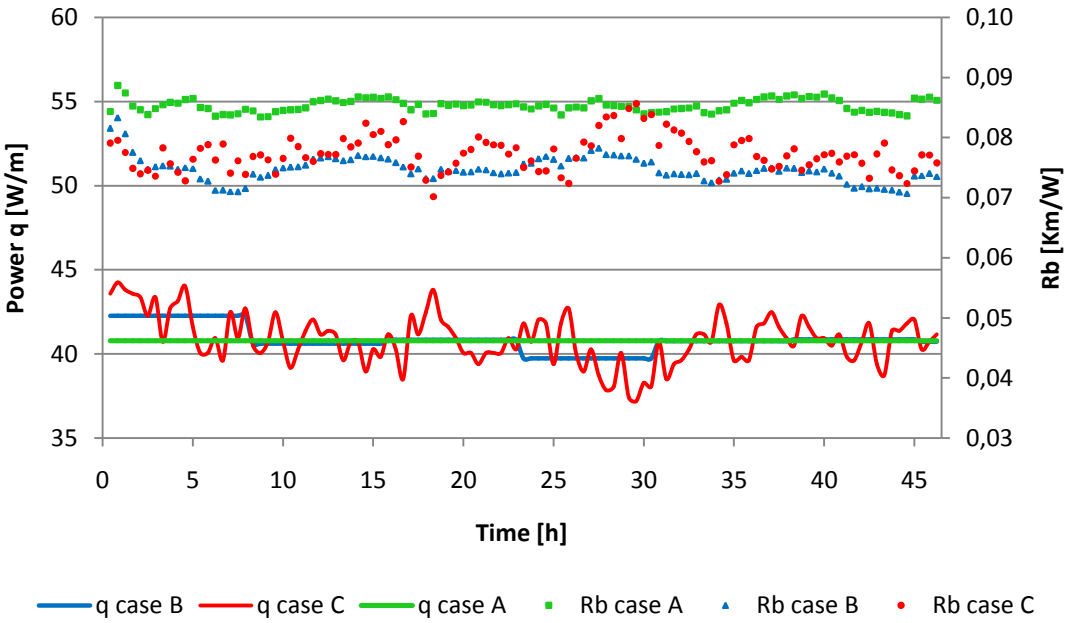

Figure 30. *Section 5: Thermal resistance profiles according to three different cases of power supplied.*

In accordance with *Figure 30,* case A presents the highest value of the estimated thermal resistance on average. For case B and C, this value is very close. Regarding thermal resistance variation on its mean value, case C shows the highest ones due to heat power variations.

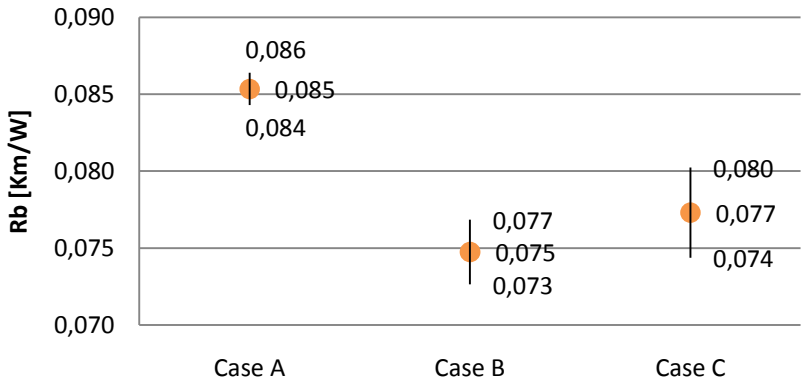

Figure 31. *Section 5: Averages thermal resistance and its variation in each case of power supplied.*

The profile of calculated temperatures during DTRT, shows that case B and C present a better fit with the measured temperature profile. In case A, the most significant deviations show up at the beginning of the test.

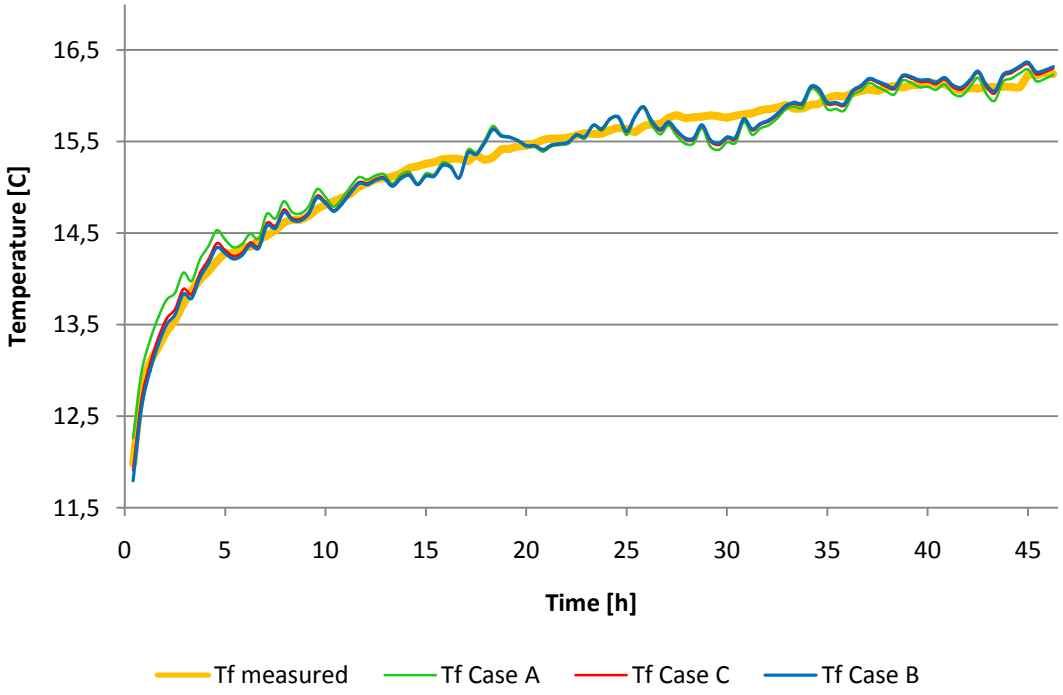

Figure 32. *Section 5: Temperatures measured and temperatures calculated in each power supplied case.*

Averaging ($T_{fmeasured}$-$T_{fcalculated}$), case B presents the less difference between the profile of measured temperature and its calculated. However, the greatest difference shows up in case A, which is about 0.01 [C] superior than the average in case B. Case C presents values in the same range as case B.

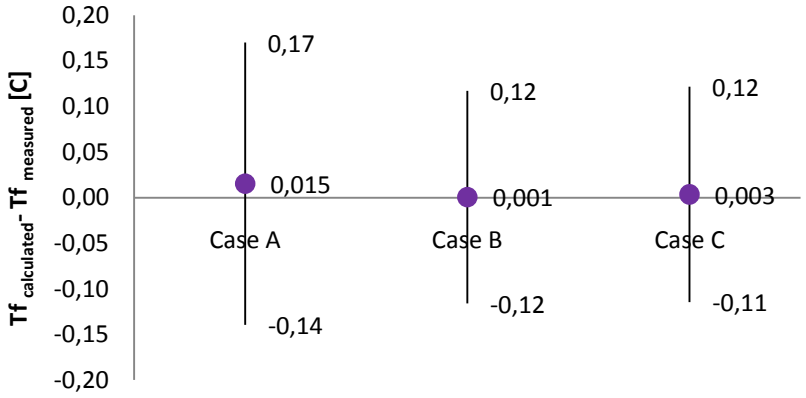

Figure 33. *Section 5: Average of ($Tf_{calculated}$- $Tf_{measured}$) and its variation in each power supplied case.*

- ***SECTION 6***

In Section 6, the thermal conductivity estimated is 3.53 [W/Km] in case A, 3.31 [W/Km] in case B and 3.55 [W/Km] in case C. The thermal resistance profiles are very close in every cases of heat power supplied. As above sections, case A trends to a constant line, whereas case C profile presents high variations. The Case B profile shows small variations distributing by steps.

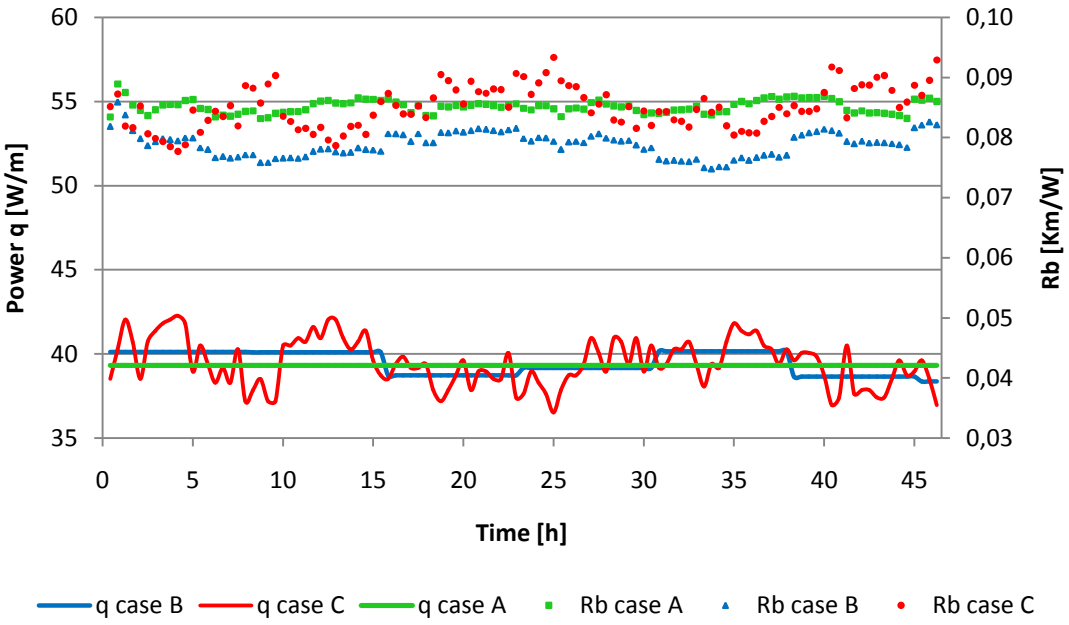

Figure 34. *Section 6: Thermal resistance profiles according to three different cases of power supplied.*

In this section, case B presents the smallest value of the average thermal resistance, whereas case A and C shows the same value on average. According to thermal resistance dispersion, case C presents the highest ones as it can be observed on the whiskers length in *Figure 35*.

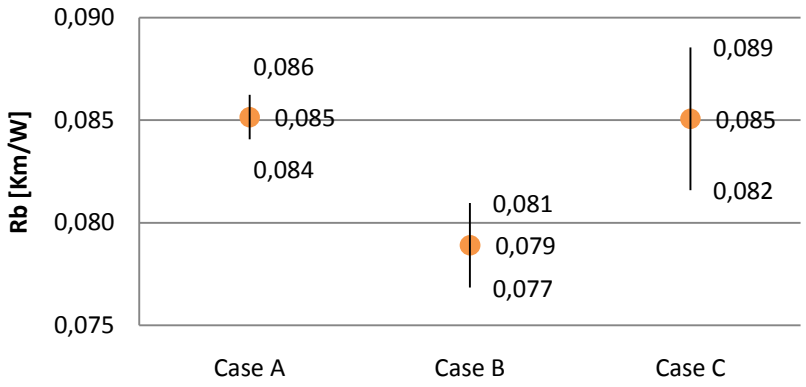

Figure 35. *Section 6: Averages thermal resistance and its variation in each case of power supplied.*

Figure 36 shows that the calculated temperature profile in case B presents the best fit during the whole DTRT. Since the parameters estimation is very close, case A and C present a similar temperature profile.

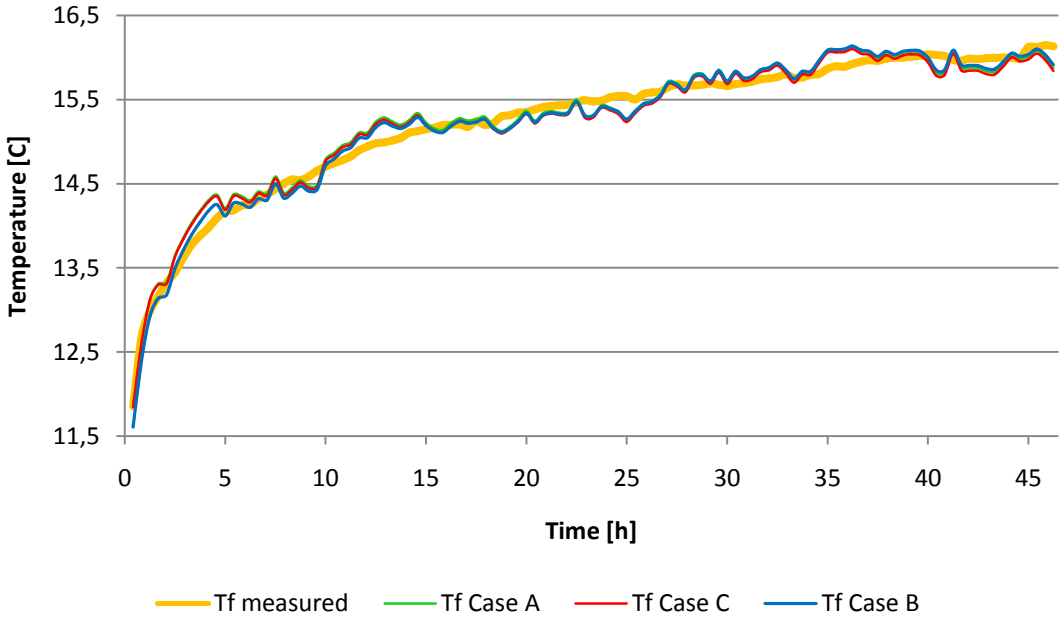

Figure 36. *Section 6: Temperatures measured and temperatures calculated in each power supplied case.*

Although case A and C presents a close profile temperatures, next figure shows that case C fits better than case A, on average. Furthermore, the results show that case B presents the less difference between the measured temperatures on average. Three cases present the same value of dispersion of ($T_{fmeasured}$-$T_{fcalculated}$).

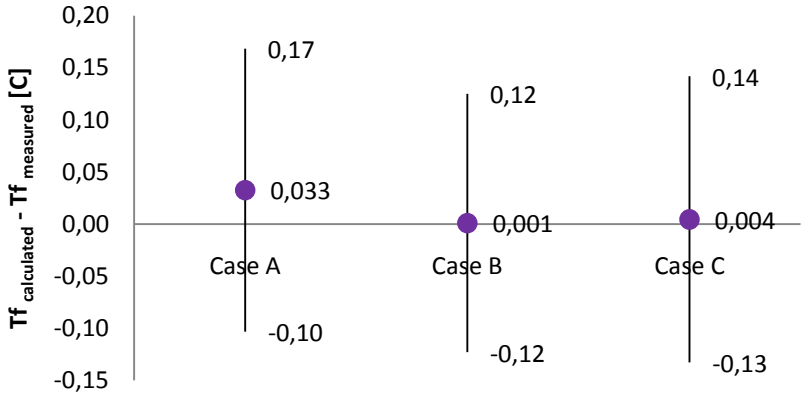

Figure 37. *Section 6: Average of ($Tf_{calculated}$- $Tf_{measured}$) and its variation in each power supplied case.*

- ***SECTION 7***

In Section 7, the thermal conductivity estimated is 3.78 [W/Km] in case A, 3.48 [W/Km] in case B and 3.76 [W/Km] in case C. Three cases present very close profiles; the main difference is the profile variation. Thus, case C presents the most significant variations along the profile according to input power variations.

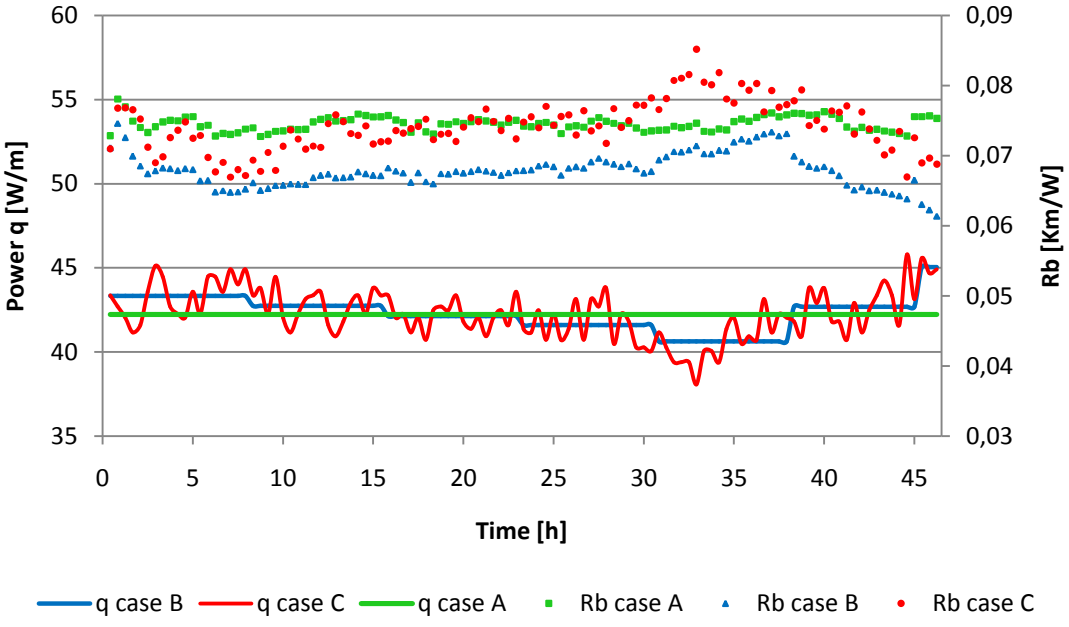

Figure 38. *Section 7: Thermal resistance profiles according to three different cases of power supplied.*

In the same way as section 6, section 7 presents the smallest value of the average thermal resistance for case B. In accordance with *Figure 38*, case A and C shows nearly the same value on average for the thermal resistance. However, case C presents the highest variation due to variations of heat power.

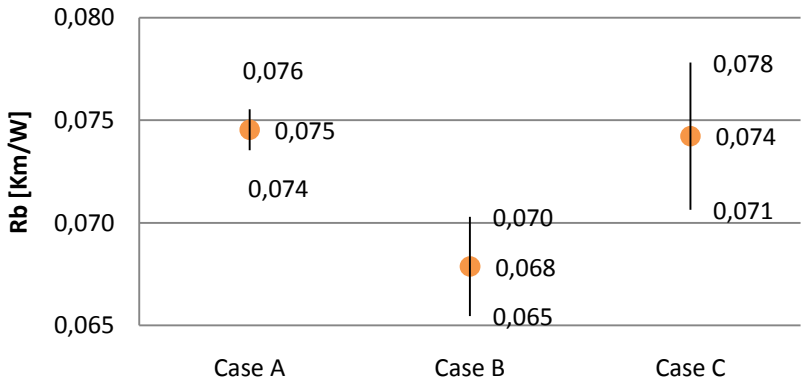

Figure 39. *Section 7: Averages thermal resistance and its variation in each case of power supplied.*

Figure 40 shows that there are not relevant differences between the profiles describing by three cases. However, it can be observed that case B trends to fit better than the other two cases during the most part of the test.

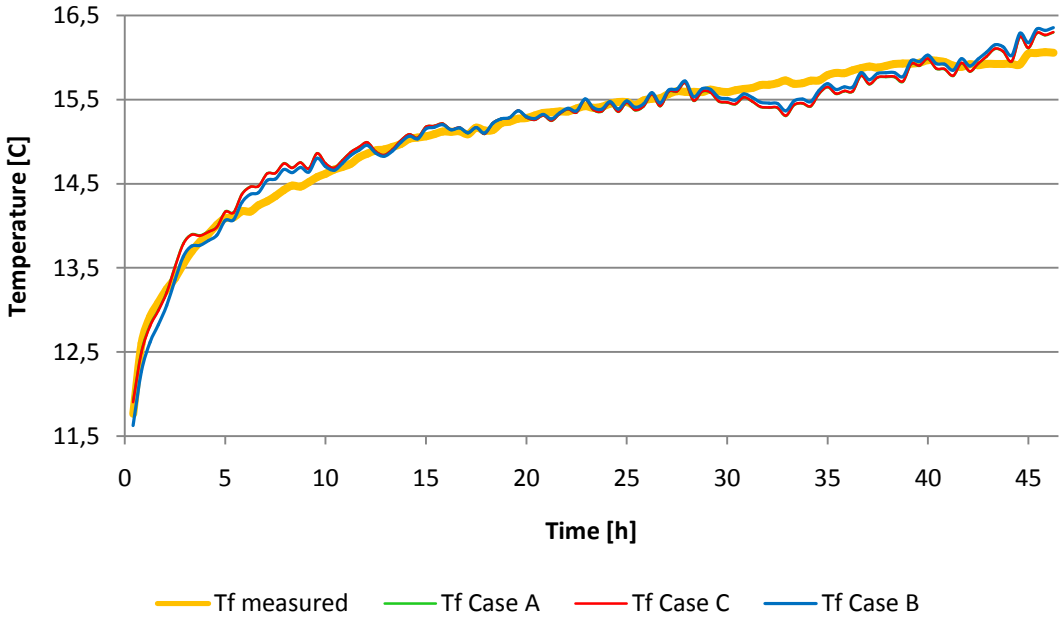

Figure 40. *Section 7: Temperatures measured and temperatures calculated in each power supplied case.*

Averaging the difference between the calculated and measured temperatures, it is nearly zero in all cases; however case B presents the less value, as illustrated in *Figure 41*.Although case A and C also present a close value to zero, they are higher than the one for case B. The dispersion of this difference in temperatures is similar in three cases.

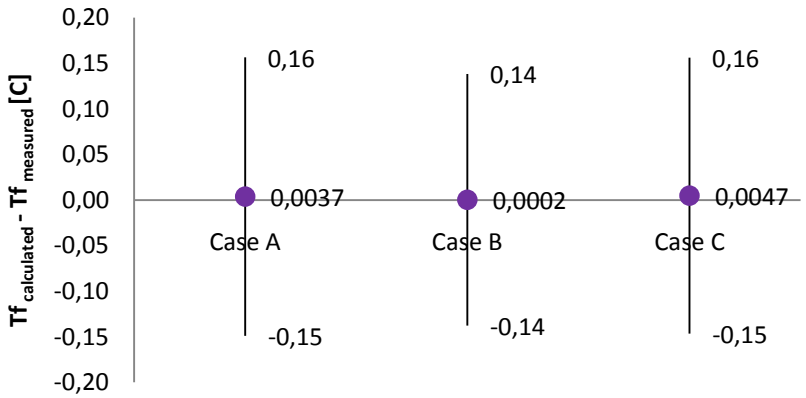

Figure 41. *Section 7: Average of ($Tf_{calculated}$- $Tf_{measured}$) and its variation in each power supplied case.*

- ***SECTION 8***

In Section 8, the thermal conductivity estimated is 3.84 [W/Km] in case A, 4.18 [W/Km] in case B and 4.30 [W/Km] in case C. In *Figure 42*, it can be observed that case B and C present higher values of thermal resistance than case A. Since the heat steps in case B are not too much significant, the thermal resistance profile for this case does not present notable variations. According to heat power variations, case C presents the most irregular profile.

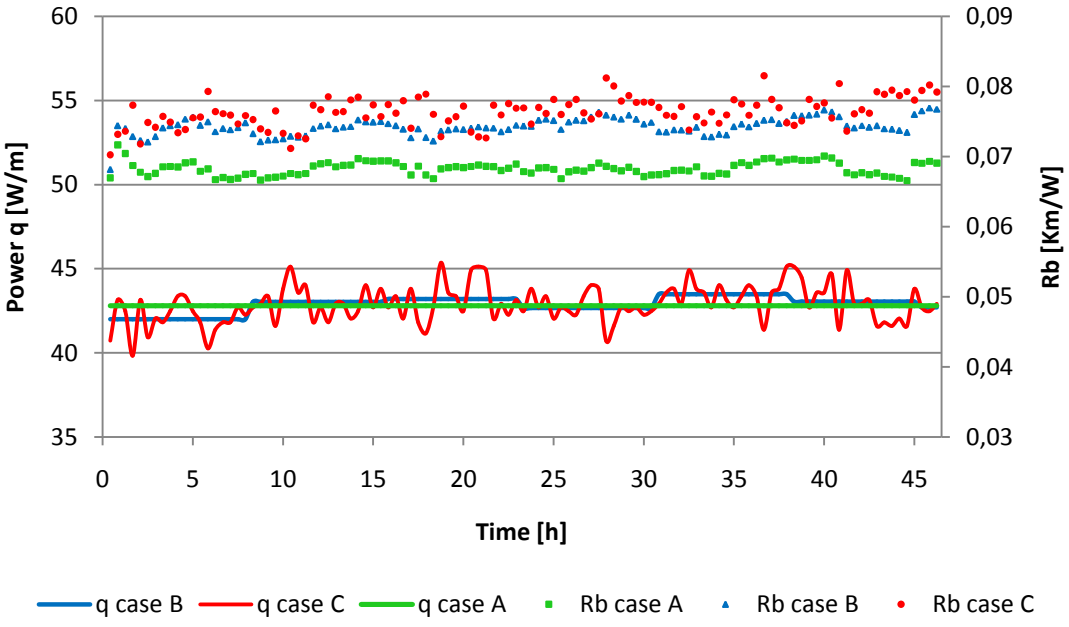

Figure 42. *Section 8: Thermal resistance profiles according to three different cases of power supplied.*

Averaging the thermal resistance, cases B and C, which assume heat steps of power, presents higher value than case A. The thermal resistance dispersion is very close in three cases.

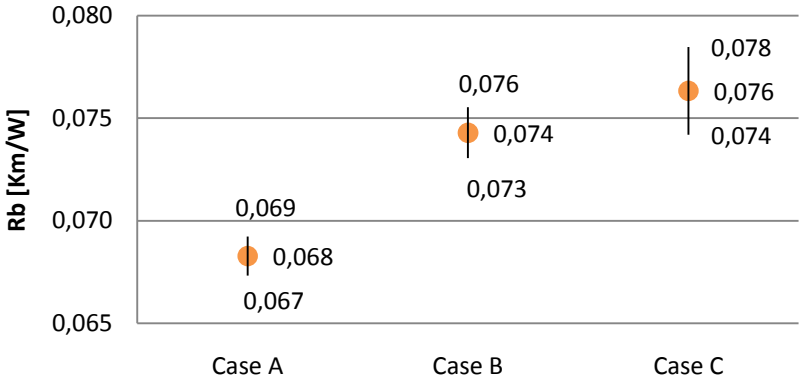

Figure 43. *Section 8: Averages thermal resistance and its variation in each case of power supplied.*

Figure 44 shows that the three cases of heat supplied present a good fit to the measured temperature. However, it cannot be observed which case present the best fit during the whole test.

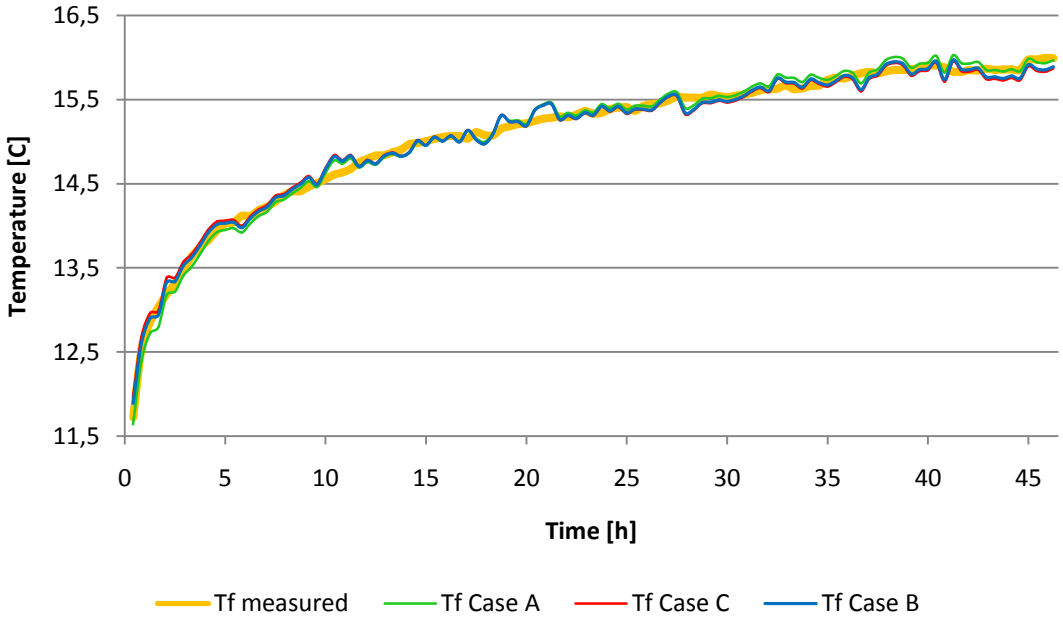

Figure 44. *Section 8: Temperatures measured and temperatures calculated in each power supplied case.*

Averaging ($T_{fmeasured}$-$T_{fcalculated}$), it can be observed that case B and C present the same deviation from the measured temperature. In contrast, case A present the highest difference from measured temperatures. The ($T_{fmeasured}$-$T_{fcalculated}$) dispersion is similar in the three cases.

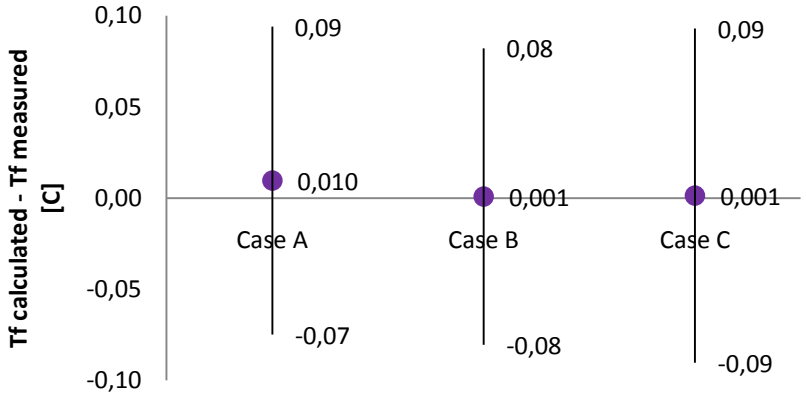

Figure 45. *Section 8: Average of ($Tf_{calculated}$- $Tf_{measured}$) and its variation in each power supplied case.*

- ***SECTION 9***

In Section 9, the thermal conductivity estimated is 2.84 [W/Km] in case A, 3.45 [W/Km] in case B and 3.65 [W/Km] in case C. In the same way as section 8, it can be observed that case B and C present higher values of thermal resistance than case A. As regards as heat power variations, case C presents the most irregular profile, which it is related to the thermal resistance variations. However, the thermal resistance profile trends to approximate a line in case A.

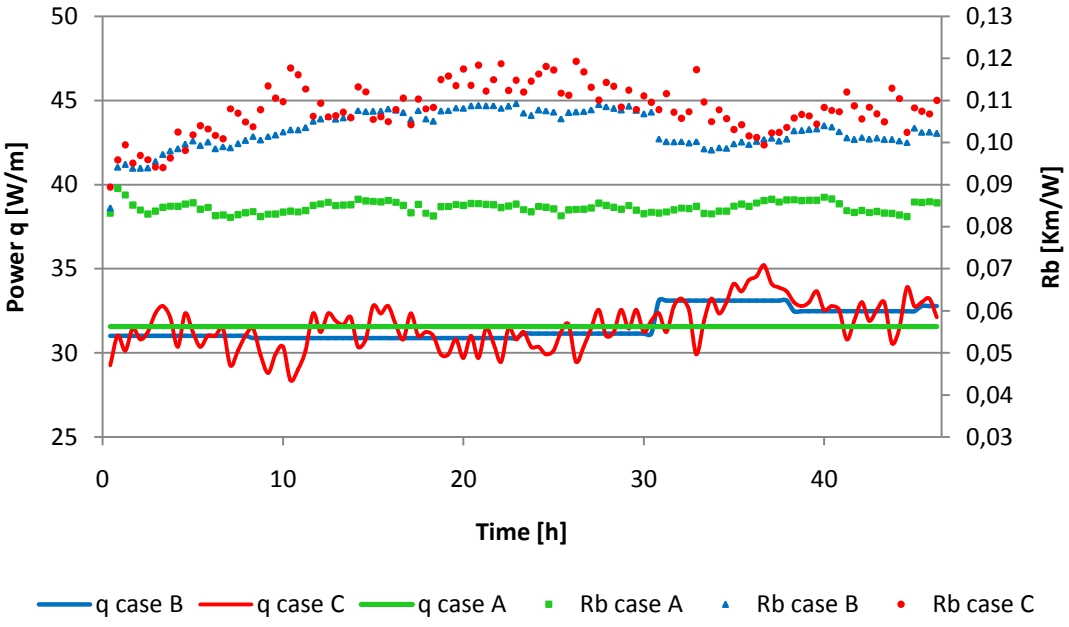

Figure 46. *Section 9: Thermal resistance profiles according to three different cases of power supplied.*

In this section, average thermal resistance for cases B and C is higher than the one for case A, as illustrated in *Figure 47*. The thermal resistance variations from its mean value show up more significant in case C, in accordance with heat power variations.

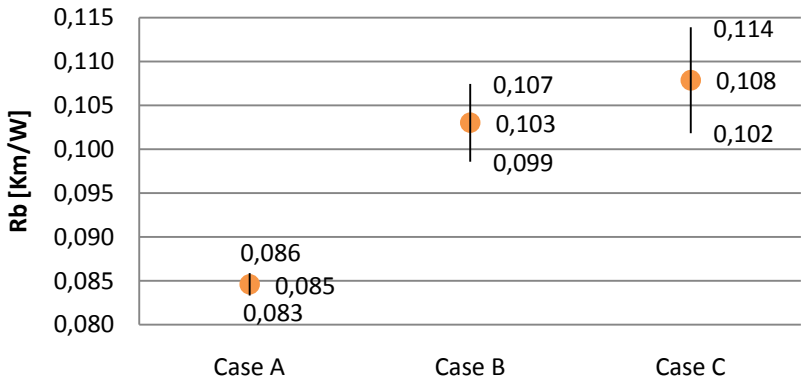

Figure 47. *Section 9: Averages thermal resistance and its variation in each case of power supplied.*

Figure 48 illustrates the profile of measured and calculated temperatures in section 9 during the DTRT heating phase. For the first five hours, case A fits better than the others; however, for the almost rest of time case B and C trends to approximate to temperature measurements.

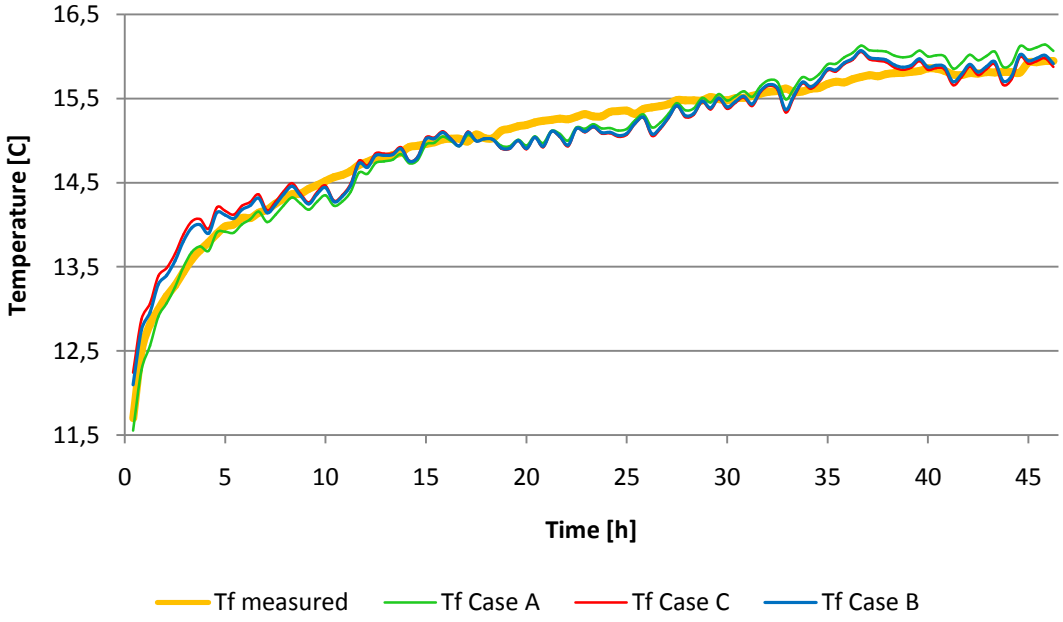

Figure 48. *Section 9: Temperatures measured and temperatures calculated in each power supplied case.*

Averaging ($T_{fmeasured}$-$T_{fcalculated}$), the best fit in temperature measurements show up in case B, as shown in *Figure 49*. The dispersion of ($T_{fmeasured}$-$T_{fcalculated}$) is similar in three cases.

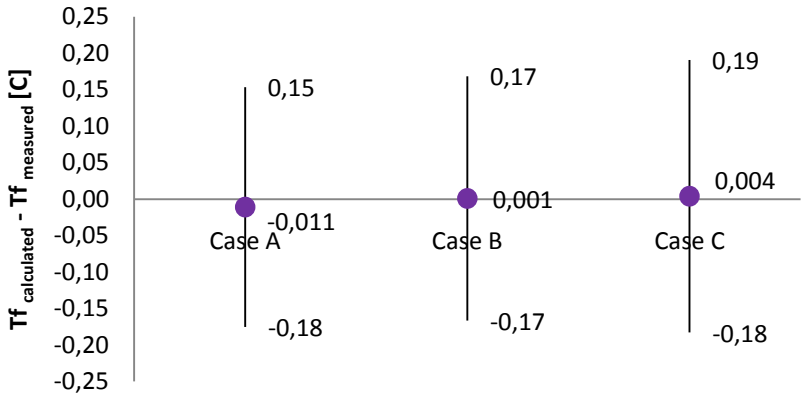

Figure 49. *Section 9: Average of ($Tf_{calculated}$- $Tf_{measured}$) and its variation in each power supplied case.*

- ***SECTION 10***

In Section 10, the thermal conductivity estimated is 3.33 [W/Km] in case A, 3.42 [W/Km] in case B and 3.80 [W/Km] in case C. When the steps heat from case B present a close value to the mean heat power, case A and B present a similar thermal resistance behavior; however, when the step is notable this behavior is quite different, as it can be observed in *Figure 50*. In the same way, case B thermal resistance varies according to heat power variations.

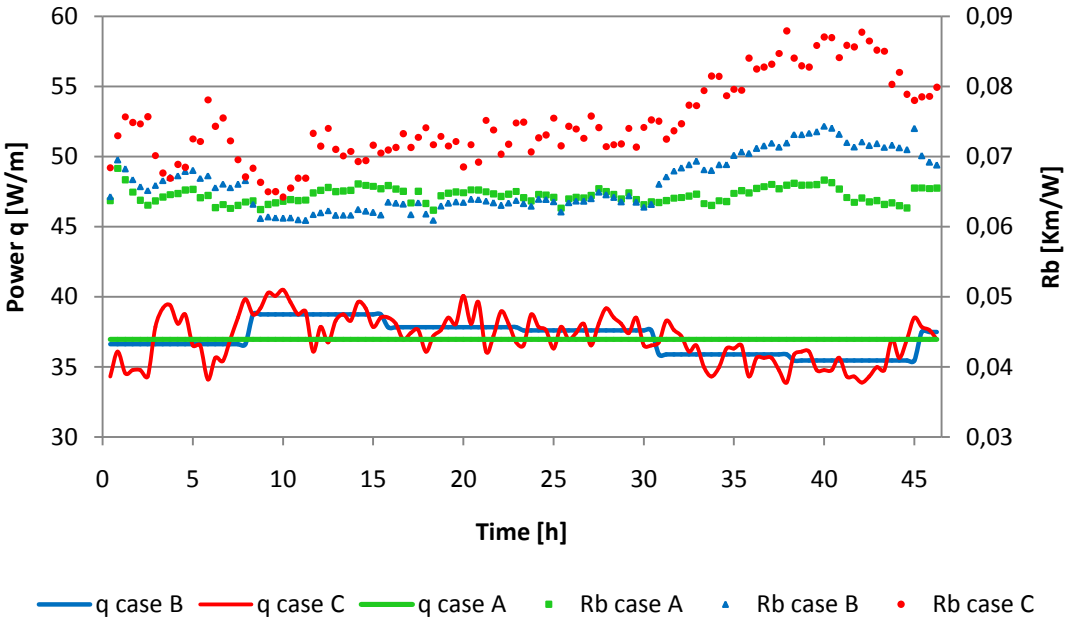

Figure 50. *Section 10: Thermal resistance profiles according to three different cases of power supplied.*

According to *Figure 51*, case A and B present a close value of the average thermal resistance, whereas case C presents the furthest value of these, which it is about 0,01 [Km/W] units in difference. As beforehand sections, the R_b dispersion is more significant in case C.

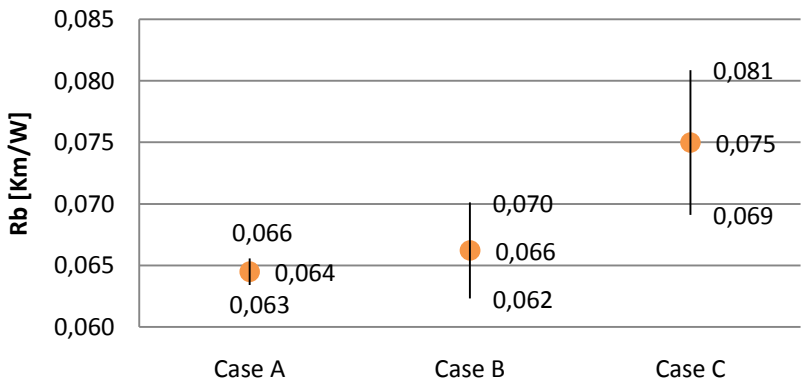

Figure 51. *Section 10: Average thermal resistance and its variation in each case of power supplied.*

Figure 52 shows that every profiles of calculated temperature bear resemblance to the profile of measured temperature. Since each case fits better in a different interval of the test, it cannot be established which case describes better the temperature measurements for the whole period.

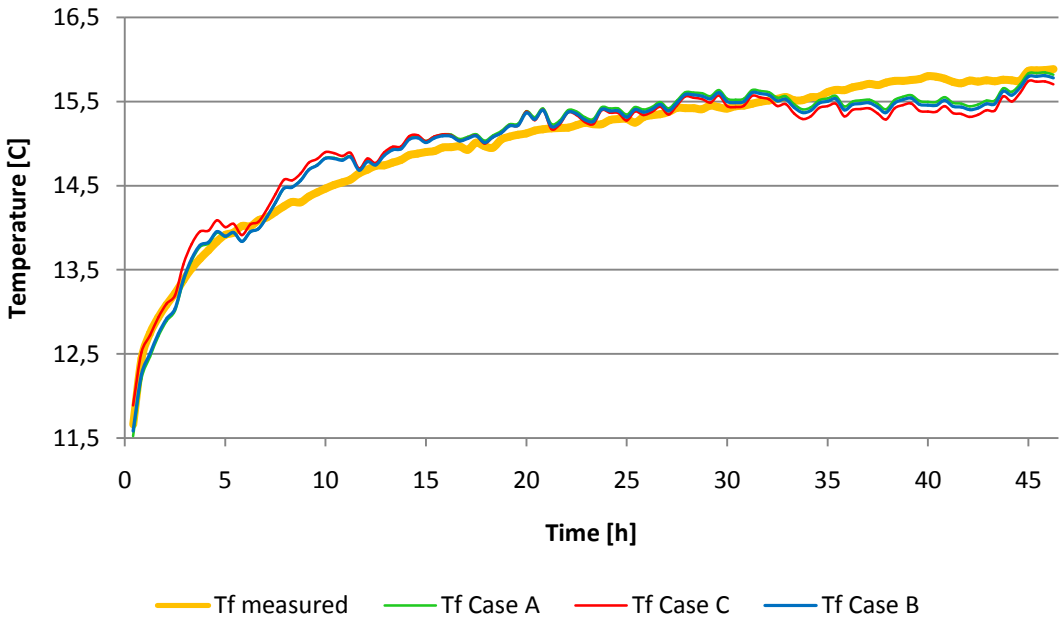

Figure 52. *Section 10: Temperatures measured and temperatures calculated in each power supplied case.*

Figure 53 illustrates the difference between the calculated and the measured temperature. Thus, it can be observed that case B fits better to the measured temperature on average. In contrast, case A present the highest difference in measured temperature. The dispersion of ($T_{fmeasured}$-$T_{fcalculated}$) is similar in every case.

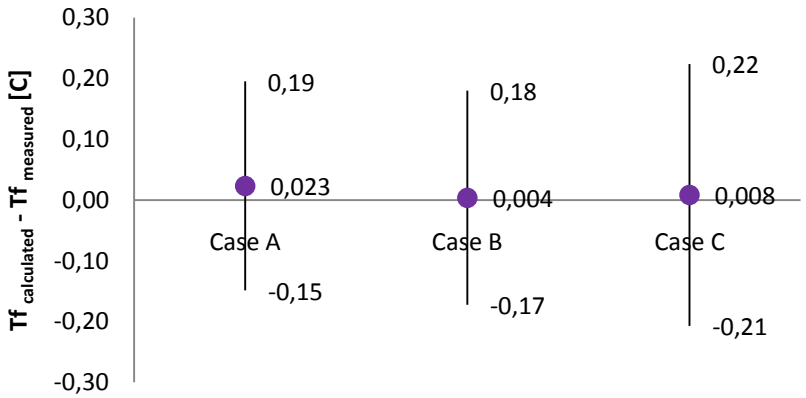

Figure 53. *Section 10: Average of ($Tf_{calculated}$- $Tf_{measured}$) and its variation in each power supplied case.*

- ***SECTION 11***

In Section 11, the thermal conductivity estimated is 3.24 [W/Km] in case A, 4.13[W/Km] in case B and 4.36 [W/Km] in case C. *Figure 54* shows the profile thermal resistance in case A, which trends to a line around 0,06 [Km/W] in accordance with constant heat power assumed. Moreover, the estimated value for case A show up further than the one of cases B and C, in 0,02-0,03 [Km/W] units of difference. As well as, it can be seen the influence of the heat power supply in the estimation of the thermal resistance.

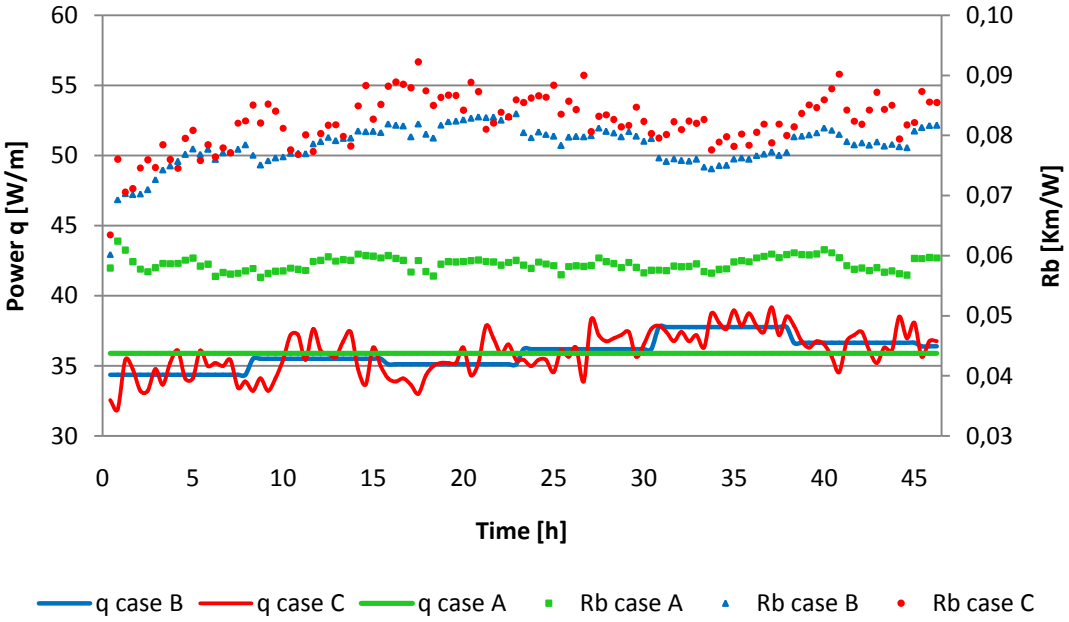

Figure 54*. Section 11: Thermal resistance profiles according to three different cases of power supplied.*

Case A presents the smallest average thermal resistance estimation, whereas case C does the highest one. In accordance with graphic results, the dispersion from the mean value it is more significant in case C, in which the heat power is not constant.

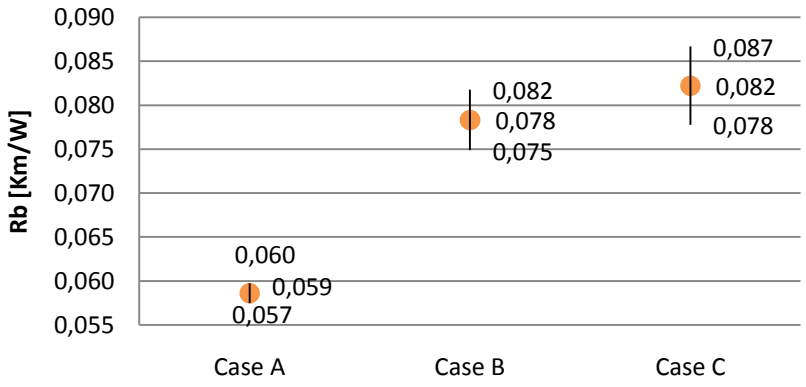

Figure 55. *Section 11: Average thermal resistance and its variations in each case of power supplied.*

Figure 56 shows the temperature profile of experimental measurements and calculated temperatures in each heat power supplied case. It can be observed that each case fits better in a different interval of the test. To assess which case presents the best fit to measured temperature, it is calculated the difference between the measured and calculated temperature, as shown in *Figure 57*.

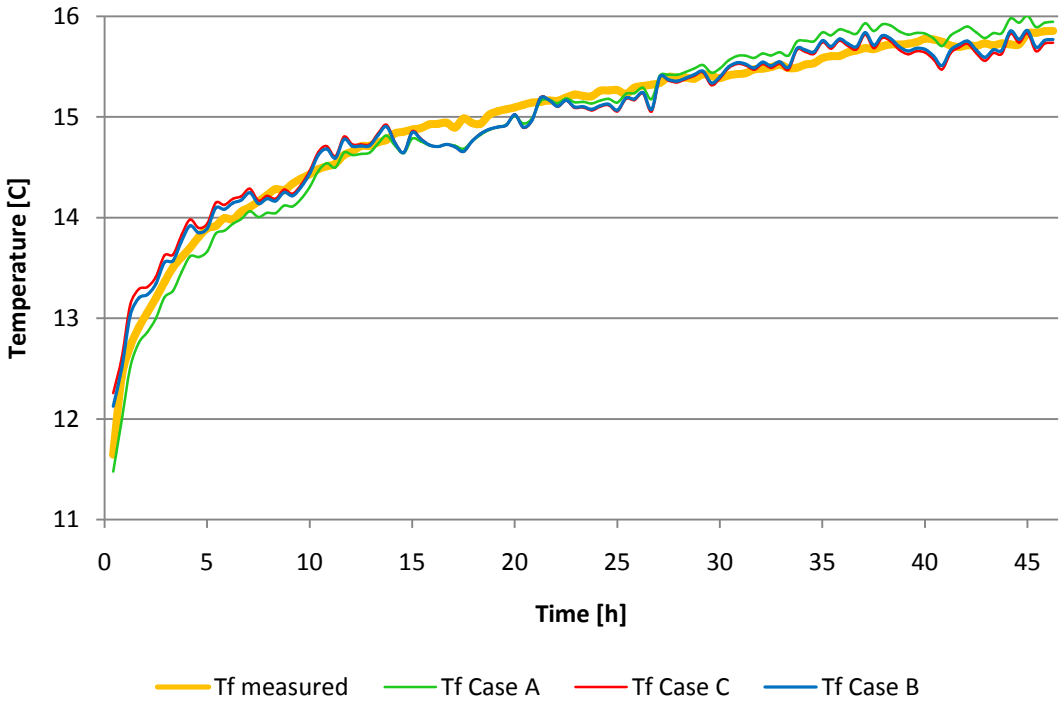

Figure 56. *Section 11: Temperatures measured and temperatures calculated in each power supplied case.*

Case C presents the smallest deviation from the measured temperature, which is only about 0,001 [C] on average. However, case A presents a deviation of - 0,013 [C] from measured temperature. The dispersion of ($T_{fmeasured}$-$T_{fcalculated}$) is similar in every case.

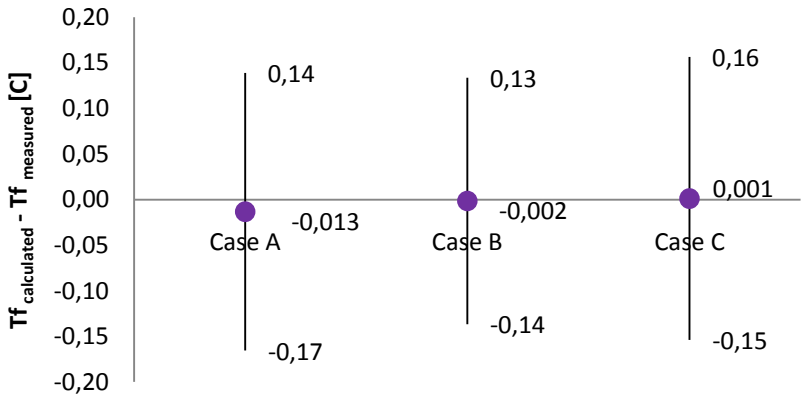

Figure 57. *Section 11: Average of ($Tf_{calculated}$- $Tf_{measured}$) and its variation in each power supplied case.*

- ***SECTION 12***

In Section 12, the thermal conductivity estimated is 3.01 [W/Km] in case A, 3.26 [W/Km] in case B and 3.62 [W/Km] in case C. In *Figure 58*, it can be observed that C presents the highest values of thermal resistance during the whole test. Case B and C show a similar profile, being higher the values from case B. As regards as heat power variations, case C presents the most irregular profile.

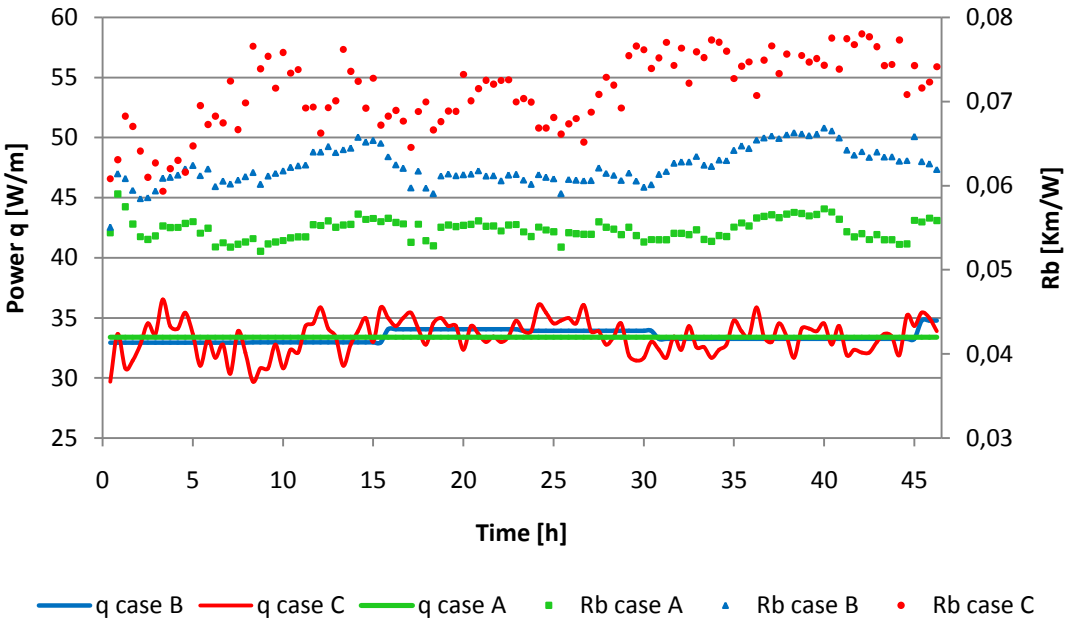

Figure 58. *Section 12: Thermal resistance profiles according to three different cases of power supplied.*

Case A presents the smallest thermal resistance on average, it is 0.016 [Km/W] in difference from case C and 0.007 [Km/W] from case B. The dispersion of this parameter is related to the heat power, so that case C presents the highest value.

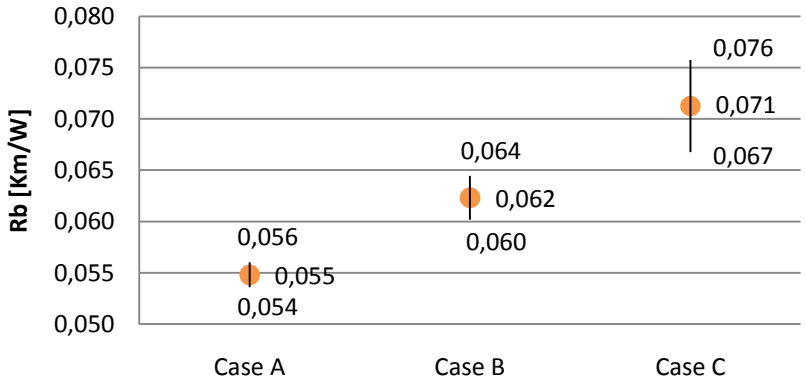

Figure 59. *Section 12: Average thermal resistance and its variations in each case of power supplied.*

Figure 60 shows case A and B presents a better fit than case C at the end of the test. For the beginning and the intermediate period of the test, each case fit better in certain intervals. For that reason, the difference between the measured and the calculated temperature is assessed; these results are shown in *Figure 61*.

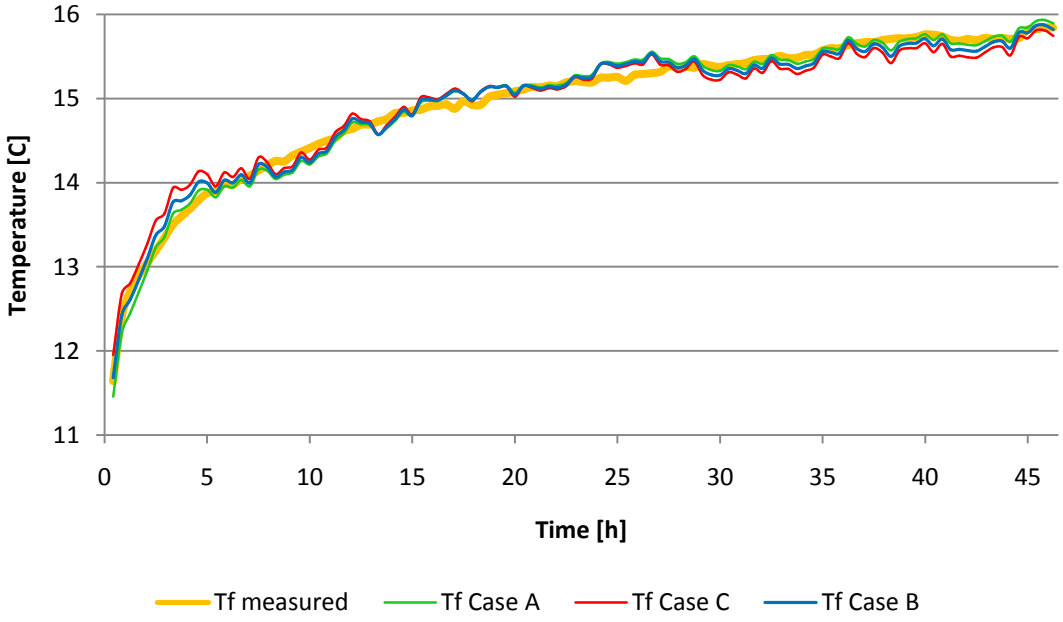

Figure 60. *Section 12: Profiles of measured and calculated temperature.*

Averaging ($T_{fmeasured}$-$T_{fcalculated}$), three cases present a good approximation to the measured temperature, as shown in next figure. The highest deviation from the mean value of ($T_{fmeasured}$-$T_{fcalculated}$) shows up in case C.

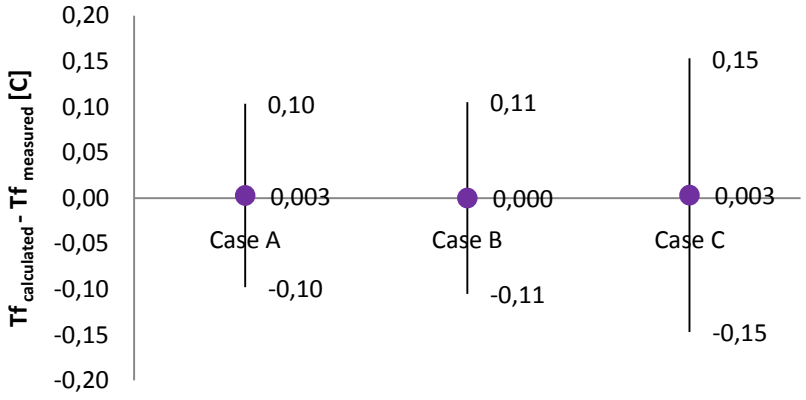

Figure 61. *Section 12: Average of ($Tf_{calculated}$- $Tf_{measured}$) and its variation in each power supplied case.*

The mean value of rock thermal conductivity and borehole thermal resistance, which have been estimated from Halo data in each case of heat power injection, are presented in *Figure 62 (a)* and *(b)* in each borehole sections.

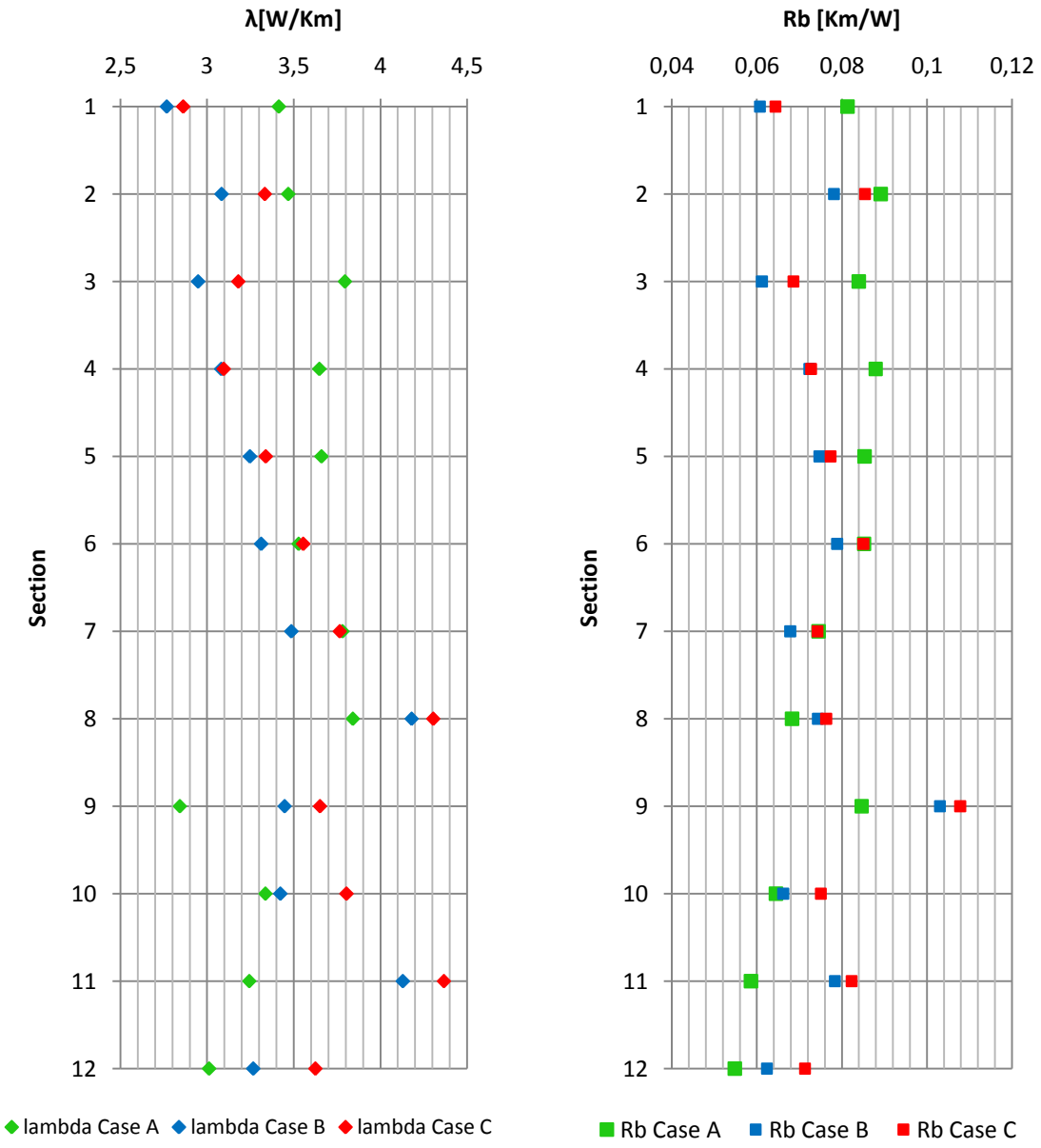

Figure 62. *Thermal conductivity and thermal resistance in each borehole section. (Halo data-Case A, B and C).*

Firstly, the uncertainties due to the assumption of constant heat power rate are analyzed considering the results of Halo case A, B and C. To assess which case of heat power supply – constant or by steps (7.5-hours or 25 minutes) - gives the best approximation to the profile of measured temperatures, it is averaged the mean values of ($T_{fmeasured}$-$T_{fcalculated}$) calculated in all sections. This result is equal to 0.001 [C] in case B. This is about 0.005 [C] in case C. And it is equal to 0.013 [C] in case A. The cases B and C, which assume heat power by steps, present a better fit than case A, which assumes a constant heat power rate. Moreover, the values of case B and C are very close; however case A differs from case B a value of 0.012 [C].

Since case C assumed the tightest heat power steps, it should have presented the best fit; however it is not the result. It may attribute to the uncertainties in measurements. This suggests that the heat power step should extend for a minimum period of time in order to remove the uncertainties of the test equipments. Therefore, case B presents the best fit between the measured and calculated temperature on average, this case of heat power rate can provide more accurate estimates. This result is in a good accordance with the influence of heat power variations to the accuracy in the borehole thermal parameters estimate.

It can be observed that in the five first sections, case A presents values of thermal conductivity higher than the values of case B and C. The results from case A are closer to the values from case C in these sections. In section 6 and 7, thermal conductivity values are almost equal in case A and C. However, case A presents the smallest values in the last sections. Moreover, in these last sections, case A and case C does not presents close values between them, being values from case A closer to the values estimated in case B. This behavior can be observed in the same way in the results of thermal resistance.

Considering the heat power rate and the estimates of thermal conductivity in each case of heat power supply by 7.5 hours steps –case B-, it can be observed that the influence of the value of the first heat power step in the estimate of the thermal parameters. If the first interval of time present significant value of heat power rate, which is lower than its mean value, the thermal conductivity estimation presents a higher value than the estimate made assuming a constant heat power, for instance this situation happens in section 8 and 10. In contrast, if the heat power rate during the first interval of time present higher value than its mean rate, the thermal conductivity presents lower value than the value provide considering a constant heat power rate; for instance in section 3. It is in a good accordance with the profile of thermal conductivity shown in case of a constant heat power rate-case A- and the profile for a 7.5 hours stepwisely constant heat power-case B-. The thermal resistance profiles in cases A, B and C present the same distribution along the borehole depth as the thermal conductivity, it may attribute to the heat power rate during the first interval of time.

In case A, the rock thermal conductivity varies within the range 3.84 to 2.84 [W/Km].Calculating the mean value for all sections, it is equal to 3.46 [W/Km]. This thermal conductivity variation is more significant in case B and C where heat power is assumed as a contribution of heat steps from past intervals of time. Thus, case B presents a mean value equal to 3.36 [W/Km], which varies in the interval 4.18 to 2.76 [W/Km]. This variation increases in case C, being its mean value equal to 3.57 [W/Km] and its variation in the range 4.36 to 2.86 [W/Km]. It is illustrated in *Figure 63*.

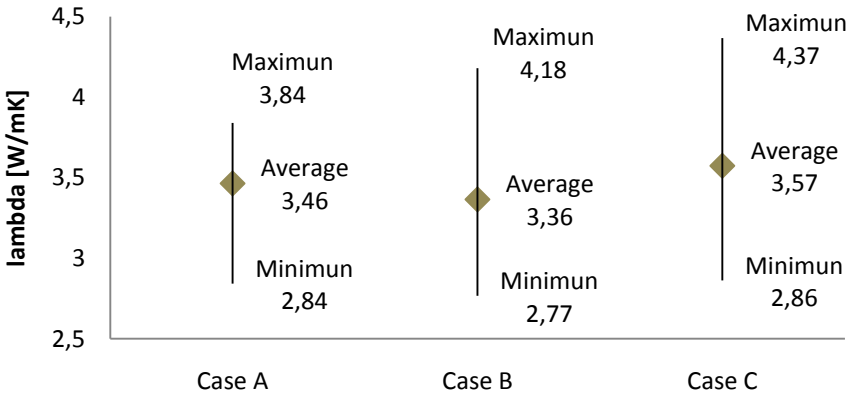

Figure 63. *Rock thermal conductivity: average, maximum and minimum (Halo data Case A, B and C).*

As regards as borehole thermal resistance, the average value is equal to 0.076 [Km/W] and it ranges between 0.089 and 0.054 [Km/W] in case A. For case B, the mean value results in 0.073 [Km/W] and this parameter varies between 0.103 and 0.061 [Km/W]. In case C, thermal resistance presents a value equal to 0.078 [Km/W] on average and its variation is within the range 0.108 and 0.064 [Km/W].

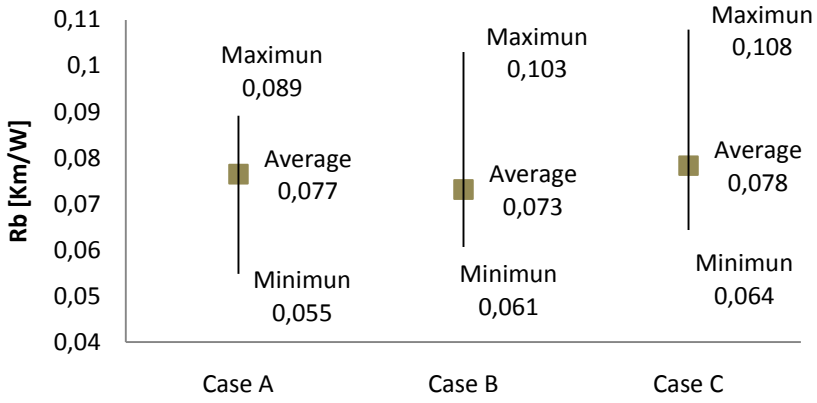

Figure 64. *Borehole thermal resistance: average, maximum and minimum (Halo data Case A, B and C).*

3.2. Results from data of Halo and Sentinel DTS-equipment.

- ***SECTION 1***

In section 1, the results from Sentinel data give a high value of thermal conductivity, which is equal to 9.00 [W/mK]. Notice that heat power presents high values of rate in comparison with Halo data and the rest of section measured by Sentinel DTS-equipment. Since thermal conductivity is connected with heat power, the high heat power rate explains the high value of thermal conductivity. Moreover, it can be observed great fluctuations of input heat power during the heating phase, which are range between 30 and 20 [W/m].

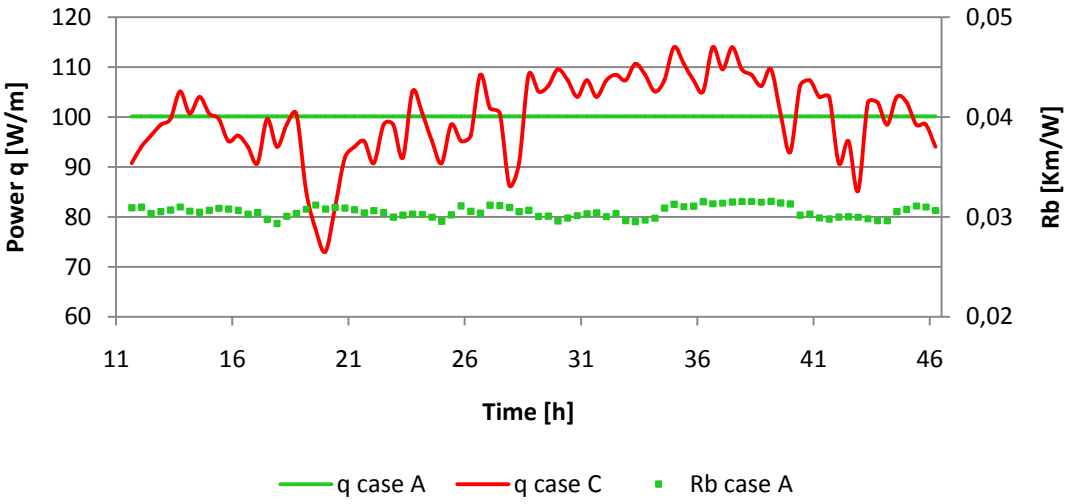

Figure 65. *Section 1: Thermal resistance profile according to constant heat power supply.*

According to thermal resistance profile in Sentinel results, this parameter varies around 0.03 [Km/W], as illustrated in *Figure 65*. This value differs from the expected value. Since the thermal resistance is calculated using the heat power rate and the estimated thermal conductivity, this irregularity is attributed to these anomalous values of heat power rate and thermal conductivity. Next figure shows the mean value of thermal resistance and its deviation calculating by standard deviation for Sentinel and Halo data assuming a constant heat power

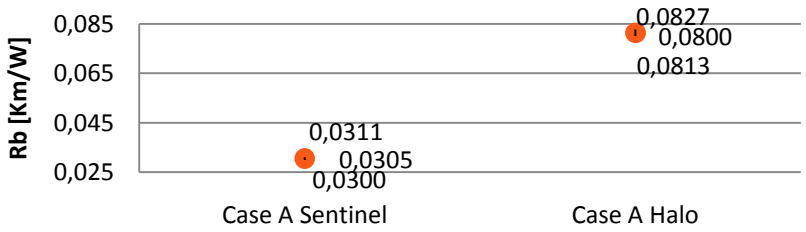

Figure 66. *Section 1: Average thermal resistance and its variation.*

Figure 67 shows the profile of measured and calculated temperature from Halo and Sentinel data during the last part of DTRT heating phase. It can be observed that Sentinel result present significant fluctuations in some intervals of the test, as shown in the periods around of 21 and 27 hours test, in a good accordance with the heat input variations showed in *Figure 65*.

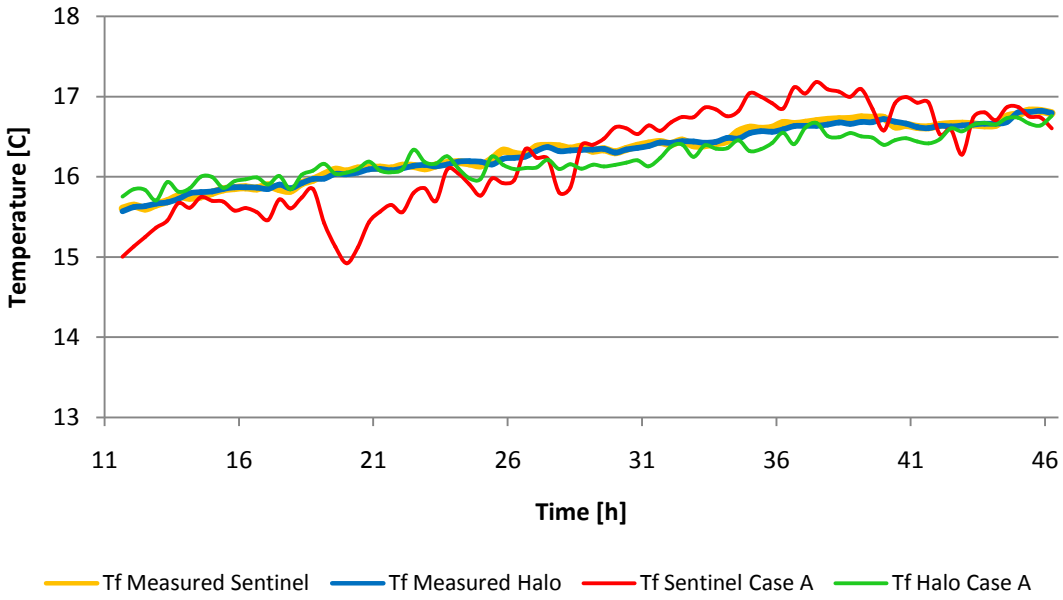

Figure 67. *Section 1: Profiles of measured and calculated temperatures.*

Averaging ($T_{fmeasured}$-$T_{fcalculated}$), this difference is equal to 0.07 [C] in Sentinel results and its variation from the mean difference is shown in *Figure 68*. The average of these differences is lower in Halo results, in a good accordance with the results shown in *Figure 67*.

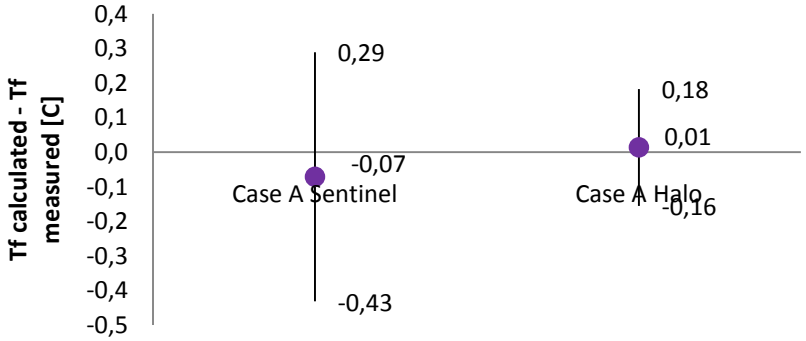

Figure 68. *Section 1: Average of ($Tf_{calculated}$- $Tf_{measured}$) and its variation.*

Since the heat power input presents high values of rate and then the estimated parameters present anomalous values, the results from section 1 are neglected for assessment of the whole borehole.

- ***SECTION 2***

In section 2, the thermal conductivity estimated is 3.53 [W/Km] in Sentinel data by assuming a constant heat power injection - case A -. In *Figure 69*, it can be observed that heat power input presents great fluctuations during the whole phase, which influences in results.

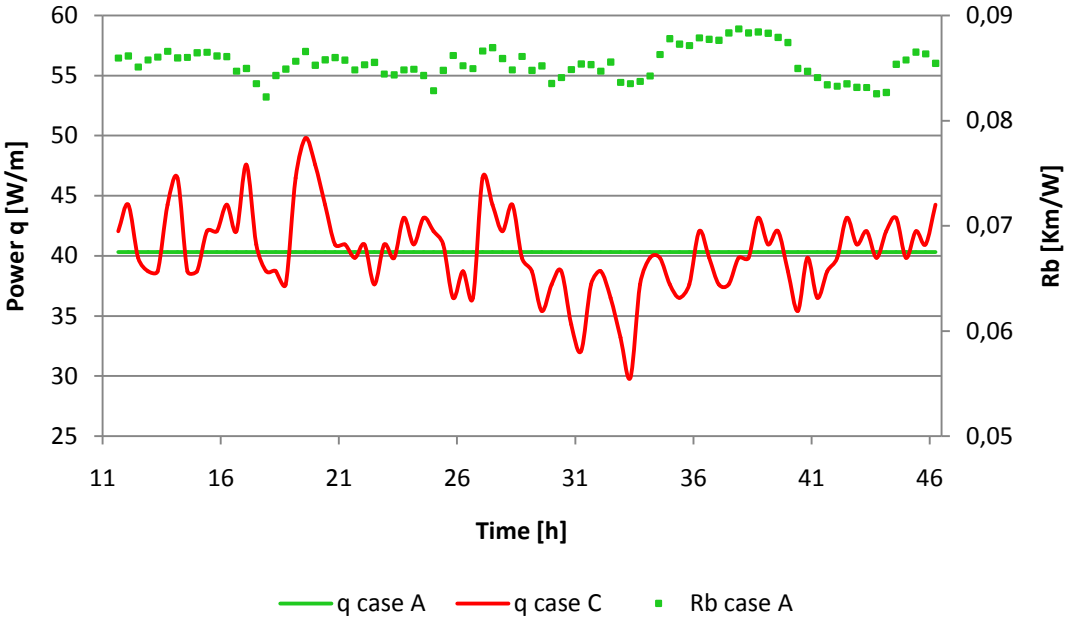

Figure 69. *Section 2: Thermal resistance profile according to constant heat power supply.*

The mean of the thermal resistance is equal to 0.085 [Km/W] in Sentinel case and its deviation from the mean value is shown in *Figure 70*, which is about 0.0015 [Km/W]. In this figure, it is also shown the results from Halo data obtained by assuming a constant heat power rate.

Figure 70. *Section 2: Average thermal resistance and its variation.*

As regards as Sentinel results, the most significant deviations of calculated temperatures show up in the same interval of time, in which the most significant heat power variations occur. This fact can be observed around 21 and 34 hours test, in which the deviation is about 1 [C]. In next figure, it is also shown the results from Halo data for a constant heat power.

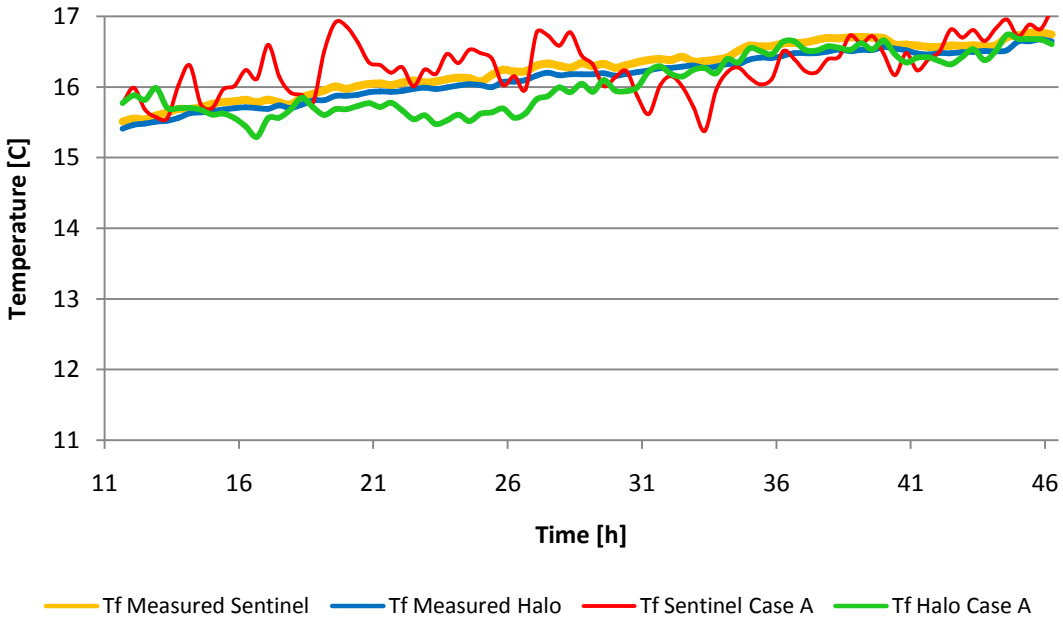

Figure 71. *Section 2: Profiles of measured and calculated temperatures.*

Averaging the difference between the calculated and measured temperatures for the last period of DTRT, it is equal to 0.03 in Sentinel results. Its deviation from the mean value of this difference is about ±0.3 [C]. The difference between the measured temperature and the calculated temperature is similar in Sentinel and Halo results, on average. However, the variation of this difference is higher in Sentinel results. Consequently, the calculated temperature profile from Halo data fits better to the measured temperature profile.

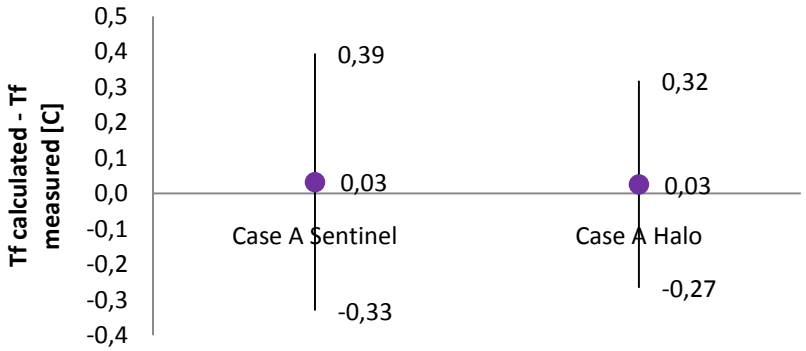

Figure 72. *Section 2: Average of ($Tf_{calculated}$- $Tf_{measured}$) and its variation.*

- ***SECTION 3***

Assuming a constant heat power input in Sentinel data, the thermal conductivity calculated in section 3 is equal to 3.99 [W/Km].In *Figure 73*, it can be observed the variations of heat power rate, which ranges between 54 and 37 [W/m].

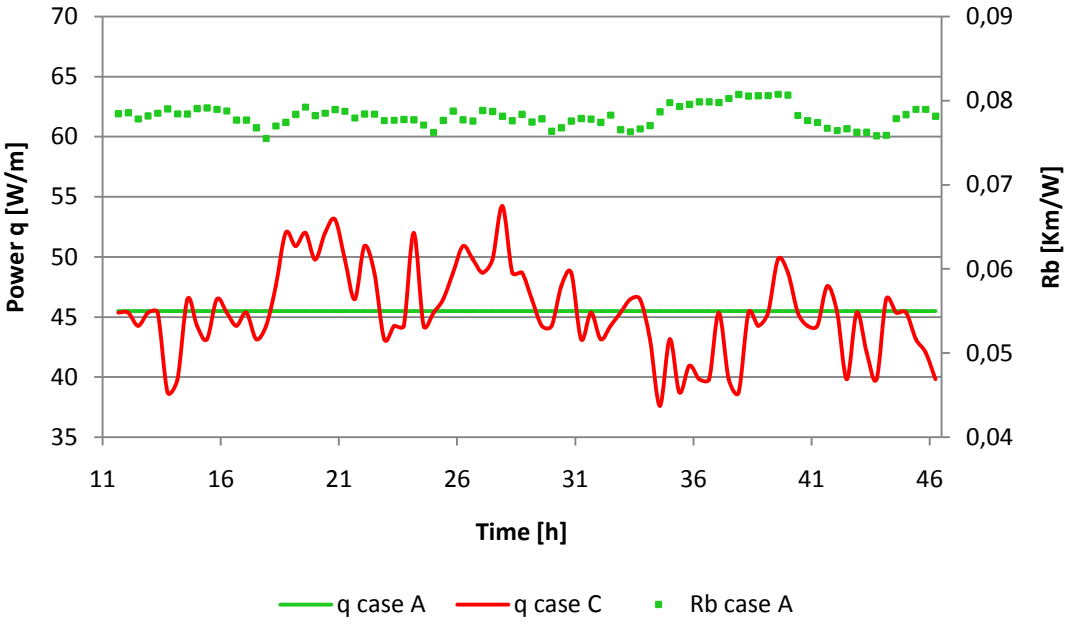

Figure 73. *Section 3: Thermal resistance profile according to constant heat power supply.*

Assuming a constant heat power, the average of thermal resistance is equal to 0.078 [Km/W] in Sentinel case. Since the heat power is constant, its deviation from the mean value is only about 0.001 [C]. It is illustrated in *Figure 74* together with the results of Halo DTS-equipment.

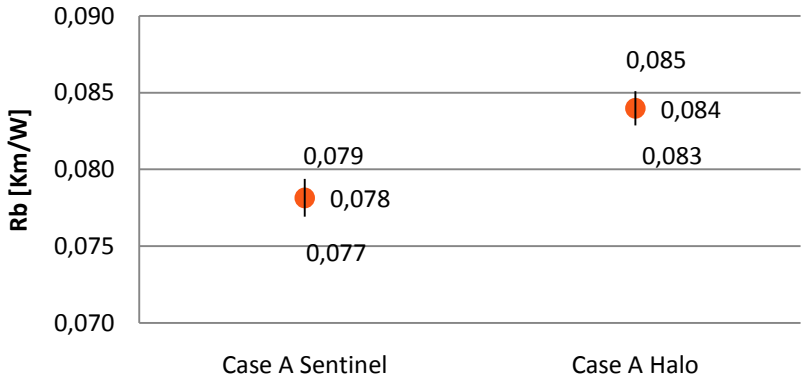

Figure 74. *Section 3: Average thermal resistance and its variation.*

According to Sentinel results, the comparison between the measured and calculated temperature shows similar results as given in section 2. Since 25-minutes stepwise of heat power is used to calculate the temperature profile, significant heat power variations result in relevant differences in calculated temperatures. It is shown in *Figure 75* together with the profile of measured and calculated temperature resulting from Halo measurements.

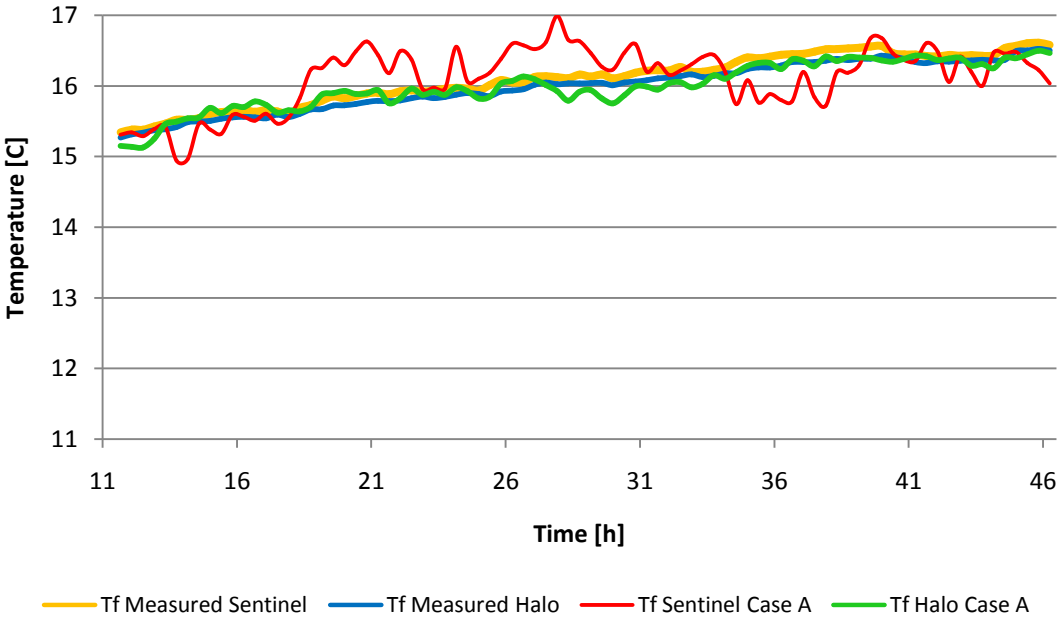

Figure 75. *Section 3: Profiles of measured and calculated temperatures.*

Averaging ($T_{fmeasured}$-$T_{fcalculated}$), it is equal to 0.02 [C] in Sentinel results and its deviation ranges between -0.35 and 0.39 [C], as shown in *Figure 76*.It is also included the results from Halo data. Comparing Sentinel and Halo results, both of them present the same difference to the measured temperature profile, on average. However, the variation of this difference is higher in Sentinel results. Consequently, the calculated temperature profile from Halo data fits better to the measured temperature profile.

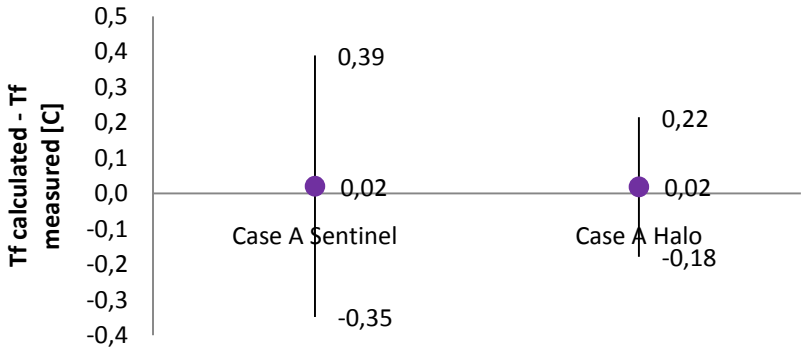

Figure 76. *Section 3: Average of ($Tf_{calculated}$- $Tf_{measured}$) and its variation.*

- ***SECTION 4***

In section 4, the value of thermal conductivity is estimated at 3.61 [W/Km] by assuming a constant heat power – case A – in Sentinel data. The thermal resistance profile varies over 0.08 [W/m]. It can be also observed the fluctuations in the heat power injection, which range between 48 and 34 [W/m]. These results are shown in *Figure 77*.

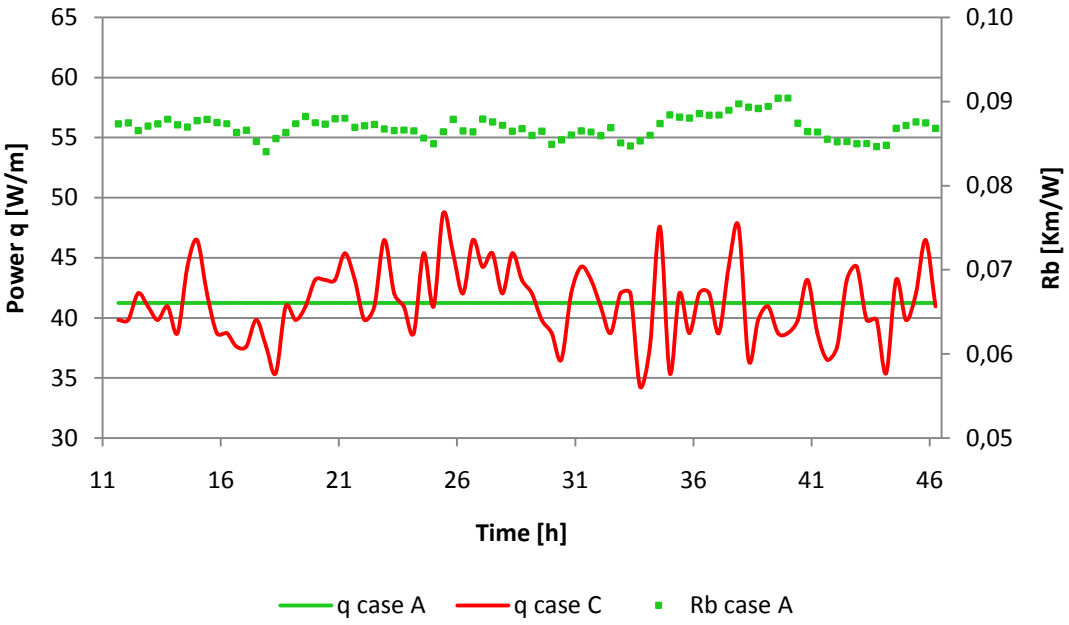

Figure 77. *Section 4: Thermal resistance profile according to constant heat power supply.*

According to Sentinel results, the mean value of thermal resistance is equal to 0.087 [Km/W], and its deviation from the mean value is only about 0.001 [Km/W]. Next figure shows also the results from Halo data.

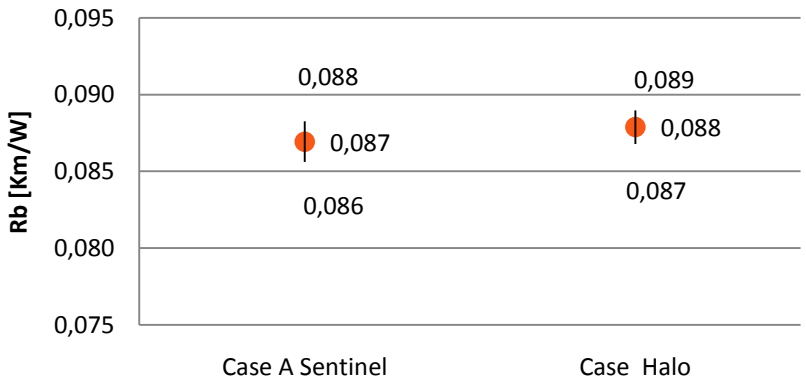

Figure 78. *Section 4: Average thermal resistance and its variation.*

In *Figure 79*, it can be observed that the profile of calculated temperature in Sentinel case presents deviations from measured temperature during the whole period of time. To assess these deviations, it is calculated the difference between the measured and calculated temperature. It is illustrated in *Figure 80*. The results from Halo-case A- are also included in next figures.

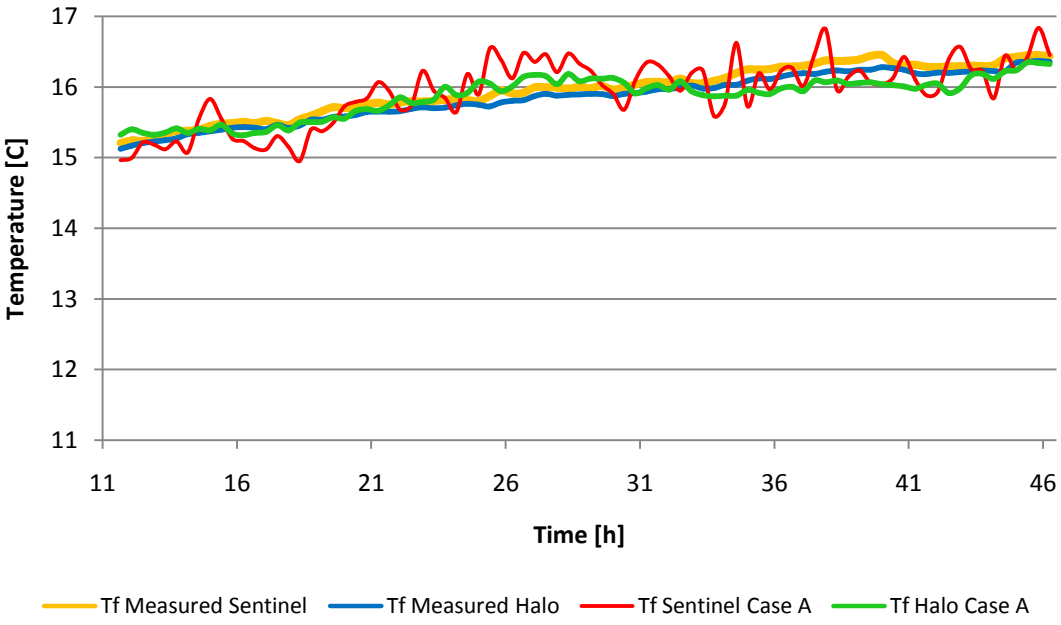

Figure 79. *Section 4: Profiles of measured and calculated temperatures.*

As regards as Sentinel results, the mean value of the difference between the measured and calculated temperature is equal to -0.02 [C]. Considering the standard deviation, this difference fluctuates from the mean value within the range -0.31 to 0.27 [C]. Besides, the average difference between temperatures in Halo –case A- is shown in next figure.

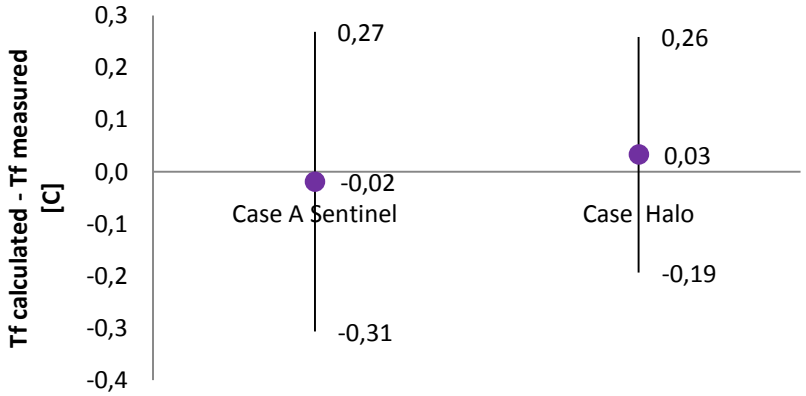

Figure 80. *Section 4: Average of ($Tf_{calculated}$- $Tf_{measured}$) and its variation.*

- ***SECTION 5***

The rock thermal conductivity estimation is equal to 3.80 [W/Km] calculating by a constant heat power injection in Sentinel data. However, the heat power rate varies within the range 49 to 36 [W/m], as presented in *Figure 81*. In this figure is also shown the thermal resistance profile, which presents small variations around 0.08 [Km/W].

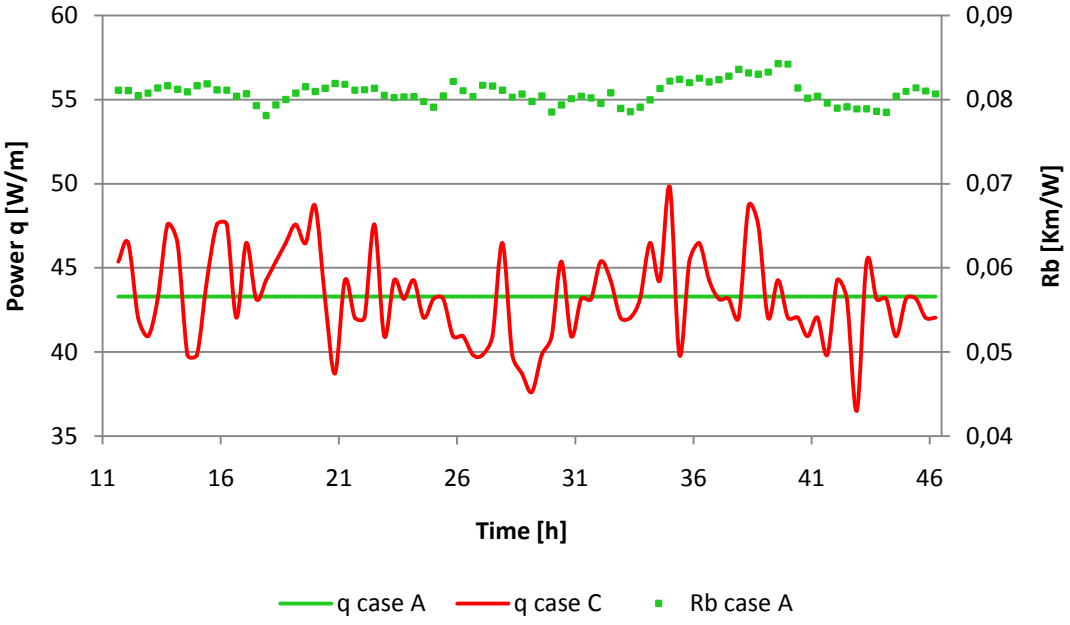

Figure 81. *Section 5: Thermal resistance profile according to constant heat power supply.*

Since thermal resistance profile varies around 0.08 [Km/W] in Sentinel results, its mean value is equal to 0.081 [Km/W]. Since the thermal resistance profile is calculated by a constant heat power, thermal resistance deviation from its mean value is only about 0.001 [Km/W]. In next figure, the results from Halo data are also shown.

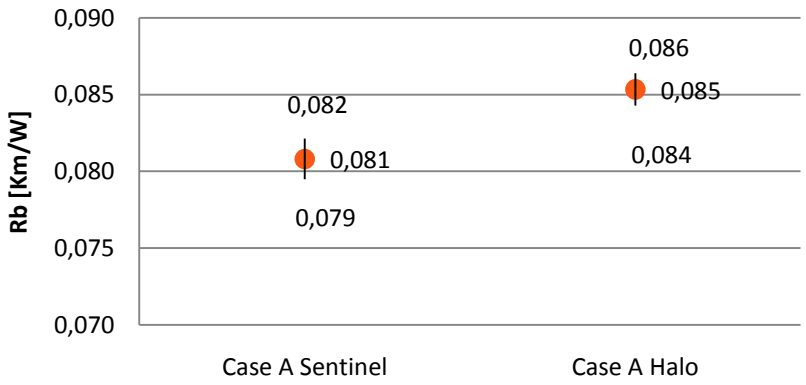

Figure 82. *Section 5: Average thermal resistance and its variation.*

To compare the results with the temperature measurements, the calculated temperature from Halo and Sentinel are plotted together with their measurements of temperature in the same graph, as illustrated in *Figure 83*. The most relevant deviations are related to the most significant heat power variations. The difference between the calculated and measured profiles is calculated to assess these deviations. It is illustrated in *Figure 84*.

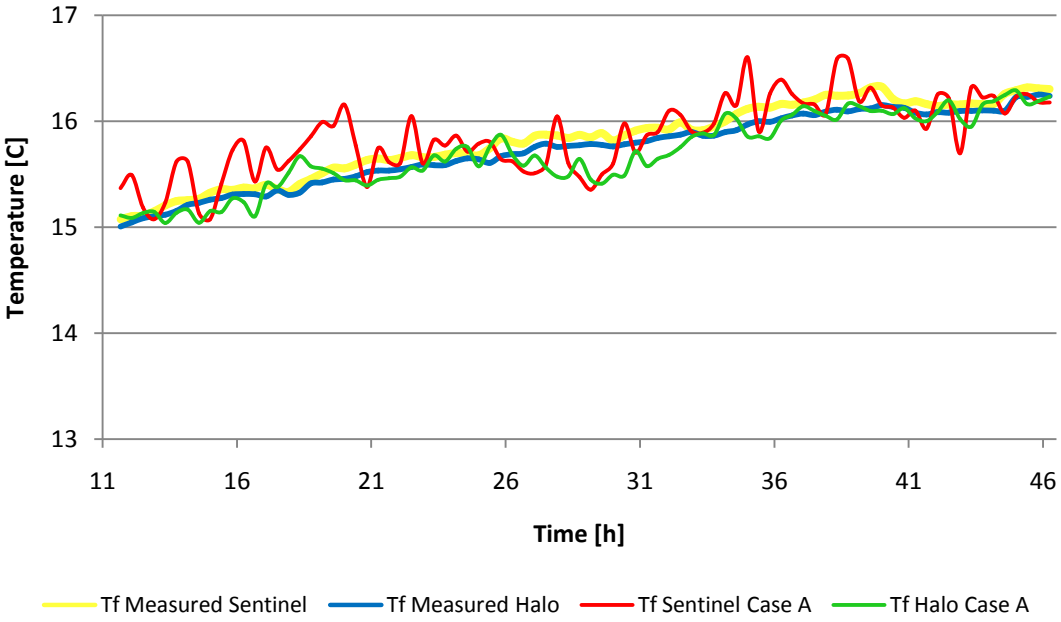

Figure 83. *Section 5: Profiles of measured and calculated temperatures.*

According to Sentinel results, these deviations from the measured temperatures is equal to 0.04 [C] on average. The fluctuation of ($T_{fmeasured}$-$T_{fcalculated}$) is within the range -0.20 to 0.28 [C] in Sentinel case. For Halo results, this average difference is lower and its variation is also lower, which indicate a better fit to the measured temperature profile.

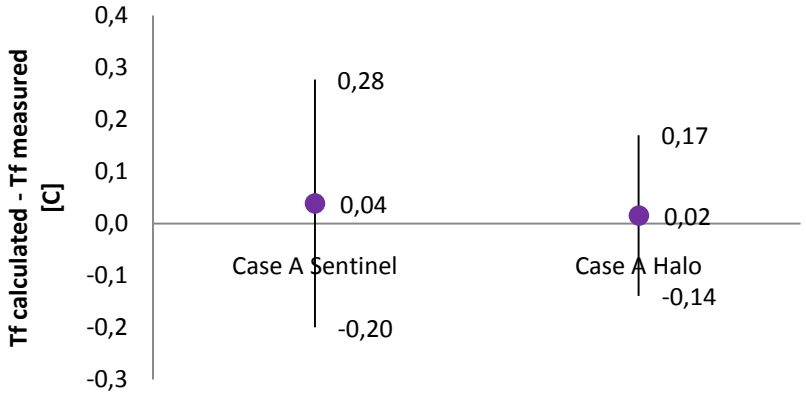

Figure 84. *Section 5: Average of ($Tf_{calculated}$- $Tf_{measured}$) and its variation.*

- ***SECTION 6***

Assuming a constant heat power input in Sentinel data, the thermal conductivity is equal to 3.76 [W/Km]. In the same way as the above sections, it can be observed significant variations of heat power rate, which varies within the range 48 to 32 [W/m]. According to thermal resistance profile, it is varies around 0.08 [Km/W] for a constant heat power rate, as presented in *Figure 85*.

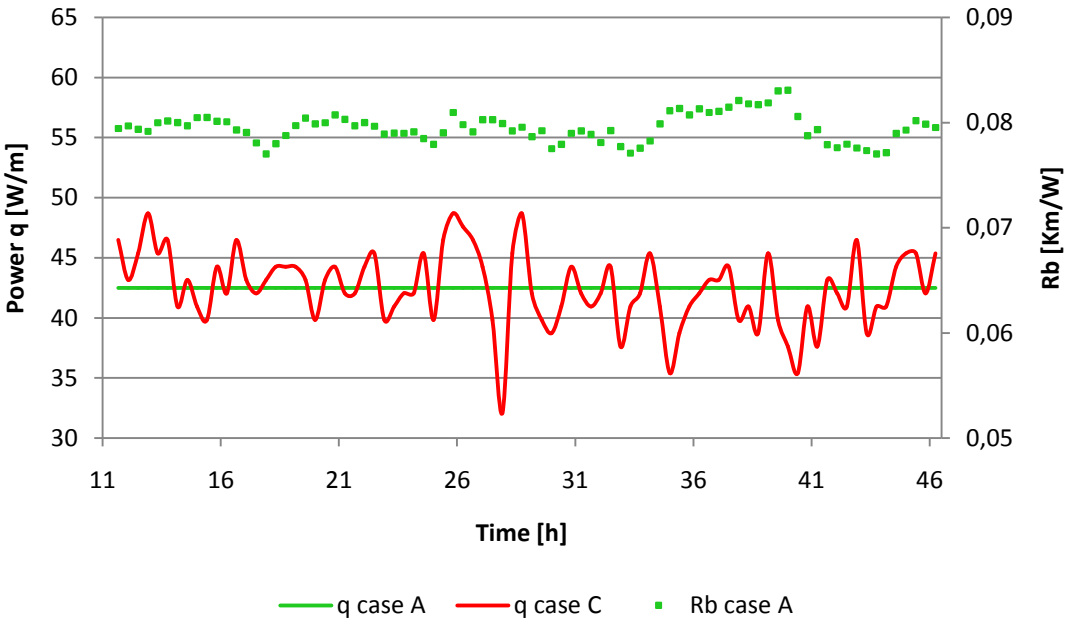

Figure 85. *Section 6: Thermal resistance profile according to constant heat power supply.*

In Sentinel results, the average of thermal resistance is equal to 0.080 [Km/W] and its deviation from the mean value is only about ±0.001 [Km/W]. In next figure, it is also included the results from Halo data for a constant heat power.

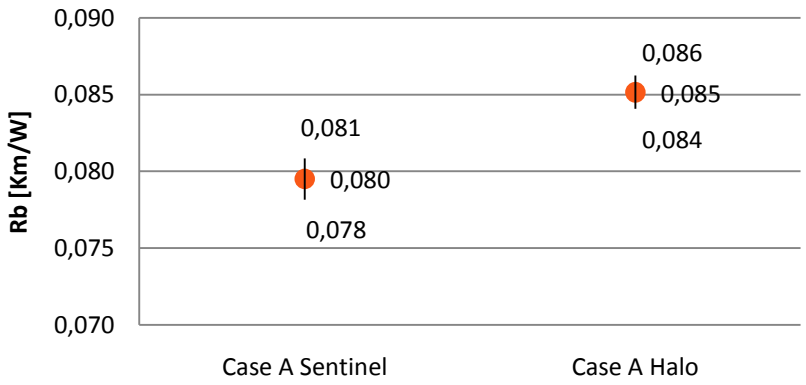

Figure 86. *Section 6: Average thermal resistance and its variation.*

Figure 87 shows the measured and calculated temperature profiles obtained by means of Sentinel and Halo data for a constant heat power. It can be observed more significant deviations between the calculated and measured profile in Sentinel case, which are related to the most significant heat power variations.

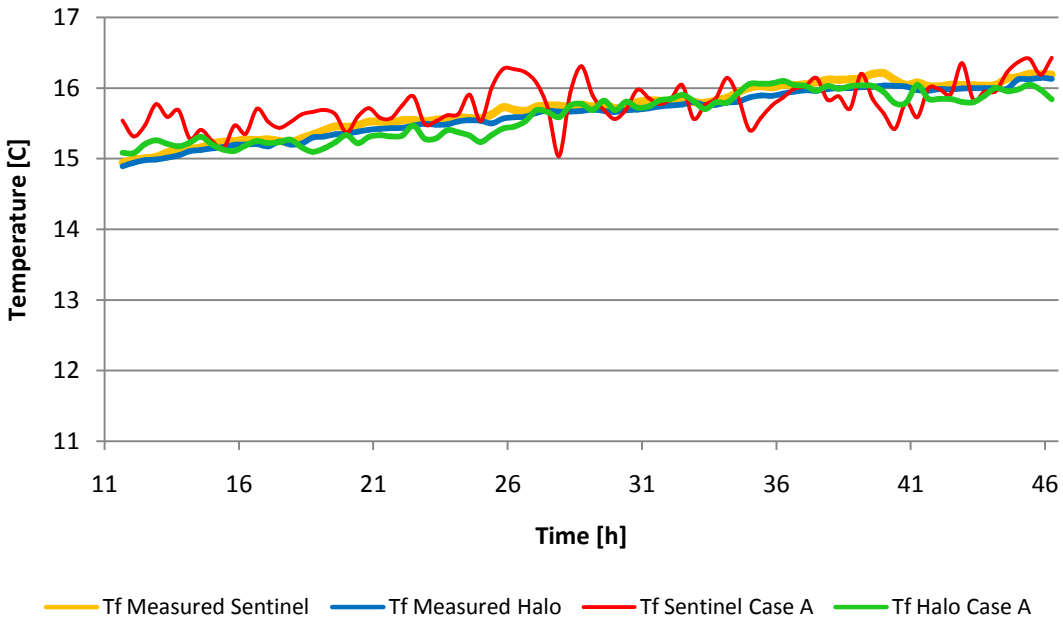

Figure 87. *Section 6: Profiles of measured and calculated temperatures.*

To measure the deviation between the calculated and measured temperatures, it is calculated its difference in each interval of time. It is shown in *Figure 88,* being the average difference is equal to 0.07 [C] in Sentinel results. Its variation ranges between -0.23 to 0.37 [C].In next figure, it is also shown the results of Halo-case A-. It can be observed that Halo results present a less difference.

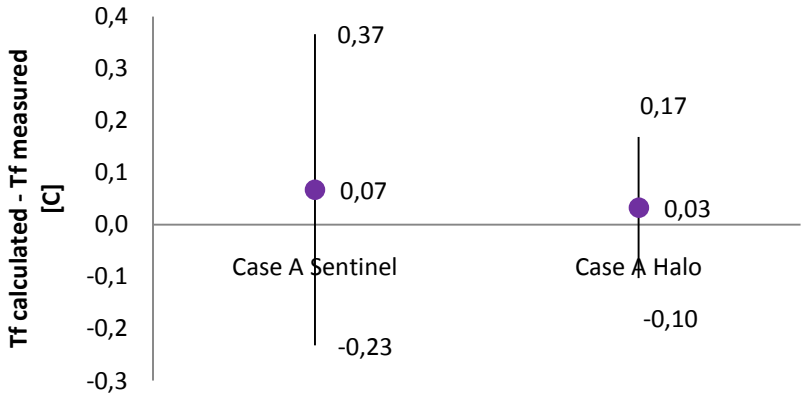

Figure 88. *Section 6: Average of ($Tf_{calculated}$- $Tf_{measured}$) and its variation.*

- ***SECTION 7***

The thermal conductivity is equal to 3.92 [W/mK] in section 7, in which it is assumed a constant heat power in Sentinel data. As regards as heat power rate, it can be observed that it varies in wide range between 52 and 37 [W/m]. In this section, the thermal resistance profile fluctuates over 0.07 [Km/W].

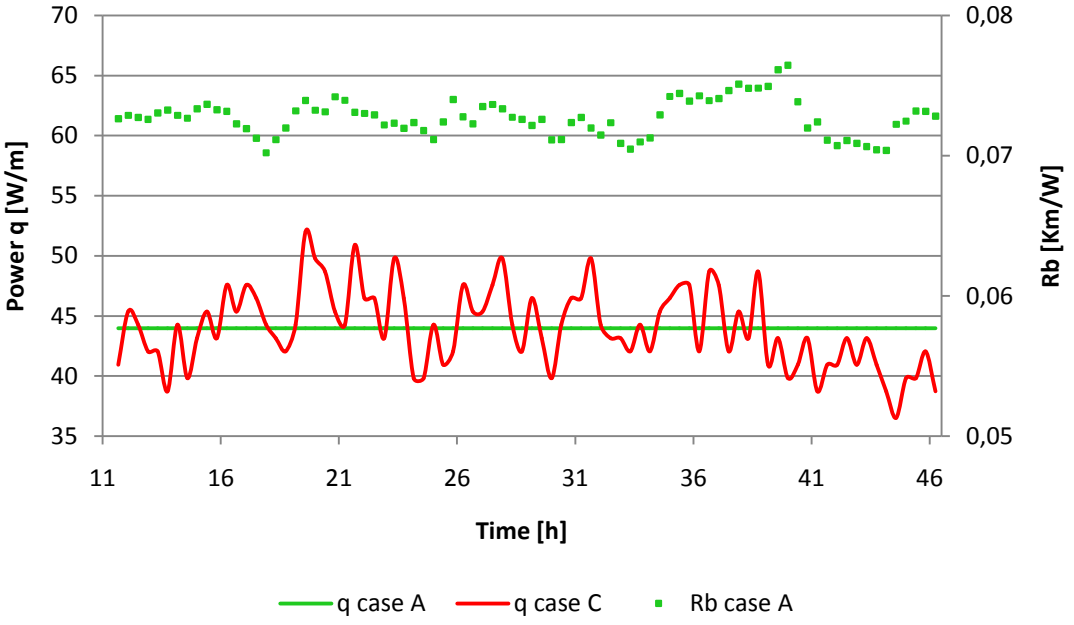

Figure 89. *Section 7: Thermal resistance profile according to constant heat power supply.*

Averaging all values from thermal resistance profile, it is equal to 0.073 [Km/W] in Sentinel results. Its deviation from the average thermal resistance is about ± 0.0015 [Km/W].In next figure, it is also included the results from Halo data for a constant heat power.

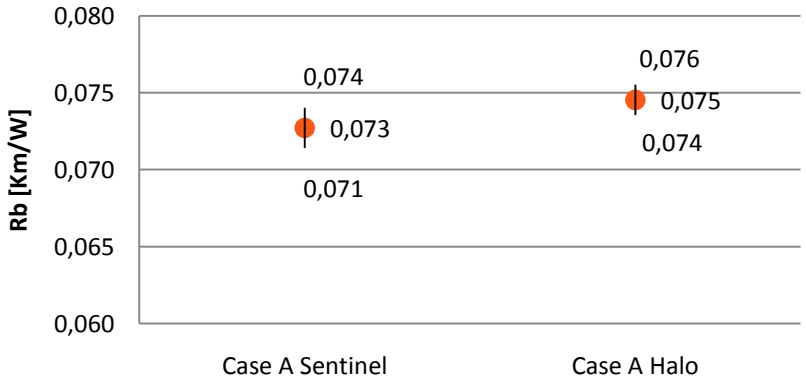

Figure 90. *Section 7: Average thermal resistance and its variation.*

According to Sentinel results, *Figure 91* shows the profiles of the measured and calculated temperatures. In this figure, it is also included the measured and calculated temperature from Halo data. It can be observed that results from Halo data present the best fit to the profile of measured temperatures.

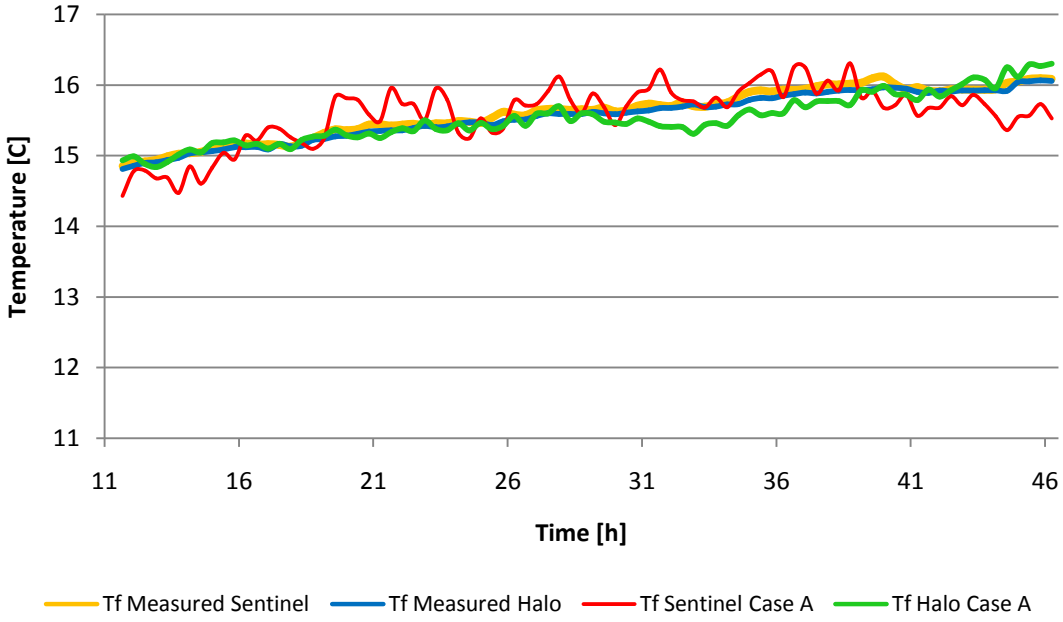

Figure 91. *Section 7: Profiles of measured and calculated temperatures.*

Evaluating Sentinel results, the average of the difference between the measured and calculated temperature is equal to -0.02 [C]. Taking into account its standard deviation, the ($T_{fmeasured}$-$T_{fcalculated}$) values fluctuate from its mean value within the range -0.30 to 0.26 [C]. Next figure also shows the results from Halo data.

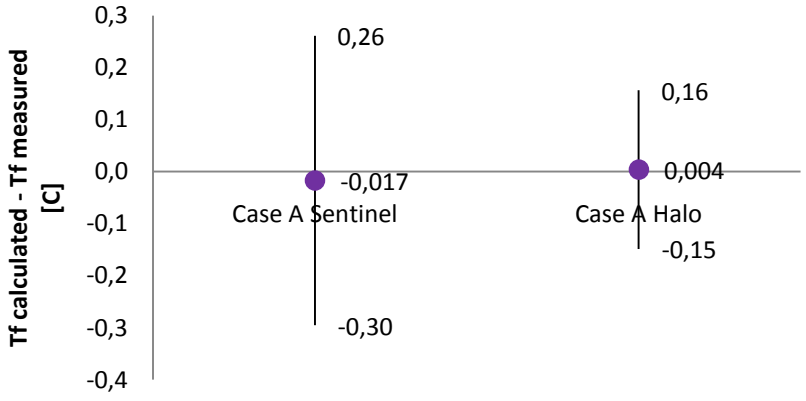

Figure 92. *Section 7: Average of ($Tf_{calculated}$- $Tf_{measured}$) and its variation.*

- ***SECTION 8***

Assuming a constant heat power in Sentinel data– case A -, the thermal conductivity is equal to 3.78 [W/Km]. In this section, it can be observed that heat power rate varies within the range 31 to 52 [W/m]. Moreover, the thermal resistance profile varies around 0.07 [Km/W] as shown in *Figure 93*.

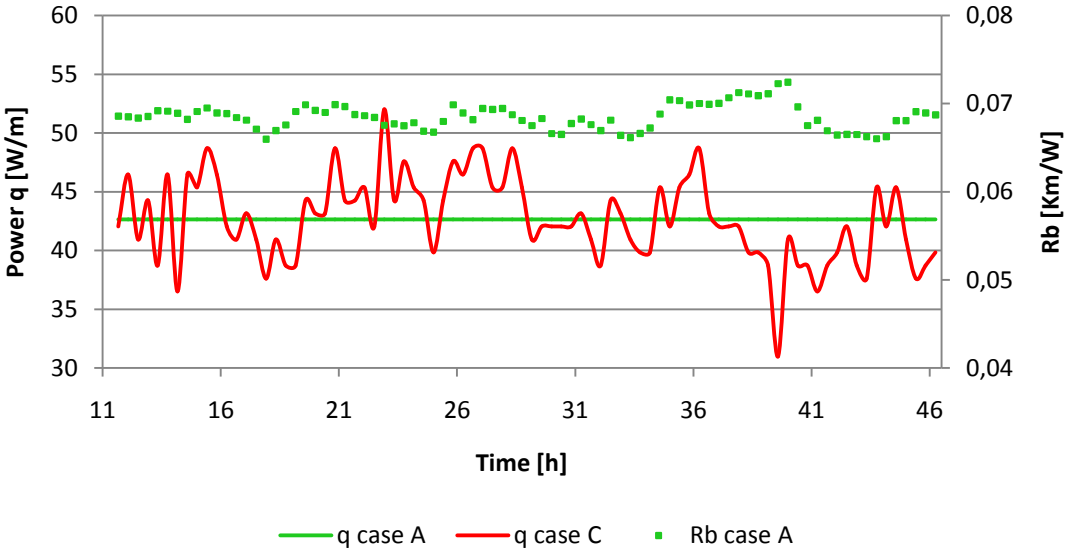

Figure 93. *Section 8: Thermal resistance profile according to constant heat power supply.*

In section 8, the average thermal resistance is equal to 0.068 [Km/W] in Sentinel results and its standard deviation is about 0.0015 [Km/W].

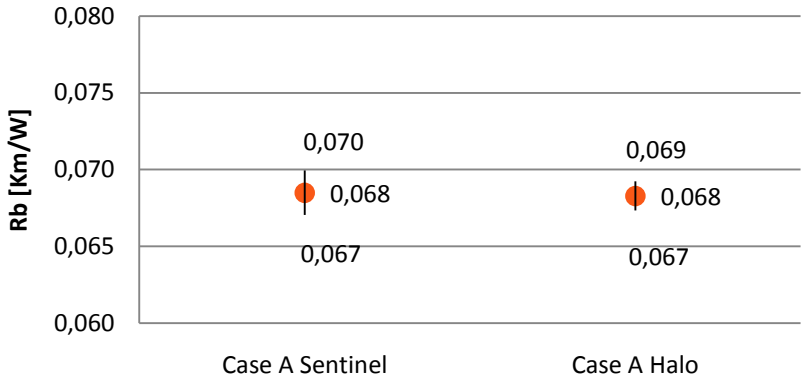

Figure 94. *Section 8: Average thermal resistance and its variation.*

Figure 95 presents the profile of measured and calculated temperatures in section 8 from Sentinel and Halo data for a constant heat supply. In the same way as results from section 7, there is a good fit between both profiles for certain periods of time in Sentinel results. However, Halo results present the best fit during the whole period. To evaluate the approximation of calculated temperatures to measured temperature, it is calculated the difference between both results.

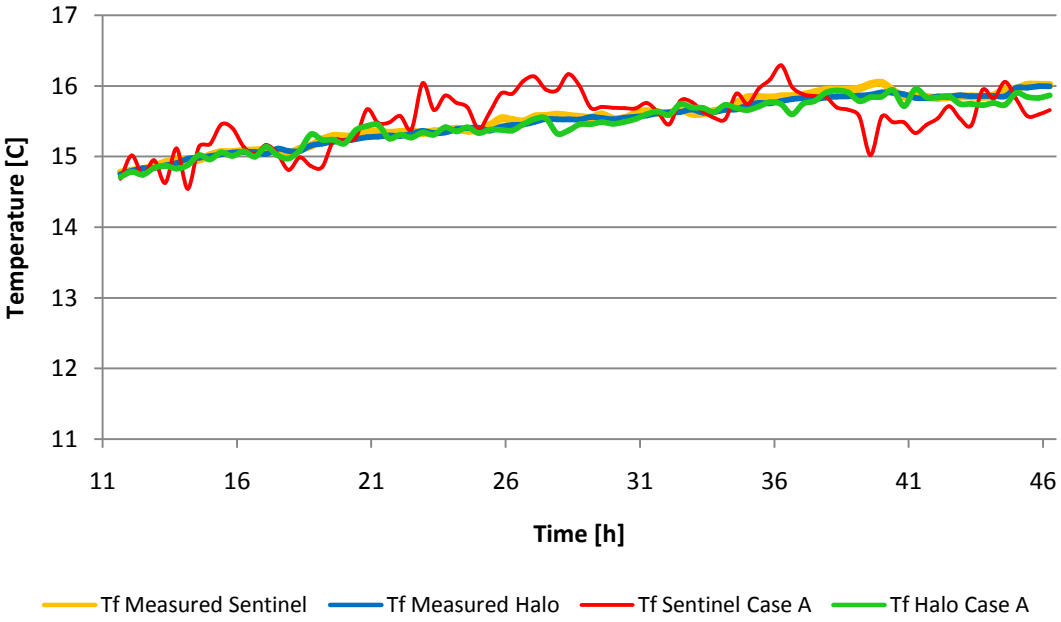

Figure 95. *Section 8: Profiles of measured and calculated temperatures.*

As regards as Sentinel results, averaging difference between the measured and calculated temperature, it is equal to -0.02 [C]. Calculating its standard deviation, this difference fluctuates from its mean value within the range -0.32 to 0.29 [C]. Next figure shows also the results from Halo data. Comparing Sentinel and Halo results, Halo case presents the lowest difference between the measured and calculated temperature, on average.

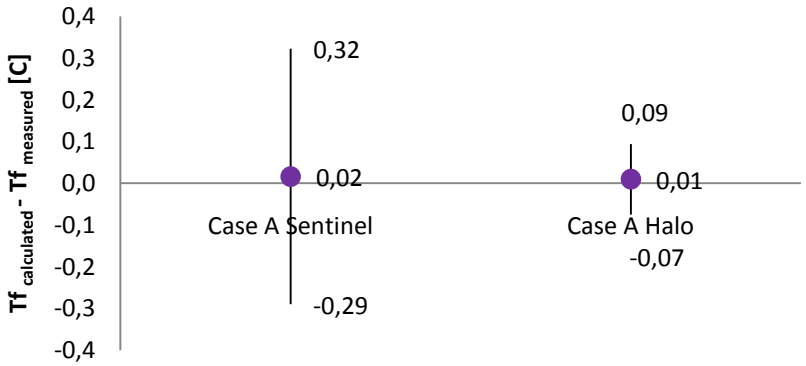

Figure 96. *Section 8: Average of ($Tf_{calculated}$- $Tf_{measured}$) and its variation.*

- ***SECTION 9***

In section 9, the thermal conductivity estimated is 3.77 [W/Km] by assuming a constant heat power in Sentinel data. Moreover, it can be observed important variations in the power rate during the heating phase. The heat power range between 35 and nearly 50 [W/m].As regards as thermal resistance profile, it is varies over 0.06 [Km/W].

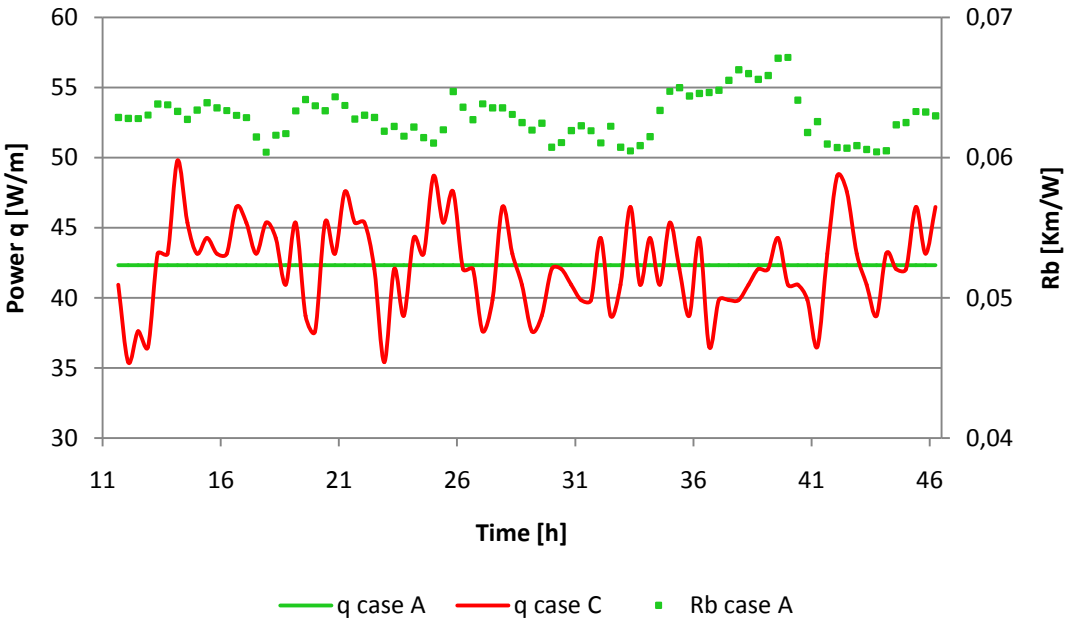

Figure 97. *Section 9: Thermal resistance profile according to constant heat power supply.*

Averaging all values of thermal resistance profile in Sentinel results, it is equal to 0.063. Calculating its standard deviation, the variation from its mean value is between 0.061 and 0.064 [Km/W].In next figure, it is also included the results from Halo data for a constant heat power.

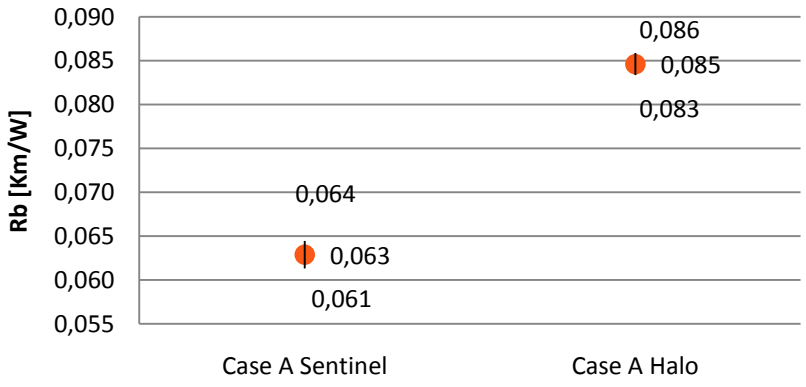

Figure 98. *Section 9: Average thermal resistance and its variation.*

Figure 99 shows the profiles of the measured and calculated temperatures evaluating by Halo and Sentinel data. In Sentinel data, the profile of calculated temperatures varies around the profile of measured temperatures; however, the Halo profile of calculated temperatures presents the best fit to its profile of measured temperatures.

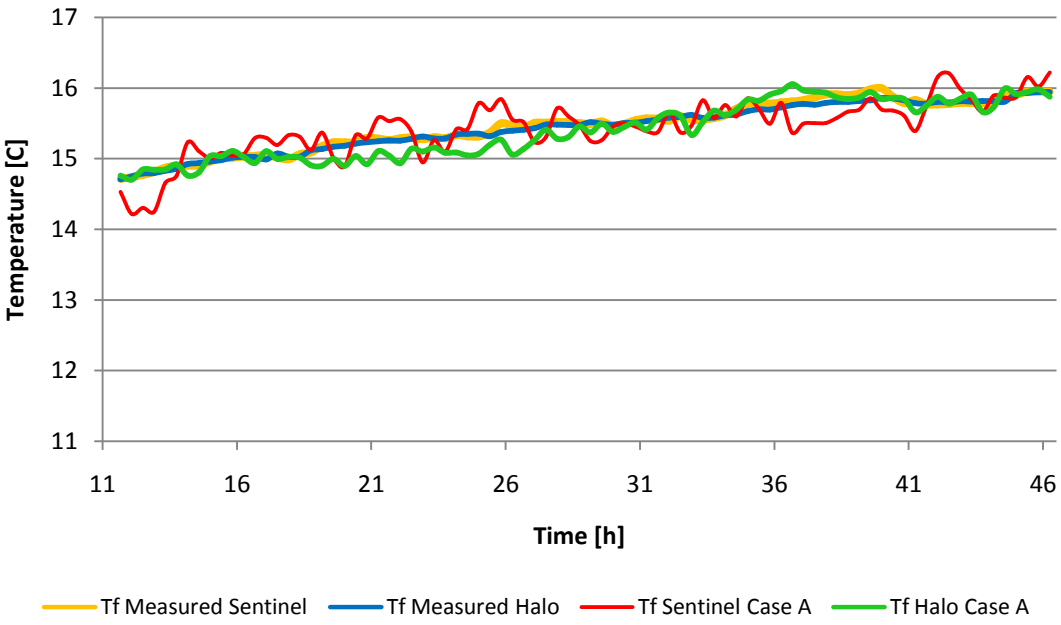

Figure 99. *Section 9: Profiles of measured and calculated temperatures.*

Averaging the difference between the profiles of measured and calculated temperatures, this value is equal to -0.02 [C] in Sentinel case and it varies between -0.26 and 0.22 [C]. In next figure, it is also shown the results from Halo data assuming a constant heat power -case A-. Comparing Halo and Sentinel results, the lowest difference between the measured and calculated temperature is observed in Halo case, in a good accordance with the results show in the previous figure.

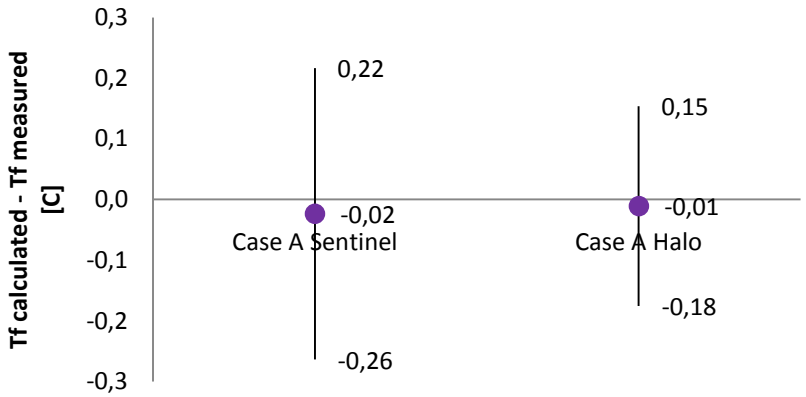

Figure 100. *Section 9: Average of ($Tf_{calculated}$- $Tf_{measured}$) and its variation.*

- ***SECTION 10***

The thermal conductivity is equal to 3.24 [W/mK] considering Sentinel data for a constant heat power supply. In this section the heat power rate varies within the range between 31 and 43 [W/m], as presented in *Figure 101*. Moreover, it can be observed the thermal resistance profile, which presents values over 0.06 [Km/W].

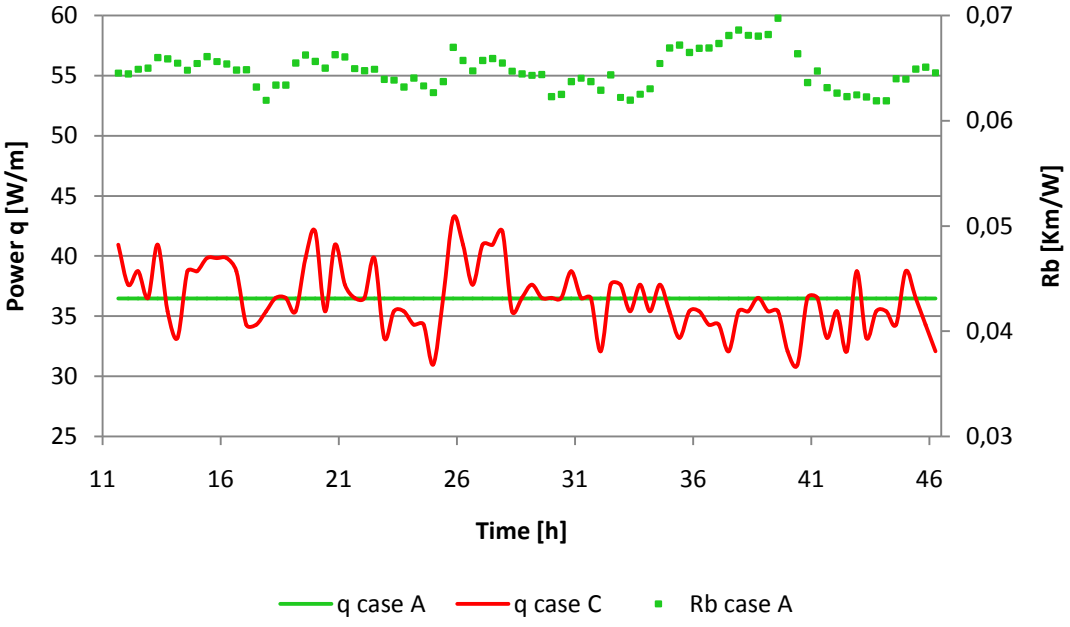

Figure 101. *Section 10: Thermal resistance profile according to constant heat power supply.*

In Sentinel results, the mean value of thermal resistance is equal to 0.065 [Km/W]. The Sentinel profile of the thermal resistance varies from its average within the range 0.063 to 0.067. In next figure, it is also shown the results from Halo data.

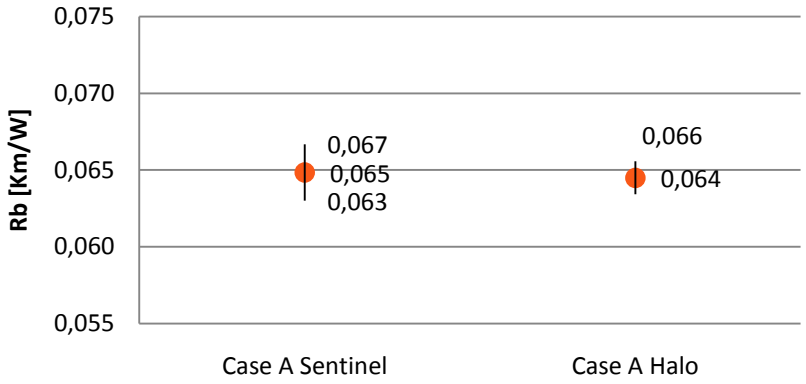

Figure 102. *Section 10: Average thermal resistance and its variation.*

The profiles of measured and calculated temperatures of Halo and Sentinel cases are compared in *Figure 103*. It is calculated the difference between both profiles in each equipment data in order to evaluate the fit. The results are presented in *Figure 104*.

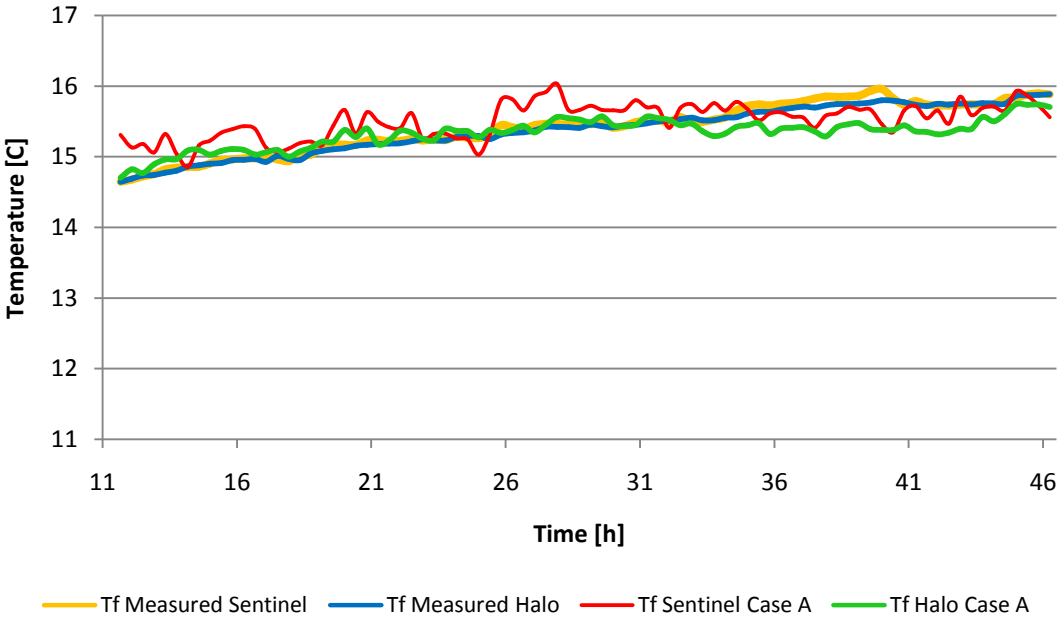

Figure 103. *Section 10: Profiles of measured and calculated temperatures.*

According to Sentinel results, the difference between the measured and calculated temperatures is equal to 0.1 [C] on average. This difference varies between -0.15 and 0.36 [C] according to its standard deviation. In next figure, it is also included the results from Halo data. On average, the calculated temperature profile from Halo data fit better to its measured temperature profile.

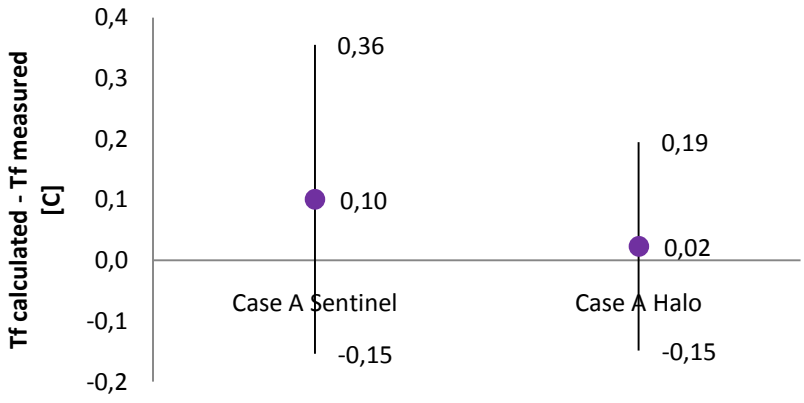

Figure 104. *Section 10: Average of ($Tf_{calculated}$- $Tf_{measured}$) and its variation.*

- ***SECTION 11***

The rock thermal conductivity is equal to 3.16 [W/Km] in section 11 for a constant heat power in Sentinel data. In *Figure 105*, it can be observed the constant heat power using in calculations. However, the heat power presents significant variations of the flow injection. The flow varies between 26 and 50 [W/m], approximately. Moreover, it is presented the profile of thermal resistance, which shows a significant variation on 40-hours test according to the variation of temperature measurements in this interval, as presented in *Figure 107*.

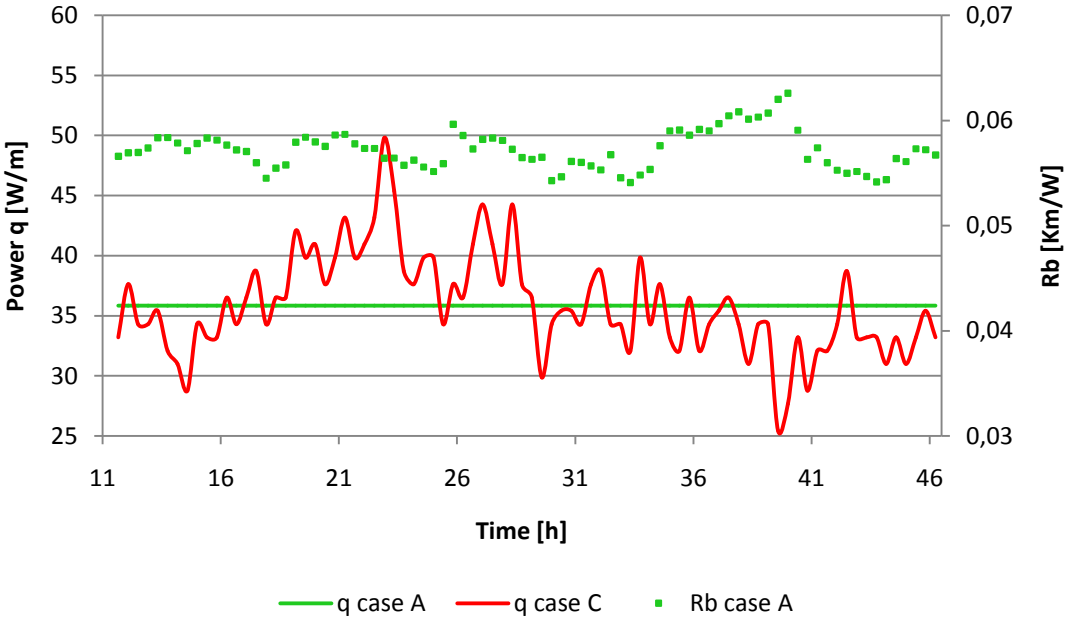

Figure 105. *Section 11: Thermal resistance profile according to constant heat power supply.*

In Sentinel data, the average thermal resistance is equal to 0.057 [Km/W] and its standard deviation presents a value of ±0.002 [Km/W].

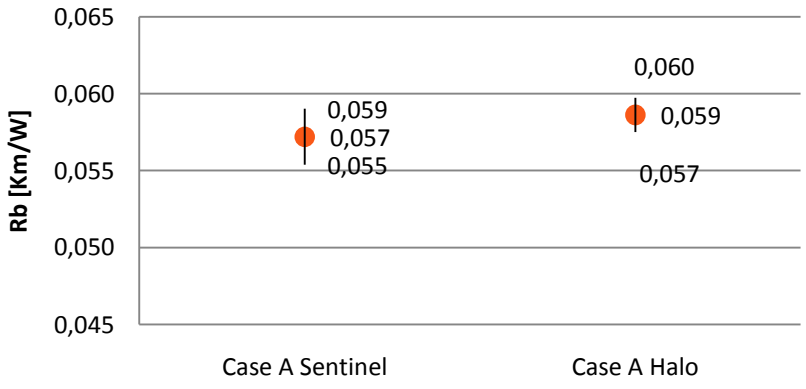

Figure 106. *Section 11: Average thermal resistance and its variation.*

Figure 107 shows the profiles of measured and calculated temperatures in section 11 obtained by means of data from Halo and Sentinel DTS-equipment. It can be observed significant differences between the measured and calculated profiles in Sentinel case. Evaluating Sentinel results, these differences happen when the heat power rate presents high variations. However, the calculated temperature profile presents a good fit when the heat power fluctuates within a tight range. It can be observed that profile of calculated temperature from Halo data fits better to its profile of measured temperature than profiles of temperatures from Sentinel.

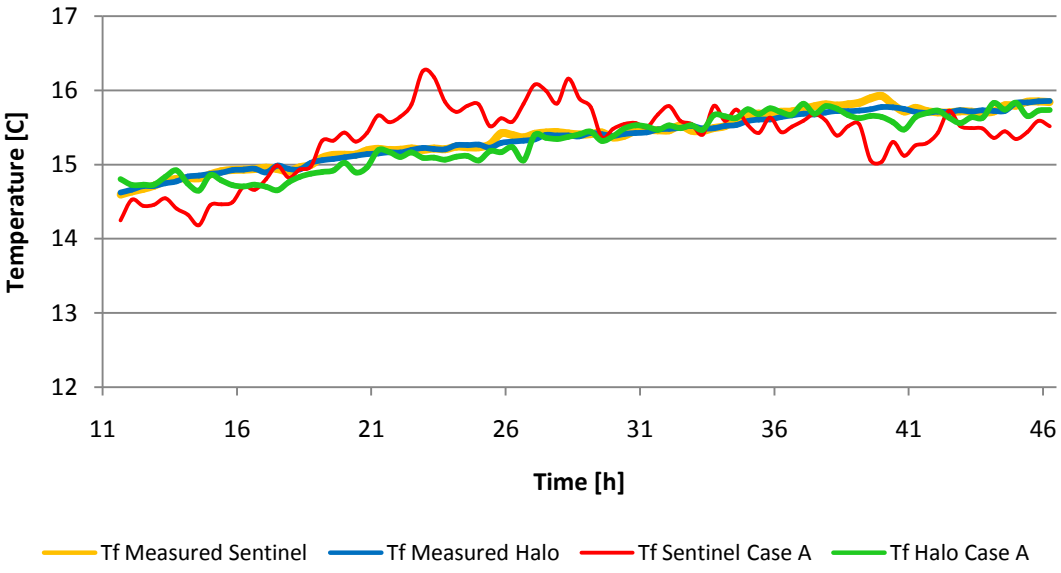

Figure 107. *Section 11: Profiles of measured and calculated temperatures.*

Although there are some periods in which the difference between the measured and calculated temperature is about 1[C] in Sentinel results, the average of this difference is equal to 0.01 because of the periods with good fit. The standard deviation of the difference between the measured and calculated temperature profile in Sentinel case is about ±0.40 [C], which is higher than the difference from Halo case.

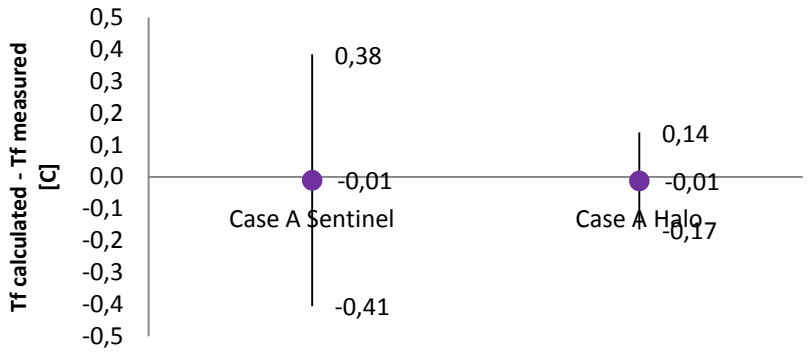

Figure 108. *Section 11: Average of ($Tf_{calculated}$- $Tf_{measured}$) and its variation.*

- ***SECTION 12***

In section 12, the thermal conductivity is equal to 3.15 [W/Km] for a constant heat power –case A- in Sentinel data. In *Figure 109*, it can be observed the variations of heat power, which range between 30 and 45 [W/m]. Moreover, the thermal resistance profile is also presented in this figure, which varies around 0.05 [Km/W].

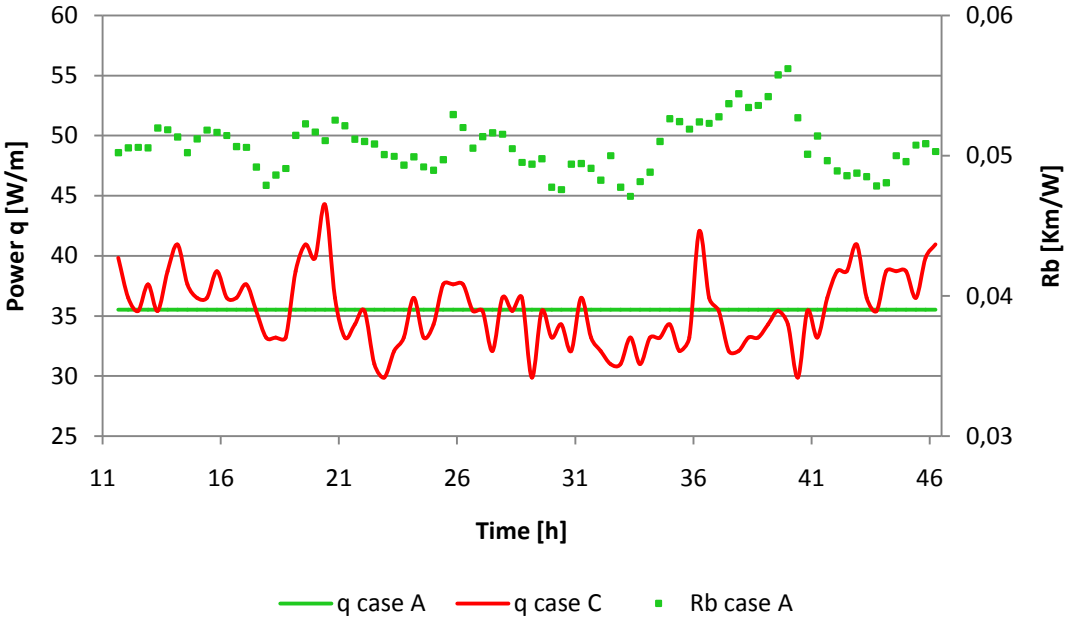

Figure 109. *Section 12: Thermal resistance profile according to constant heat power supply.*

Averaging all values of thermal resistance profile in Sentinel results, thermal resistance is equal to 0.051 in section 12. Its standard deviation is about ±0.002 [Km/W].

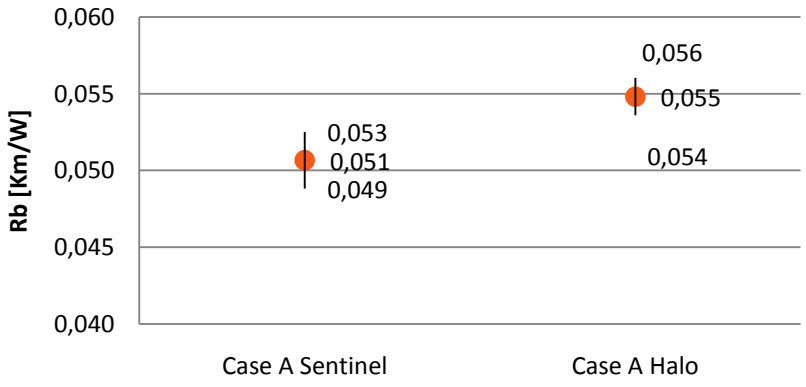

Figure 110. *Section 12: Average thermal resistance and its variation.*

The profiles of the measured and calculated temperatures are presented in *Figure 111*.It is shown the results from Halo and Sentinel data. For 21-hours Sentinel test, it can be observed a significant difference in temperature. To evaluate the fit between both in each readout equipment, it is calculated the differences between every pair of $T_{fmeasured}$ and $T_{fcalculated}$ in each interval of time.

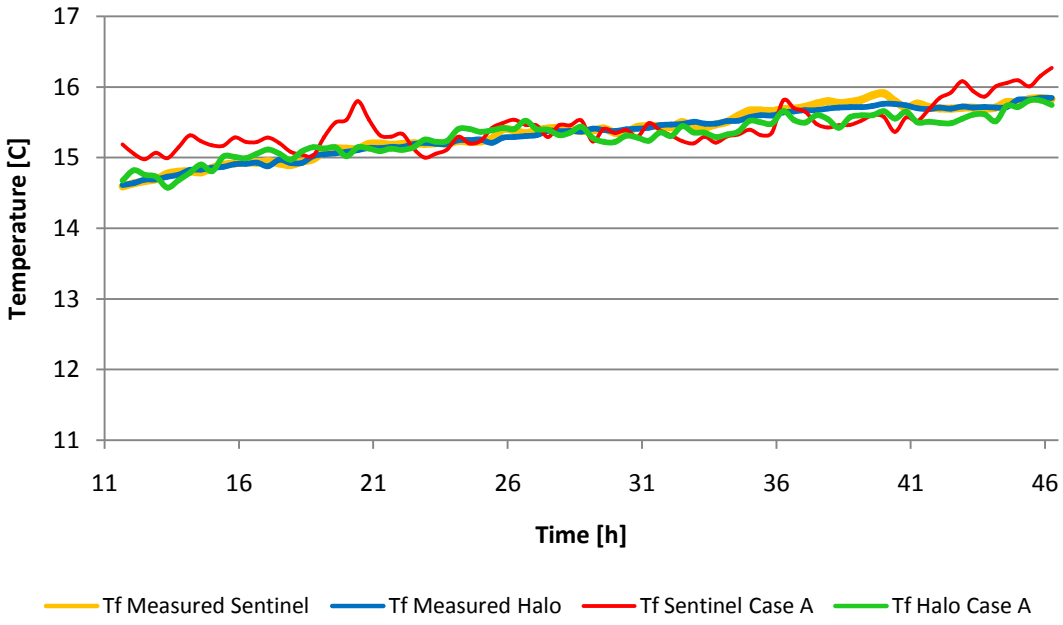

Figure 111. *Section 12: Profiles of measured and calculated temperatures.*

As regards as Sentinel data, averaging the difference between both temperatures, it is equal to 0.07 [C] and its standard deviation is about 0.25 [C]. It is shown in *Figure 112* together with the results from Halo data. It can be observed that the average difference is lower in Halo results, which is in a good accordance to the results show in *Figure 111*.

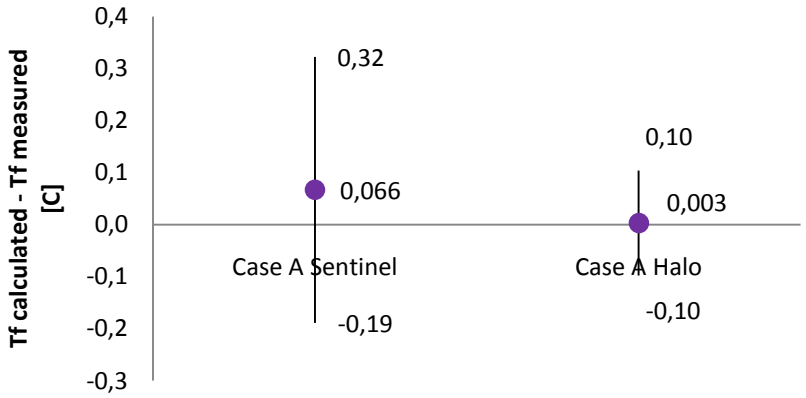

Figure 112. *Section 12: Average of ($Tf_{calculated}$- $Tf_{measured}$) and its variation.*

For each borehole section, the value of thermal conductivity and the average thermal resistance, which result from Sentinel data, are presented together with the results from Halo- case A- in *Figure 113.*

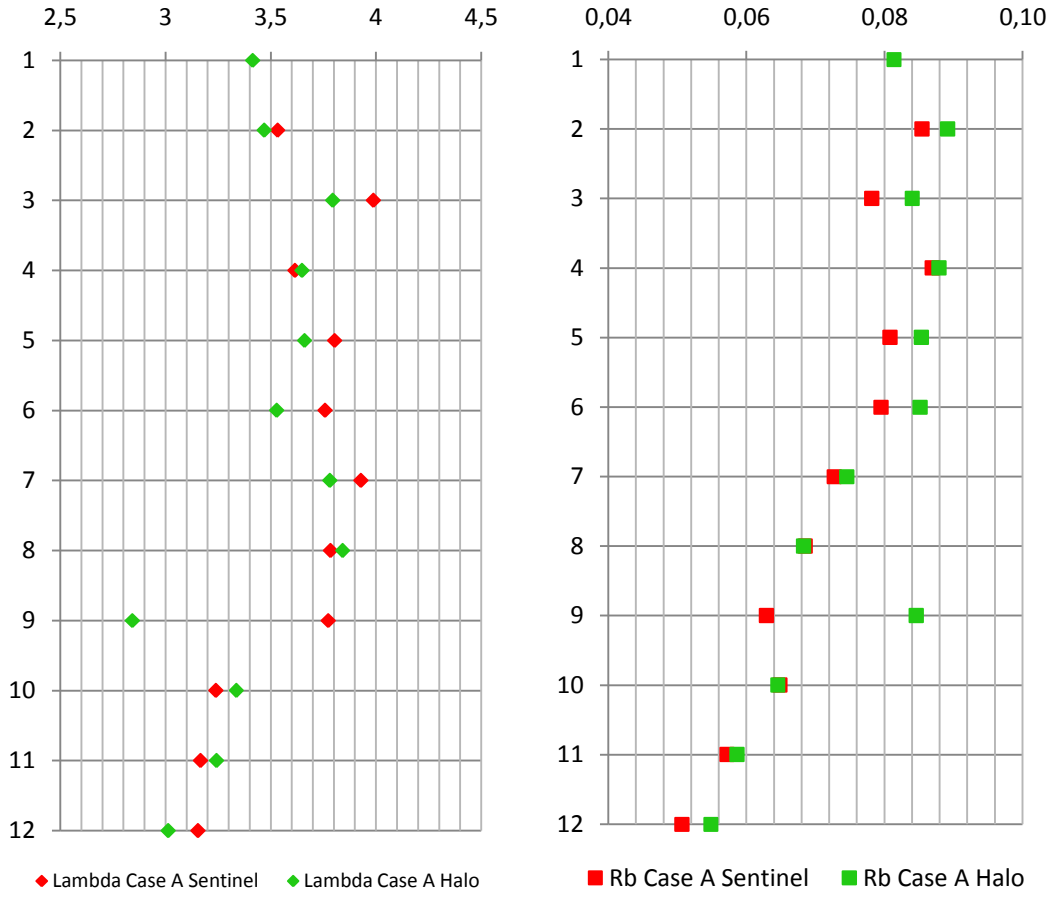

Figure 113. *Thermal conductivity and thermal resistance in each borehole section. (Sentinel data-Case A and Halo data-Case A).*

In *Figure 113*, it can be observed that section 1 presents anomalous results of the thermal conductivity and the thermal resistance. As shown above, the heat power data in section 1 present the highest values in comparison with the rest of borehole sections. This may be related to the anomaly detected in results of thermal parameters. Moreover, these results present a significant deviation from the results of Halo –case A- and Integral Method. Therefore, the results from section 1 are not taking into the account to assess the borehole thermal parameters and to compare with Halo and Integral Method results from Acuña (2010).

For Sentinel data, the average of the rock thermal conductivity is equal to 3.61[W/Km] and this parameter varies within the range 3.99 to 3.15 [W/Km]. Notice that the average does not take into account the value of section 1. It is presented in *Figure 114.*

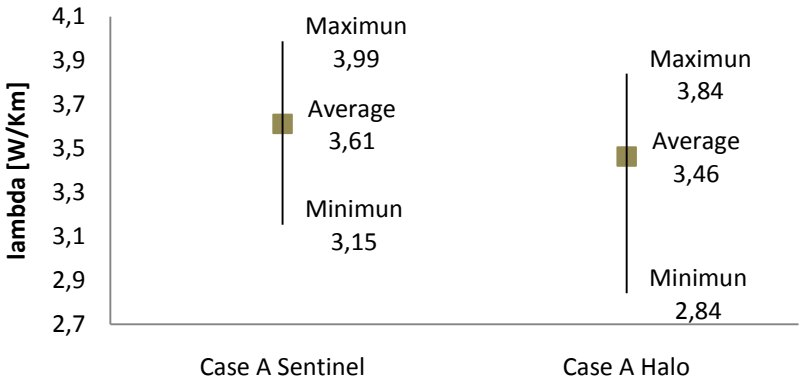

Figure 114. *Rock thermal conductivity: average, maximum and minimum. (Sentinel data-Case A and Halo data-Case A).*

In the same way, the mean value of the borehole thermal resistance without considering section 1, estimating by means of measurements from Sentinel equipment, is equal to 0.072 [Km/W] and its values range between 0.051 and 0.087 [Km/W] along the borehole sections.

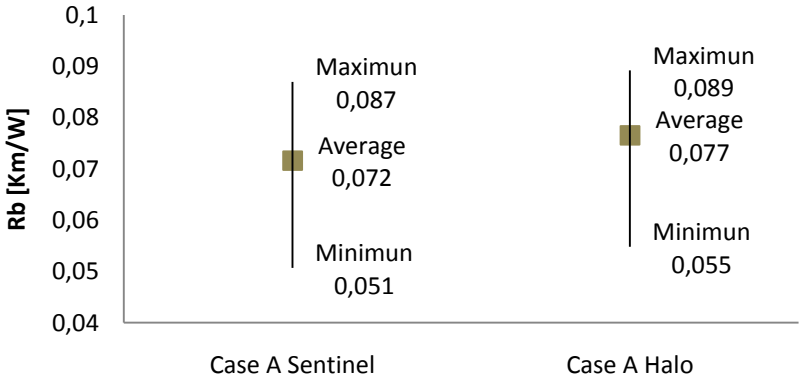

Figure 115. *Borehole thermal resistance: average, maximum and minimum (Sentinel data-Case A and Halo data-Case A).*

3.3. Results comparison.

3.3.1. Comparison of Halo and Integral Method results.

The results of thermal conductivity and thermal resistance from Halo equipment and the results of Integral Method from Acuña(2010) are shown in *Figure 116* (a) and (b), respectively.

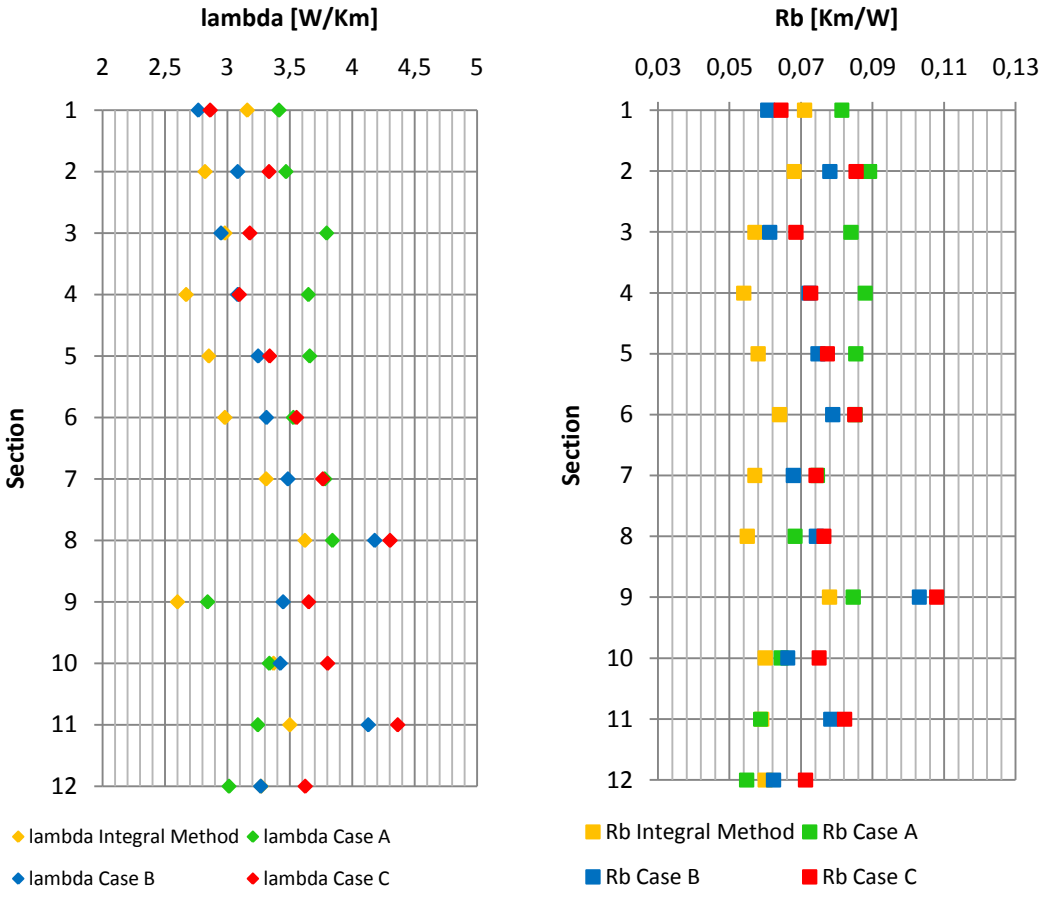

Figure 116. *(a) Thermal conductivity and (b) Thermal resistance in each borehole section (Integral Method and Halo - (Case A, B and C) results).*

Firstly, the uncertainties due to the assumption of constant heat power rate are analyzed considering the results of Halo case A, B and C. To assess which case of heat power supply – constant or by steps (7.5-hours or 25 minutes) - gives the best approximation to the profile of measured temperatures, it is averaged the mean values of ($T_{fmeasured}$-$T_{fcalculated}$) calculated in all sections. This result is equal to 0.001 [C] in case B. This is about 0.005 [C] in case C. And it is equal to 0.013 [C] in case A. The cases B and C, which assume heat power by steps, present a better fit than case A, which assumes a constant heat power rate. Moreover, the values of case B and C are very close; however case A differs from case B a value of 0.012 [C].

Since case C assumed the tightest heat power steps, it should have presented the best fit; however it is not shown up in the results. It may attribute to the uncertainties in measurements. This suggests that the heat power step should be determined considering more measurements points in order to get a better fit in the estimation of the heat power rate injected. Therefore, case B presents the best fit between the measured and calculated temperature on average; thus, this case of heat power rate can provide more accurate estimates. This result is in a good accordance with the influence of heat power variations to the accuracy in the borehole thermal parameters estimate.

Considering the heat power rate and the estimates of thermal conductivity in each borehole section for a 7.5 hours stepwisely heat power supply –case B-, the value of these estimates may be attributed with the value of the first heat power step considered in the analysis. If the first interval of time presents a significant value of heat power rate, which is lower than its mean value, the thermal conductivity estimation presents a higher value than the estimate made by assuming a constant heat power, for instance this situation happens in section 8 and 10. In contrast, if the heat power rate during the first interval of time presents a higher value than its mean rate, the thermal conductivity presents lower value than the value provides for a constant heat power rate; for instance in section 3. It is in a good accordance with the profile along the borehole depth of the thermal conductivity shown in case of a constant heat power rate -case A- and the profile for a 7.5 hours stepwisely constant heat power-case B-.

According to the thermal resistance profiles in cases A, B and C present the same distribution along the borehole depth as the thermal conductivity, the differences in the estimates between the three different cases of heat power supply may be attributed to the heat power rate during the first intervals of time. Since the thermal resistance is a sum of thermal resistance of heat carrier fluid circulating through the pipe, the thermal resistance of the filling material and the borehole wall thermal resistance, the variation in the value of thermal resistance along the borehole depth may be attributed to the convective heat and the variation in the geological characteristics of the ground.

The results of thermal conductivity in Halo case A, B and C are compared with the results of Integral Method; mostly sections present the smallest value for the results from integrating calculations (Acuña (2010)). This is an exception in sections 1, 10, 11 and 12, in which the cases by steps of Halo data present a lower thermal conductivity. It is shown in *Figure 116* (a). However, there are not significant variations between all results in each section. Since the results of the Integral Method were obtained by means of the main equation of Line Source Theory - without any approximation- and using Halo data, comparing with the results obtained in this thesis by Halo data-which have been compiled in section 3.1.-, the analysis procedure is assessed. For this purpose, the difference between the values of the Integral Method and the values of Halo are calculated. As a result, the case B presents the smallest deviation of thermal conductivity on average and it is equal to 0.27 [W/Km]. The results of all cases are presented in *Figure 117*.

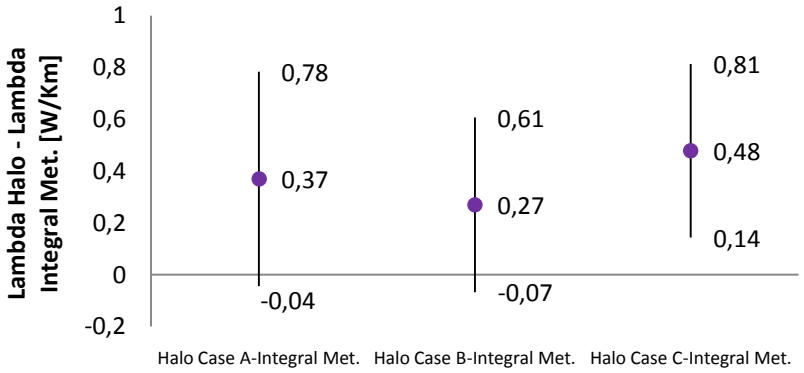

Figure 117. *Comparison of rock thermal conductivity (Halo vs Integral Method).*

As regards as the borehole thermal resistance, *Figure 116* (b) shows that the results from Acuña (2010) present the smallest values, except in section 1 and 12 where the thermal resistance is smaller in Halo results. However, it can be observed that the thermal resistance profile along the borehole depth is very similar in all borehole section analyzed. In the same way as thermal conductivity, it is calculated the difference between the result from Integral Method and Halo. The results show that the less difference in the estimation of borehole thermal resistance show up in case B, which is only about 0.011 [Km/W].It is presented in *Figure 118*. Consequently, this comparison suggests that case B presents the best fit in estimation for the rock thermal conductivity and the borehole thermal resistance.

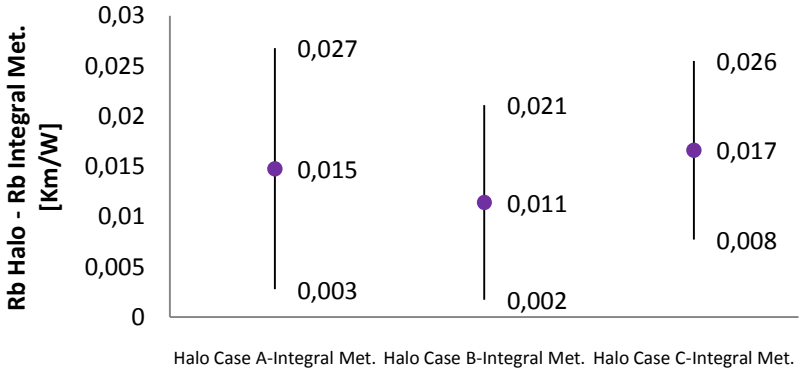

Figure 118. *Comparison of borehole thermal resistance (Halo vs Integral Method)*

3.3.2. Comparison of Sentinel and Integral Method results.

The rock thermal conductivity and borehole thermal resistance from Integral Method and Sentinel results are presented in *Figure 119*. Since the results of both thermal conductivity and thermal resistance in section 1 present anomalous values, these are not included in the graph. As mentioned in section 3.2, the data of Sentinel equipment are only analyzed assuming a constant heat power –case A-.

Firstly, the results from Sentinel are analyzed according to the temperature measurements. In section 3.2, the mean value of the difference between the calculated and measured temperature is presented in each section as well as its deviation. Averaging all sections, the result of these differences is equal to 0.017 [C]. Since Sentinel data are only analyzed for a constant heat power supply, it cannot compare with the results from a heat power supply by steps.

There are two differences between the results of Integral Method and Sentinel equipment: the calculating procedure and the data. Whereas Integral Method applied the line source theory to the data of Halo, the results from Sentinel are determined by means of an approximation of line source theory and the data from Sentinel DTS-equipment. It is important to bear in mind that the resolution of Sentinel equipment is greater than Halo DTS-equipment and Sentinel data are only analyzed assuming a constant heat power, as explained above in section 3.2.

In *Figure 119* (a), it can be observed that there are not relevant differences between both estimations in thermal conductivity. The seven first sections present more differences in the estimation of this parameter, showing up the smallest value in Integral Method results. In section 7 and onwards, the values are closer between both cases. However, there is an exception in section 9, where the values are extreme in opposite directions and Integral Method estimation is greater than Sentinel parameter. Moreover, it should be noticed that there is not a relevant difference in parameters between section 8 and 9 in Sentinel case.

The thermal resistance distribution along depth of borehole is very similar to the path drawn by the thermal conductivity, as shown in *Figure 119* (b); it may be attributed with the heat power considered in the analysis. In eight first section, the estimations of Integral Method present smaller values. As thermal conductivity results, in section nine the value from Sentinel data is smaller. In the last sections, the values from both cases have not the same tendency as thermal conductivity, but they present a close estimation in both analyzed cases.

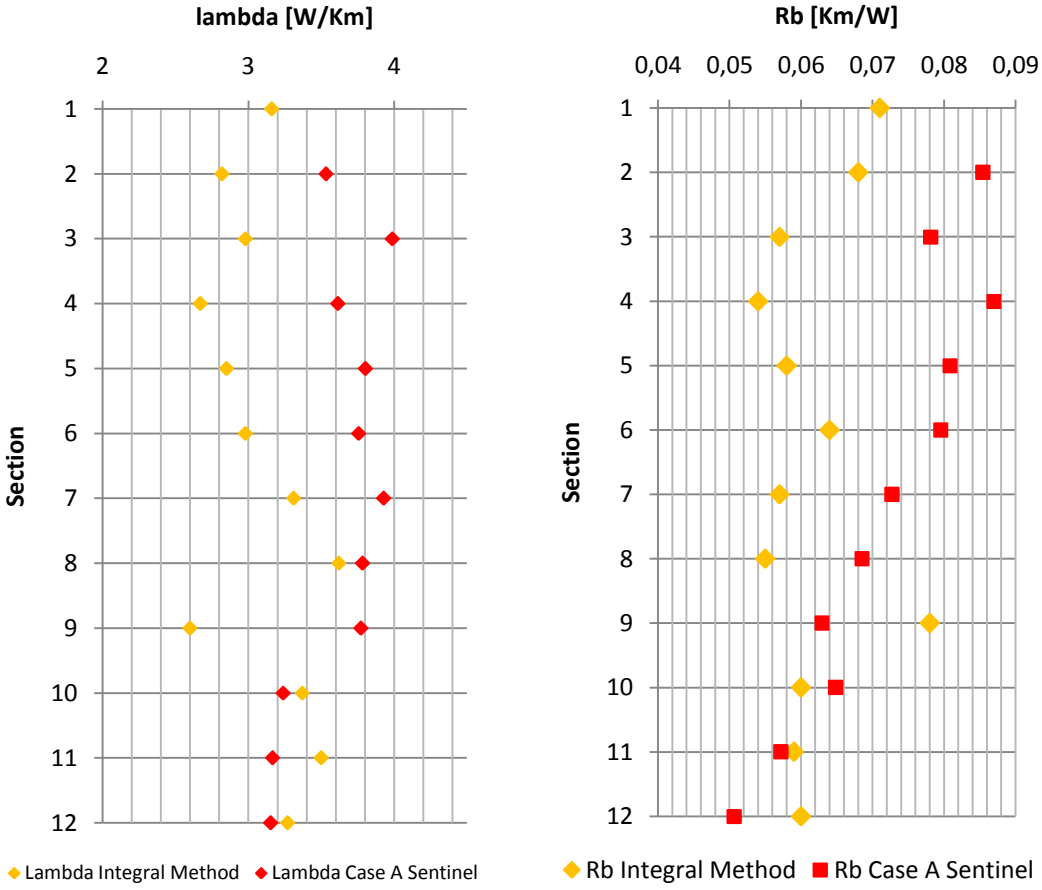

Figure 119. *(a) Thermal conductivity and (b) Thermal resistance in each borehole section (Integral Method from Acuña (2010) and Sentinel - (Case A) results).*

It is calculated the difference between the result from Integral Method and Sentinel for both estimates of thermal parameter. The rock thermal conductivity difference between the Integral Method and Sentinel case A results is equal to 0.52 [W/Km] on average. In the same way, the difference in the thermal resistance is equal to 0.011 [Km/W]. These results and their deviation, which are calculated according to its standard deviation, are presented in *Figure 120* (a) and (b), respectively.

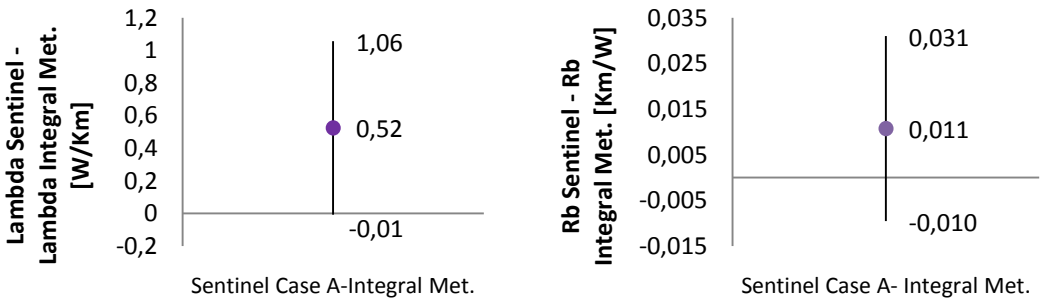

Figure 120. *Comparison of (a) rock thermal resistance and (b) borehole thermal resistance (Sentinel vs Integral Met).*

3.3.3. Comparison of Halo, Sentinel and Integral Method results.

In this chapter, the rock thermal conductivity and the borehole thermal resistance result from Halo and Sentinel data, both in the case of a constant heat power supply, are compared with the values estimated from Integral Method. All these results of both parameters in each borehole section are presented in *Figure 121*.

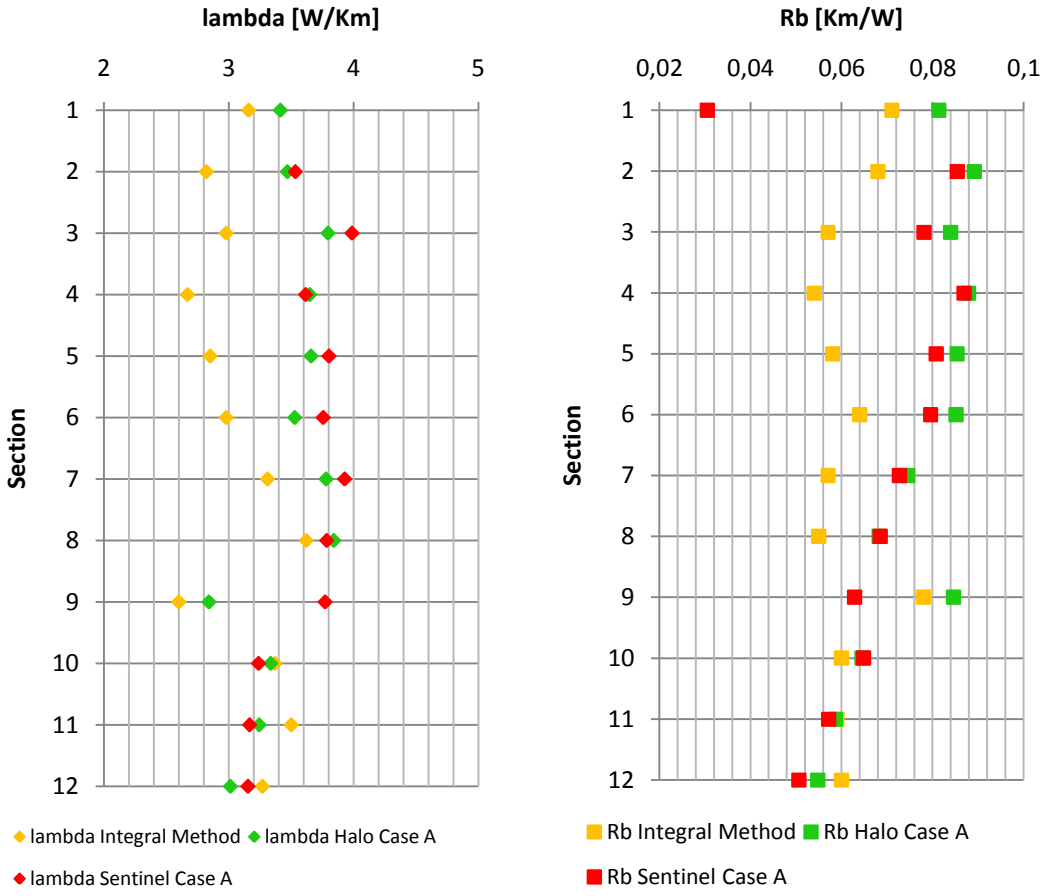

Figure 121. *Comparison of thermal conductivity and thermal resistance in each borehole section. (Integral Met. from Acuña (2010), Halo Case A and Sentinel Case A results).*

The thermal conductivity profile resulting from Halo and Sentinel present a similar distribution along the depth profile. There is only an exception in section 9, in where the value of Halo presents a value closer to the value of Integral Method. Since Halo and Sentinel are evaluated by the same procedure and Integral Method is estimating by Halo data, this result may indicate an anomaly in the measurements of Halo DTS-equipment.

Comparing Halo data with Sentinel data in each section, there are not any anomalies in temperature measurements. However, the heat power presents a significant difference in the average flow between the data of Halo and Sentinel equipments. In *Figure 122*

and *Figure 123,* it can be observed that there is a relation between the difference in heat power of Halo and Sentinel data and the differences in the both estimated parameter from Halo and Sentinel data. Thus, this suggests that there is no relevant difference in the estimation of parameters between the data read by the two different resolution equipments: Halo and Sentinel DTS-equipment.

Moreover, it can be observed that the heat power flow in Halo data trends to a certain value around 40 [W/m] in every borehole section, except in section 9. Consequently, this may be attributed to an anomaly in the measurement of heat power flow in section 9 by Halo DTS- equipment. Notice that in the results of Integral Method from Acuña (2010), this deviation is may relate to an anomaly detected in the differential groundwater flow measurements.

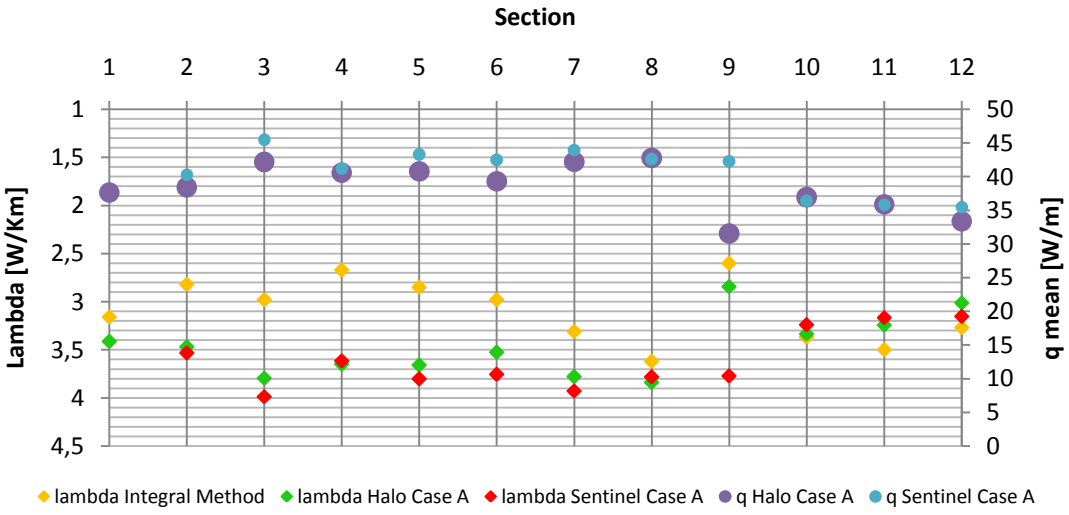

Figure 122. *Rock thermal conductivity (Halo Case A- Sentinel Case A- Integral Method) and Average power flow (Halo and Sentinel in Case A)*

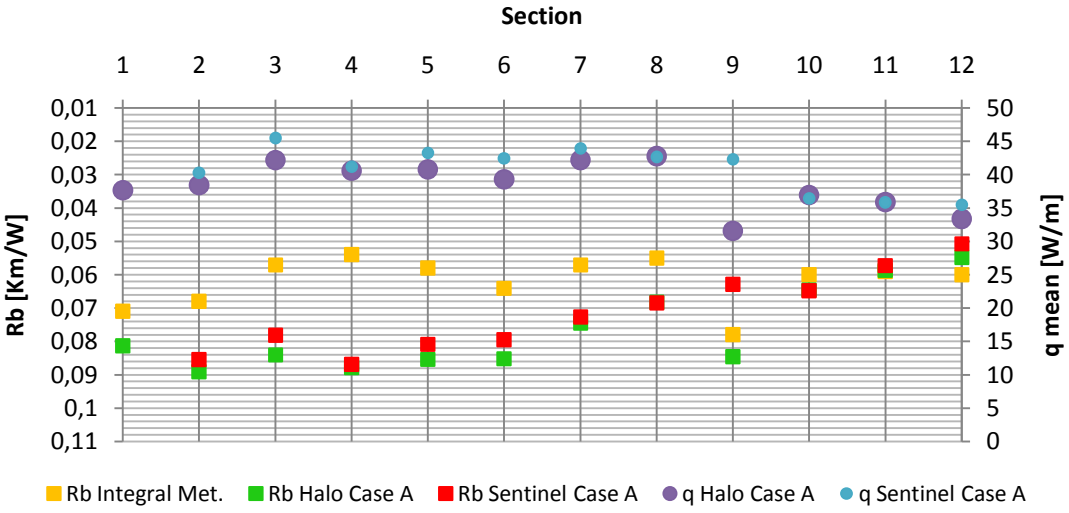

Figure 123. *Borehole thermal conductivity (Halo Case A-Sentinel Case A-Integral Method) and Average heat power flow (Halo and Sentinel in Case A).*

Since the Halo and Sentinel data has been analyzed by the same calculating procedure and present a similar distribution along the borehole depth, the difference observed between these results and the results of Integral Method may explain the uncertainties in the estimated parameters due to the approximations made in analytical model. In Halo results, the uncertainties respect to Integral Method are estimated in average values of 0.37 [W/Km] and 0.014 [Km/W] for thermal conductivity and thermal resistance, respectively. Notice that it is estimated without considering results of section 9. The deviation from the mean value of the uncertainties in thermal conductivity varies with the range -0.06 and 0.80 [W/Km]. In thermal resistance, it ranges between 0.027 and 0.002 [Km/W].

The difference between the estimated parameters in Sentinel results and Integral Method, averaging these differences between the estimates in all section except section 9, the thermal conductivity uncertainties are equal to 0.42 [W/Km] and varies within the range -0.09 and 0.92 [W/Km]. In the same way, the average uncertainties of thermal resistance are equal to 0.012 and its variation is within the range -0.07 and 0.031. Although the uncertainties due to the analytical procedure are not too much relevant, the analysis of Sentinel measurements should carry out considering a stepwisely heat power. And then, the comparison of Halo and Sentinel assuming a stepwisely heat power with Integral Method results may made again.

According to uncertainties due to the test equipment, Halo and Sentinel, there are not significant variations in the estimates of both thermal parameters, without considering results in section 9.

Since the data from Halo DTS-equipment evaluated considering 7.5 hours stepwisely heat power present the best fit according to the measurements of temperature, in next figure are illustrated the profile of thermal conductivity and the profile of borehole thermal resistance estimated in this case- Halo data case B- together with the estimates from Halo and Sentinel data assuming a constant heat power and the results of Integral Method.

It can be observed that the profile of the thermal parameters, which has been obtained by assuming a 7.5 hours stepwisely heat power, present values closer to the values from Integral Method than the results by assuming a constant heat power during the test. In section 1, 8 and 11, it is observed that this behavior in thermal conductivity is different and these estimates present a notable deviation from the estimates of Integral Method. It is may be attributed to the value of the first step heat power considering in the procedure by steps, as regards as the value of the constant heat power assumed in Sentinel and Halo date in case A- constant heat power-.

Considering the borehole thermal resistance profiles, the estimates in case B are closer to the estimates of Integral Method than the estimates obtained in Halo and Sentinel

Case A, in a good accordance with the fit to the measured temperature profile. There are exceptions in section 9 and 11, they may relate to the heat power supply.

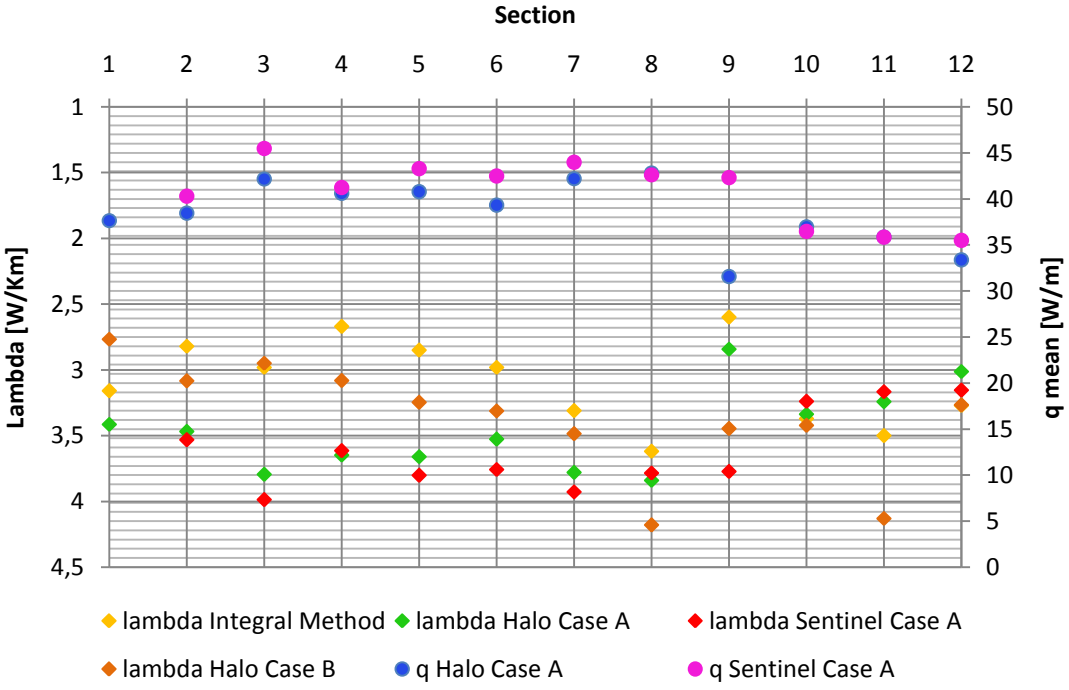

Figure 124. *Rock thermal conductivity (Halo Case A and Case B- Sentinel Case A- Integral Method) and Average power flow (Halo and Sentinel in Case A).*

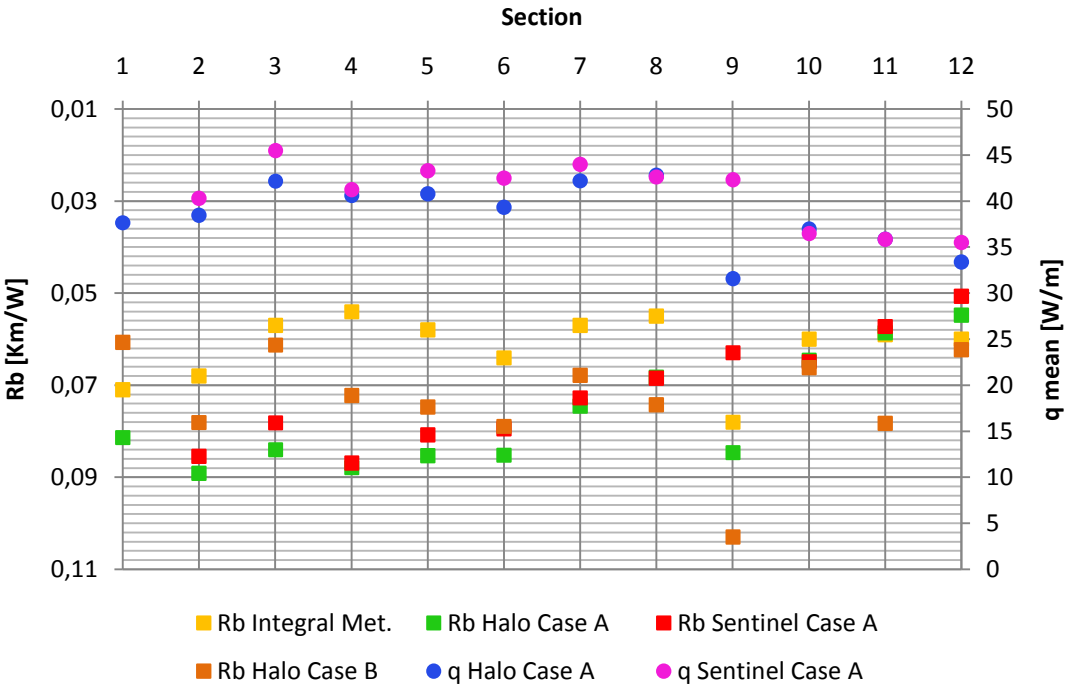

Figure 125. *Borehole thermal conductivity (Halo Case A and Case B-Sentinel Case A-Integral Method) and Average heat power flow (Halo and Sentinel in Case A).*

4. Conclusion.

The Distrubuted Thermal Response Test (DTRT) was carried out using two different resolution equipment - HALO and SENTINEL DTS-equipment -their resolution are 1 and 2 meters, respectively. The analytical procedure to determine the rock thermal conductivity and the borehole thermal resistance is an approach based on the Line Source Model, which is applied to each 20 meters section along the borehole depth.

- The comparison of the results of TRT depending on the heat power supply considered in the analysis –constant and by steps- analyzes the influence of the heat power supply in the estimation of the thermal parameters. The results show that considering the heat power supply as a contribution of 7.5 hours heat power step from past intervals of time, the calculated temperature profile fits better to the profile of temperature measurements in every borehole section.

- Evaluating the results from two different resolution equipments, it is compared Halo and Sentinel results in each borehole section. The profiles of the thermal conductivity and thermal resistance present a similar distribution along the borehole depth in both cases. For Halo data – constant heat power- , the average of the rock thermal conductivity is equal to 3.46 [W/Km], which varies within the range 2.84 and 3.84 [W/Km]. By averaging the thermal resistance in all sections, it is equal to 0.077 and ranges between 0.055 and 0.087 [Km/W].On the other hand, the rock thermal conductivity estimated from Sentinel data presents a mean value of 3.61 [W/Km], which ranges between 3.15 and 3.99 [W/Km] in borehole sections. The average of thermal conductivity is 0.072 [Km/W] and it is varies within the range 0.051 and 0.087 [Km/W]. This suggests that there are no relevant uncertainties in the estimated thermal parameters due to the test equipment measurements. The difference in the estimation of the thermal conductivity along the borehole depth may be attributed to differences in the geological properties along the borehole, although the ground has been considered homogeneous and isotropic for calculations. The variations in the estimation of the borehole thermal resistance can be due to the convective heat, which is not considered, and the physical deviation of U-pipe along the borehole depth.

  It should be noticed that the value of these parameters differs significantly in section 9; this may be attributed to an anomaly in the measurement of heat

power flow. Notice that in Acuña (2010), this deviation is may relate to an anomaly detected in the differential groundwater flow measurements.

- The uncertainties due to the analytical procedure are analyzed comparing the results from Halo and Sentinel data with the results of Integral Method from Acuña (2010). In Halo results, the thermal conductivity uncertainties respect to Integral Method results are equal to 0.37 [W/Km] by averaging the values of all sections except values from section 9 and it is within the range between -0.06 and 0.80 [W/Km].The average of uncertainties of thermal resistance in all sections, except section 9, are equal to 0.014 [Km/W] and it is range between 0.027 and 0.002 [Km/W]. Comparing Sentinel and Integral Method results, the thermal conductivity uncertainties are equal to 0.42 [W/Km] and varies within the range -0.09 and 0.92 [W/Km]. The average uncertainties of thermal resistance are equal to 0.012 and its variation is within the range -0.07 and 0.031. In both cases, it is done by averaging these differences between the estimates in all section except the results from section 9. This suggests that results from Halo present less uncertainties respect to Integral Method results (Acuña 2010). Since the comparison is carried out by means of the estimates result in assuming a constant heat power, it may carry out considering a stepwisely constant heat power for both HALO and SENTINEL measurements in order to provide the best estimation of thermal parameters.

5. Future Work

- Since the heat power is established by means of four measurements points at the inlet and outlet fluid temperatures in each section (Acuña 2010). It is suggested more points of measurements in the fluid inlet and outlet in each borehole section to get more accuracy in the estimation of temperature. Consequently, it may estimate a more accurate heat power rate.

- The case B- 7.5 hour stepwisely constant heat power- presents the best fit to measurements of temperature. However, it may be established other time size of the heat power step which may provide a better approximation. This suggests the analysis of the duration in the heat power step in order to estimate the most accurate values of thermal parameters.

- In the approach by steps, the value of the first heat power step is considered during the whole test and the rest steps of heat power injected depend on the value of the first one. It is suggested the analysis of the influence of the earlier heat power step in the estimation of thermal parameters.

6. References

Acuña J. (2010). *Improvements of U-pipe Borehole Heat Exchanger*. Licentiate Thesis in Energy Technology 2010. Stockholm: KTH.

Acuña, J. (2008). *Characterization and Temperature Measurements Techniques of EnergyWells for Heat Pumps*. Master os Sicinece Thesis Energy Technology 2008:450. Stockholm: KTH.

Austin W.A. (1998). *Development of an in-situ system for measuring ground thermal properties [Master's Thesis].* Oklahoma State University.

Austin W.A., Y.C. (2000). *Development of an in-situ system and analysis procedure for measuring ground thermal properties*. ASHVE Transactions Vol. 106 (1).

Bandos T.V., M.A. (2009). *Finite line-source model for borehole heat exchangers:effect of vertical temperature variations*. Geothermics 38, 263-270.

Carlslaw H.S., J.J.C. (1959). *Conduction of Heat in Solids*, 2d ed Great Britain: Oxford Science Publications.

Cruickshanks F., B.J. (2000). *In-situ measurements of thermal properties of cunard formation in a borehole, Halifax, Nova Scotia*. Proceeedings of the 8th International Conference of Thermal Energy Storage, Terrastock 2000, 28 August-1 September 2000, Stuttgart, Germany.

Eklöf C, G.S. (1996). *TED- A Mobile Equipment for Thermal Response Test*. Master Thesis 1996:198 E. Luleå: Luleå University Technology.

Eskilson, P. (1987). *Thermal Analyses of Heat Extraction Boreholes*. Lund, Sweden: Department of Mathematical Physics, Lund Institute of Technology.

Fujii H., O.H. (2006).*Thermal Response Test Using Optical Fiber Thermometers*. GRC Transactions, 2006.-Vol. 30. , Kyushu University, Fukuoka.

Fujii H., O.H. (2009). *An improved thermal response test for U-tube ground heat exchanger based on optical fiber thermometers.* Geothermics 38, 399-406

Gehlin S. (1998). *Thermal Response Test – In-situ measurements of thermal properties in hard rock.* Licentiate Thesis 1998:37. Luleå: Luleå University Technology.

Gehlin S. (2002). *Thermal Response Test-Method, Development and Evaluation.* Luleå: Luleå University Technology.

Gehlin S., H.G. (2001). Comparison of Four Models for Thermal Response Test for BTES Application in Sweden. *Proceedings of Terrastock 2000*, Stuttgart, Germany, August 28- September 1, 2000, pp.159-164.

Gehlin S., N.B. (1997). Thermal Response Test – A mobile equipment for determining thermal resistance of boreholes. *Proceedings Meagastock'97*, Sapporo, Japan. June 18-21 1997, pp. 103-108.

Gehlin S., N.B. (1998). Thermal Response Tests of Boreholes- Results from In Situ Measurements. Proc. *Second International Stockton Geothermal Conference*. 15-16 March 1998. Richard Stockton College of New Jersey, Pomoma, USA.

Hellström G. (1991). *GROUND HEAT STORAGE, Thermal Analyses of Duct Storage System* .Doctoral Thesis. Lund: LTH.

IEA ECES Annex 21. *Thermal Response Test for Underground Thermal Energy Storages (Annex 21).* Available at: <http://www.iea-eces.org/annexes/ongoing-annexes.html> (8 Oct.2010).

Ingersoll L.R., P.H (1948). *Theory of the Ground Pipe Heat Source for the Heat Pump.* ASHVE Transactions, Vol.54.

Marcotte D., P.P. (2008). *Fast fluid and ground temperature computation for geothermal ground-loop heat exchanger system.* Geothermics 37, 651-665.

Mogensen, P. (1983). *Fluid to Duct Wall Heat Transfer in Duct System Heat Storages.* The international Conference on Subsurface Heat Storage in Theory and Practice, (ss.[Appendix, Part II, p.652-657]). Stockholm.

Sanner B., H.G. (2000).*Thermal response test-current status and worldwide applications.* In: Proceedings of the 2005 World Geothermal Congress, Antalya, Turkey, p.9, Paper 1436.

Schiavi L. (2009). *3D Simulation of the Thermal Response Test in a U-pipe Borehole Heat Exchanger.* Proceedings of *The COMSOL Conference*. Milan.2009

Shonder J.A., B.J.V.(1999). *Determining effective soil formation properties from field data using a parameter estimation technique.* ASHRAE Transactions. 105(1):458-466.

Signorelli S., B.S. (2007). Numerical evaluation of thermal response test. Geothermics 36, 141-166.

Spiltler J.D., Y.S.J. (2000). *In Situ Measurement of Ground Thermal Properties*. Proceeedings of the 8th International Conference of Thermal Energy Storage, Terrastock 2000, Vol.1., 28 August-1 September 2000, Stuttgart, Germany.

Sundberg J. (1998). *Thermal Properties of Solids and Rocks*. Publ. A57, Geology, Chalmers University of Technology, Sweden.

Wang H., Q. C. (2009). *Improved method and case study of thermal response test for borehole heat exchangers of ground source heat pump system*. School of Energy and Enviroment Engineering, Hebei University of Technology, Tianjin, China. Renewable Energy 35, 727-733.

Witte H.J.L., G.G.J. (2002). *In situ measurements of ground thermal conductivity: The Dutch Perspective.* ASHRAE Transactions 2002, No.1.